Universidade do Minho
Escola de Ciências

Catarina Sofia Rodrigues do Carmo

Role of sirtuin 3 on mitochondrial dynamics in Huntington's disease striatal cells

Outubro 2015

Universidade do Minho
Escola de Ciências

Catarina Sofia Rodrigues do Carmo

Role of sirtuin 3 on mitochondrial dynamics in Huntington's disease striatal cells

Tese de Mestrado
Mestrado em Genética Molecular

Trabalho efectuado sob a orientação de
Professora Doutora Ana Cristina Rego
Professora Doutora Olga Coutinho

Outubro 2015

DECLARAÇÃO

Nome: Catarina Sofia Rodrigues do Carmo

Endereço electrónico: ccarmo0@hotmail.com **Telefone:** +351 964 321 097

Número do Bilhete de Identidade: 14187861

Título da dissertação de Mestrado:

Role of sirtuin 3 on mitochondrial dynamics in Huntington's disease striatal cells

Orientadores:

Professora Doutora Ana Cristina Rego

Professora Doutora Olga Coutinho

Ano de conclusão: 2015

Designação do Mestrado:

Mestrado em Genética Molecular

Universidade do Minho, 30 / 10 / 2015

_____

(Catarina Sofia Rodrigues do Carmo)

AGRADECIMENTOS

Depois de um ano intensivo mas, sem dúvida, recompensador, esta será uma das secções mais difíceis de concluir. Embora seja um trabalho apresentado por uma pessoa, não seria de todo possível sem o contínuo apoio e ajuda de um vasto número de pessoas. Não poderia assim passar a oportunidade de expressar o meu profundo agradecimento e reconhecimento a todos os que de alguma forma contribuíram para a sua realização e concretização.

Às minha orientadoras: à Professora Doutora Ana Cristina Rego pela oportunidade de poder integrar no seu grupo de investigação, pelo enorme voto de confiança que depositou em mim e por ajudar continuamente no meu crescimento científico; à Professora Doutora Olga Coutinho pelo apoio e ajuda desde o início deste trabalho e pela constante presença e disponibilidade. Quero ainda agradecer a revisão crítica desta dissertação. O meu obrigada por tudo.

Às minhas "supervisoras" não oficiais: Luana Naia e Ana Oliveira, que enalteceram grandemente o meu crescimento no laboratório, pelo apoio contínuo ao longo de todo este ano e por todo o tempo e atenção que disponibilizaram para mim. Este trabalho é tanto meu como é vosso.

Aos colegas (e amigos) do grupo *Mitochondrial Dysfunction and Signaling in Neurodegeneration* (António, Carla, Elisabete, Inês, Jorge, Luísa, Mário, Maura e Sandra), que sempre se mostraram disponíveis e prestáveis mas acima de tudo por permitirem a fácil integração no grupo e a vossa amizade, que sei que vou levar comigo.

Aos amigos de todo o país (de Braga a Lisboa, passando por Viseu), que sempre me acompanharam e partilharam comigo os sucessos e insucessos.

À minha família, em especial, aos meus pais, pelo apoio incondicional e por acreditarem em mim muito mais que o que eu acredito.

This work was funded by FEDER funds through the Operational Programme Competitiveness Factors - COMPETE, national funds by FCT - Foundation for Science and Technology (project reference: EXPL/BIM-MEC/2220/2013), 'Fundação Luso-Americana para o Desenvolvimento' (FLAD) and by *Gabinete de Apoio à Investigação*, funded by FMUC and Santander Totta Bank. Center for Neuroscience and Cell Biology (CNC) is supported by projects PEst-C/SAU/LA0001/2013-2014 and UID/NEU/04539/2013.

ABSTRACT

Altered mitochondrial dynamics has been implicated in the pathogenesis of several neurodegenerative disorders, including Huntington's disease (HD). Sirtuins, NAD^+-dependent lysine deacetylases, have emerged as important cellular targets that can interfere with mitochondrial biogenesis, fission/fusion, motility and mitophagy. Among them, sirtuin 3 (SIRT3) is particularly relevant, being the main deacetylase located in mitochondria. Here we evaluated the influence of SIRT3 on mitochondrial dynamics using striatal cells derived from HD knock-in mice (ST*Hdh*$^{Q111/Q111}$) *versus* wild-type cells (ST*Hdh*$^{Q7/Q7}$).

Increased mitochondrial fragmentation was observed in untransfected HD cells. Indeed, ST*Hdh*$^{Q111/Q111}$ cells exhibited an overall decrease in the levels of mitochondrial fusion proteins (Mfn2, OPA1) and an increase in fission-related Fis1. Drp1 (also involved in mitochondrial fission) was preferentially accumulated in the mitochondrial fraction of HD cells. Increased LC3-II/I ratio, which evaluates autophagosome formation, was observed in ST*Hdh*$^{Q111/Q111}$ cells. Moreover, the autophagy adaptor p62 was found to be decreased in mutant cells. Parkin and PINK1, two markers of mitophagy, were also assessed. Untransfected HD cells exhibited lower levels of both proteins. No significant changes were detected in phosphorylated Parkin (required for its enzymatic activation and mitochondrial translocation). These data suggest that PINK1/Parkin-dependent mitophagy is impaired in HD striatal cells.

Overexpression (OE) of SIRT3 reduced the unbalance between fission/fusion by decreasing the protein levels of Fis1 in ST*Hdh*$^{Q7/Q7}$ and ST*Hdh*$^{Q111/Q111}$ cells, and Drp1 accumulation in mitochondria in ST*Hdh*$^{Q111/Q111}$ cells. Concordantly, an increased number of mutant cells presenting tubular mitochondria was observed after SIRT3OE. An additional significant increase in LC3-II/I ratio was observed in ST*Hdh*$^{Q111/Q111}$-SIRT3 cells, indicative of macroautophagy activation.

Data suggest that enhanced SIRT3 levels restore mitochondrial morphology in mutant cells by reducing mitochondrial fission, with additional activation of macroautophagy.

KEYWORDS: HUNTINGTON'S DISEASE, MITOCHONDRIAL DYSFUNCTION, MITOCHONDRIAL DYNAMICS, FISSION/FUSION BALANCE, MITOPHAGY, SIRTUIN 3

RESUMO

Alterações na dinâmica mitocondrial têm sido relacionadas com diversas doenças neurodegenerativas, incluindo a doença de Huntington (DH). As sirtuínas são deacetilases de lisinas dependentes de NAD^+ que demonstraram ter um papel importante no re-estabelecimento do equilíbrio entre biogénese e fissão/fusão mitocondrial, e mitofagia. De todas, a sirtuína 3 (SIRT3) destaca-se por ser a deacetilase predominantemente localizada na mitocôndria com maior número de alvos proteícos. Neste trabalho avaliou-se o efeito da SIRT3 na dinâmica mitocondrial recorrendo ao uso de células estriatais derivadas de murganhos *knock-in* para a DH (ST*Hdh*$^{Q111/Q111}$) *versus* células 'wild-type' (ST*Hdh*$^{Q7/Q7}$).

As células mutantes não transfetadas apresentaram um aumento da fragmentação mitocondrial. De facto, as células ST*Hdh*$^{Q111/Q111}$ apresentaram um decréscimo dos níveis proteícos de Mfn2 e OPA1, duas proteínas envolvidas na fusão mitocondrial, e um aumento de Fis1, uma proteína relacionada com a fissão mitocondrial. Verificou-se ainda uma acumulação preferencial da Drp1 (também envolvida na fissão mitocondrial) na fração mitocondrial das células ST*Hdh*$^{Q111/Q111}$. Embora se tenha observado um aumento do rácio LC3-II/I (que avalia a formação de autofagossomas) nas células ST*Hdh*$^{Q111/Q111}$, os níveis do adaptador autofágico p62 encontraram-se diminuídos. Células mutantes não transfetadas apresentaram ainda uma redução dos níveis de Parkina e PINK1, dois marcadores do processo mitofágico. Contudo, não se observaram diferenças significativas nos níveis da forma fosforilada da Parkina (indicador da sua ativação enzimática e translocação para a mitocôndria). Estas evidências sugerem alterações deste processo mitofágico nas células mutantes.

A sobre-expressão de SIRT3 reduziu o desequilíbrio entre fissão/fusão ao diminuir os níveis de Fis1 nas células ST*Hdh*$^{Q7/Q7}$ e ST*Hdh*$^{Q111/Q111}$, e a acumulação da Drp1 na mitocôndria nas células ST*Hdh*$^{Q111/Q111}$. Consequentemente, observou-se um aumentou do número de células mutantes com mitocôndrias tubulares. Verificou-se ainda um aumento significativo do rácio LC3-II/I nas células ST*Hdh*$^{Q111/Q111}$--SIRT3, indicativo de uma ativação da macroautofagia.

Em conclusão, o aumento dos níveis de SIRT3 permite restaurar a morfologia mitochondrial em células mutantes ao reduzir a fissão mitocondrial, conduzindo ainda à ativação da macroautofagia.

TABLE OF CONTENTS

LIST OF FIGURES

LIST OF TABLES

ABBREVIATIONS

ADP, Adenosine diphosphate

ATP, Adenosine triphosphate

BDNF, Brain-derived neurotrophic factor

BSA, Bovine serum albumin

cAMP, Cyclic adenosine monophosphate

CBP, CREB binding protein

CCCP, Carbonyl cyanide *m*-chlorophenyl hydrazone

CREB, cAMP response element-binding protein

DMEM, Dulbecco's Modified Eagle's Medium

Drp1, Dynamin-related protein 1

DTT, Dithiothreitol

ER, Endoplasmic reticulum

FBS, Fetal bovine serum

Fis1, Mitochondria fission 1

GABA, γ-aminobutyric acid

GAPDH, Glyceraldehyde-3-phosphate dehydrogenase

HAP1, Huntingtin-associated protein 1

HD, Huntington's disease

HDAC, Histone deacetylase

HEAT, Huntingtin, Elongation factor 3, protein phosphatase 2A and yeast kinase TOR1

HIP, Huntingtin interacting protein

HTT, Huntingtin

H_2O_2, Hydrogen peroxide

IMM, Inner mitochondrial membrane

K, Lysine

KAT, Lysine acetyltransferase

KDAC, Lysine deacetylases

LC3, Light chain 3

Mfn, Mitofusin

mHTT, Mutant huntingtin

MPP, Mitochondrial processing peptidase

MPT, Mitochondrial permeability transition

MSN, Medium spiny neurons

mtDNA, Mitochondrial DNA

NAD^+, β-nicotinamide adenine dinucleotide

NAM, Nicotinamide

NO, Nitric oxide

Nrf2, Nuclear factor-erythroid 2-related factor-2

NRF, Nuclear respiratory factor

OE, Overexpression

OMM, Outer mitochondrial membrane

OPA1, Optic atrophy 1

OXPHOS, Oxidative phosphorylation

$O_2^{\bullet -}$, Superoxide anion radical

PGC-1α , PPARγ – coactivator-1α

PARL, Presenilin-associated rhomboid-like protease

PBS, Phosphate-buffered saline

PE, Phosphatidylethanolamine

PINK1, PTEN-induced putative kinase 1

PI3K, Phosphatidylinositol-3-kinase

PMSF, Phenylmethylsulfonyl fluoride

polyQ, Polyglutamines

PPARγ, Peroxisome proliferator-activated receptor γ

PTEN, Phosphatase and tensin homolog

ROI, Region of Interest

ROS, Reactive oxygen species

SIRT, Sirtuin

Sir2, Silent information regulator 2

SNO, S-nitrosylation

SOD2, Superoxide dismutase 2

TAF, TBP-associated factor

TBS-T, Tris Buffered Saline with Tween-20

TBP, TATA-binding protein

TCA, Trichloroacetic acid

TOR, Target of rapamycin

TSA, Trichostatin A

UPS, Ubiquitin-Proteasome System

Viniferin, Trans-(–)-ε-viniferin

YAC, Yeast artificial chromosome

$\Delta\psi_m$, Mitochondrial membrane potential

CHAPTER I – INTRODUCTION

1.1. HUNTINGTON'S DISEASE

Huntington's disease (HD) is an inherited autosomal dominant neurodegenerative disorder, with a prevalence of 2-5 per 100 000 individuals in Portugal (Costa *et al*, 2003). Unlike other neurodegenerative diseases, HD is known to be caused by an unstable expansion of CAG trinucleotide repeats in the exon 1 of *HTT* gene, located on the short arm of chromosome 4 (4p16.3) (Walker, 2007). The normal allele is transmitted according to Mendelian laws, while the mutant one shows instability during meiosis, changing in length with either slight increases or decreases (1-4 or 1-2 units, respectively) (Gil & Rego, 2008). In 73% of the cases, instability accounts for expansion, with contraction taking about 23%, occurring mainly through paternal transmission (Rosas *et al*, 2008).

The *HTT* gene contains less than 27 repeats in the general population, and although 27-35 repeats still remains under a non-pathological condition, expansion and anticipation may be manifested in offsprings (Morreale, 2015). Disease is manifested with over 39 repeats, causing long stretches of polyglutamines (polyQ) at the N-terminal of the encoded protein huntingtin (HTT). An intermediate number of repeats (36-39) is associated with a slower progression of HD, due to incomplete penetrance of the mutant allele (Bano *et al*, 2011). Disease onset and progression display an inverse correlation with the number of polyQ repeats, which is evident for CAG repeats higher than about 50. The majority of HD patients exhibit the first symptons at middle-age between 35-50 years; younger occurrences have been documented for CAG repeats higher than 60 (Gil & Rego, 2008). With a progressive decline over time, HD ultimately leads to the patient's death 15-20 years after the onset (Ross & Tabrizi, 2011).

HD is widely perceived as a movement disorder, still patients exhibit significant cognitive, behavioral and psychiatric symptoms that might precede motor abnormalities. Affected individuals demonstrate changes in behavior and personality, ranging from lack of inhibition with impulsivity and irritability to apathy and indifference. Cognitive decline is manifested with altered emotional recognition, working and learning memory with overall memory impairment, although not as pronounced as in other neurodegenerative disorders associated with dementia. The

most characteristic symptom of HD is chorea, often being the initial indication of motor illness that can be mistaken for clumsiness in early stages. It starts distally but progresses to the proximal, axial and facial musculature. Dystonia and bradykinesia develop in later stages of HD. As the disease progresses, the initial uncontrolled movements lead to impairment of nearly all movement-associated functions and cognitive deficits become more severe. HD ultimately culminates in the patient's death from complications of falls, inanition, dysphagia or aspiration pneumonia (Morreale, 2015; Ross & Tabrizi, 2011).

Neurodegeneration related with HD is specific for striatum (caudate nucleus and putamen) and in later stages for cerebral cortex (Quintanilla & Johnson, 2009). Striatal medium spiny neurons (MSN) containing γ-aminobutyric acid (GABA) are particularly vulnerable and are the reason for the characteristic involuntary movements (Mochel & Haller, 2011). The reason behind the specific neurodegeneration remains unclear to date, with several hypotheses suggested. Subramaniam and colleagues for instance, showed that Rhes, a protein that localizes particularly in striatum, has the ability to bind to mutant huntingtin (mHTT), thereby inducing its small ubiquitin-like modifier (SUMO)ylation in such a way that may result in neurotoxicity (Subramaniam *et al*, 2009). Neuronal intranuclear inclusions are also a characteristic of HD, along with protein aggregation in dystrophic neurites in striatal and cortical neurons. The number of cortical inclusions also seems to correlate with the length of CAG repeats and inversely with disease onset (Gil & Rego, 2008).

1.1.1. Huntingtin: structure, function and post-translational modifications

HTT (*OMIM:613004*) is naturally expressed among all human and mammalian cells, with a higher expression in brain and testes although it can also be found in the liver, heart and lungs (Walker, 2007).

Wild-type HTT is a ~350 kDa protein with a polymorphic stretch of 6-35 glutamine residues localized in its N-terminus (Borrell-Pagès *et al*, 2006). Longer polyQ stretches induce conformational changes, resulting in a form of HTT causative

of disease (Gil & Rego, 2008). It is mainly a cytosolic protein, where it can associate with multiple organelles (endoplasmic reticulum (ER), Golgi complex, mitochondria, among others), but can also be present in nucleus. HTT can also be found in neurites and at synapses (Mochel & Haller, 2011; Cattaneo *et al*, 2005).

The N-terminus of HTT contains an amphipatic alpha helical membrane--binding domain that can help in targeting vesicles, such as late endosomes and autophagic vesicles and ER. Due to the presence of an active nuclear localization signal in the same terminus, HTT can translocate to the nucleus in response to several stimuli, such as ER stress (Desmond *et al*, 2012; Atwal *et al*, 2007). In addition, it possesses a putative nuclear export signal near the C-terminus, regulating HTT localization towards the cytoplasm (Maiuri *et al*, 2013; Zheng *et al*, 2013; Xia, 2003). The polyQ expansion can impair the normal nuclear export and maintain the affected protein in the nucleus (Cornett *et al*, 2005). A number of HEAT (Huntingtin, Elongation factor 3, protein phosphatase 2A and the yeast kinase Target of rapamycin (TOR) 1) repeats (~40 amino acids forming two hydrophobic α-helices) downstream of the glutamine/proline-rich domain at the N-terminus (see **Fig. 1**) is also present (Andrade *et al*, 2001). This domain is highly conserved among eukaryotic proteins involved in cytoplasmic/nuclear transport-related processes, microtubule dynamics, and thus may confer the same functions to HTT (Neuwald & Hirano, 2000).

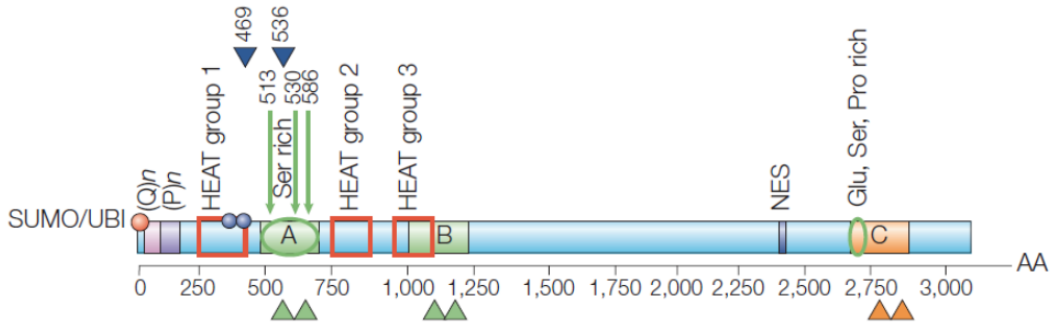

Fig. 1 | A Schematic diagram of the HTT amino acid sequence.
(Q)n indicates the polyQ tract, followed by the polyproline sequence, (P)n, and the red squares indicate the three main clusters of HEAT repeats. The arrows indicate the caspase cleavage sites and their amino acid positions. B identifies the regions cleaved preferentially in the cerebral cortex, C indicates those cleaved mainly in the striatum, and A indicates regions cleaved in both. Green and orange arrowheads point to the approximate amino acid regions for protease cleavage. NES is the nuclear export signal. The red and blue circles indicate post-translational modifications: ubiquitination (UBI) and/or SUMOylation (SUMO) (red), and phosphorylation at serine 421 and serine 434 (blue). The glutamic acid (Glu)-, serine (Ser)- and proline (Pro)-rich regions are indicated (serine-rich regions encircled in green). AA indicates number of amino acids. In E. Cattaneo, C. Zuccato, and M. Tartari, "Normal huntingtin function: an alternative approach to Huntington's disease.," Nat. Rev. Neurosci., vol. 6, no. 12, pp. 919–30, Dec. 2005.

HTT is subjected to extensive post-translational modifications (as seen in **Fig. 1**). It may be subjected to SUMOylation and ubiquitination at the N-terminal lysines (K6, K9, K15), with the former reducing the ability of HTT to form aggregates (Steffan, 2004; Kalchman *et al*, 1996). Phosphorylation has been reported at serines (S13, S16, S421, S434) and appears to play a protective role, influencing cleavage and toxicity, with lower levels associated with HD (Gu *et al*, 2009; Warby *et al*, 2009; Luo *et al*, 2005; Humbert *et al*, 2002). HTT can also be palmitoylated by huntingtin interacting protein (HIP)14, a palmitoyl transferase, at cysteine 214 and has been correlated with its trafficking and function. In the case of HD, there is a reduction in palmitoylation that can lead to increased toxic effects generated by the mutant protein due to enhanced formation of inclusion bodies (Fukata & Fukata, 2010; Yanai *et al*, 2006).

A possible role for HTT in early embryonic development was one of the first processes to be related with its function, since embryos of homozygous knockout mice do not survive after gestation (Cattaneo, 2003). Since then, it has been implicated in hippocampal neurogenesis by increasing axonal transport of brain--derived neurotrophic factor (BDNF), related with differentiation and maintenance of neurons, and in neural induction as well as in early stages of embryogenesis (Ismailoglu *et al*, 2014; Ben M'Barek *et al*, 2013; Nguyen *et al*, 2013). On the other hand, wild-type HTT appears to have an anti-apoptotic function, associated with the promoted expression of BDNF and with interaction with HIP1, a pro-apoptotic protein, preventing the later from activating caspase 8 (Gervais *et al*, 2002; Zuccato, 2001; Rigamonti *et al*, 2000).

Given its subcellular localization, ubiquitous expression and the fact that no homologues are known, a precise function of this protein is yet to be elucidated. Meanwhile, it has been proven that HTT interacts with a number of proteins involved in numerous functions – gene expression, intracellular transport, signaling and trafficking (Gil & Rego, 2008). In fact, HTT appears to be involved in endocytosis, microtubule-dependent transport of organelles (including mitochondria) or even recycling at plasma membrane by interacting with microtubules, β-tubulin, clathrin, to name a few (Brandstaetter *et al*, 2014; Li & Li, 2004). Such may implicate that HTT

may act as a scaffold protein and act to coordinate complexes composed by other proteins, as it was recently proposed by Cuervo's lab in relation to selective autophagy (Rui *et al*, 2015).

1.1.2. Mutant huntingtin and mechanisms of cytotoxicity

The mutation characteristic of HD leads to long polyQ stretches in HTT N--terminal domain, altering its conformation and protein-protein interactions combined with decreased levels of the wild-type protein. Since wild-type HTT is involved in numerous cellular functions, mHTT ultimately induces profound alterations in several signaling pathways, including transcription, apoptosis, vesicular transport and/or mitochondrial function, among others (Caviston & Holzbaur, 2009; Harjes & Wanker, 2003).

mHTT suffers a proteolytic caspase-dependent cleavage generating toxic N--terminal fragments. Both forms are prone to aggregation and its propensity is directly correlated with the polyQ tract length (Rubinsztein, 2006; Wellington *et al*, 2000). N-terminal fragments due to their smaller size can easily translocate towards the nucleus and promote apoptosis and toxicity (Wellington *et al*, 2000). One of the hallmarks of HD is, in fact, the formation of insoluble mHTT aggregates that can be found in the nucleus as neuronal intranuclear inclusions, as well as in other cellular compartments – cytoplasm, dendrites and axon terminals (Gil & Rego, 2008).

These aggregates can interfere with cell metabolism and cause cytotoxicity, though the associated mechanisms are still unclear. One possibility can be related to ER stress and another to the sequestration of proteins that have glutamine-rich domains, such as cyclic adenosine monophosphate (cAMP) response element--binding protein (CREB) and Sp1, making them unable to achieve their transcriptional function (Leitman *et al*, 2014; Schaffar *et al*, 2004; Sakahira *et al*, 2002). However, growing evidence suggests that the toxic role is not associated with the insoluble aggregates of mHTT, but rather with the soluble oligomeric mHTT, which could result in a change in therapeutic approaches (Kumar *et al*, 2014; Leitman *et al*, 2013).

When localizing in the nucleus, abnormal protein-protein interactions may occur between mHTT and nuclear proteins and transcription factors by including them into the protein aggregates or inhibiting their normal transcriptional activity. The later could occur either through chromatin modification or direct interaction with genomic DNA. Abnormal interactions of mHTT were described with TATA--binding protein (TBP)/TFIID, p53 or CREB binding protein (CBP), resulting in a wide transcription deregulation (Kumar *et al*, 2014; Moumné *et al*, 2013).

In fact, mHTT interaction with p53 not only highlights nuclear dysfunction but also mitochondrial dysfunction (see section **1.2.1.**). Additionally, mitochondrial dysfunction can aggravate cellular homeostasis by increasing oxidative stress. Mitochondria constitue the major sources for reactive oxygen species (ROS) production as a byproduct of oxidative phosphorylation (OXPHOS). Increased ROS levels can also induce oxidative DNA damage (nuclear and mitochondrial) that, if not repaired, will result in DNA instability and further pathogenesis (Ayala-Peña, 2013).

Expression of mHTT leads to protein aggregation, recruiting other proteins than just the modified protein. It can overcome the ability of the cell's protein quality control/degradation pathways to successfully degrade protein aggregates, resulting in a greater accumulation of the mHTT (Rubinsztein, 2006). It was initially thought that soluble mHTT would not be successfully degraded by physically blocking the channel of the 20S proteolytic chamber, leading to further Ubiquitin-Proteasome System (UPS) dysfunction with accumulation of 26S proteasome (McKinnon & Tabrizi, 2014). Hipp and colleagues studied the relation between aggregation of N-terminal fragments and UPS function, elegantly demonstrating that such fragments, aggregated or not, could not block the 26S proteasome (Hipp *et al*, 2012). Meanwhile, the 26S proteasome was also reported to be sequestered into mHTT--derived aggregates which could explain protein accumulation (Jana, 2001). Consequently, with general decreased protein degradation, inhibition of ER--associated protein degradation (ERAD) pathway occurs. Ultimately, it culminates in reduced protein load in the ER, with accumulation of unfolded/misfolded proteins in ER and activation of the unfolded protein response (UPR) (Leitman *et al*, 2013). As a result, Bax incorporates in the ER membrane leading to caspase 7 activation and cell death (Ueda *et al*, 2014).

Autophagy impairment has long been implicated in HD, preventing an efficient starvation response and nutrient recycling (Tan *et al*, 2014; Levine & Kroemer, 2008). Alterations in autophagy can also increase the susceptibility to apoptosis and formation of ubiquitinated inclusions (Ghavami *et al*, 2014). mHTT contributes not only to sequestration of mTOR, thereby inducing autophagy, but also with autophagosome motility and impedes cytosolic cargo from being recognized (Wong & Holzbaur, 2014; Ghavami *et al*, 2014; Martinez-Vicente *et al*, 2010). It results in an increased number of empty autophagosomes, with aggregated mHTT as well as damaged organelles kept from degradation, which then accumulate in the cytoplasm and increase cytotoxcicity (Martin *et al*, 2015).

mHTT has been studied as a target for treatment of HD and a great effort has been made in exploring new techniques that culminate in mHTT clearance or silencing (Appl *et al*, 2012; Lu & Yang, 2012; Carroll *et al*, 2011). Meanwhile, recent findings demonstrate the presence of mHTT in genetically normal cells from unrelated neural tissue grafts that were transplanted in the brain of affected HD patients. The authors suggest several hypotheses for their intriguing findings including cell-to-cell transport/transmission (Cicchetti *et al*, 2014). This has yet to be further explored to determine the therapeutic, and even scientific, implications for patients and the complete elucidation of HD pathogenesis.

1.2. CHANGES IN MITOCHONDRIAL FUNCTION AND DYNAMICS IN HD

The presence of mHTT alters profoundly the cellular homeostasis further leading (directly or not) to excitotoxicity, oxidative stress, nucleolar and mitochondrial dysfunction and overall metabolic impairment (Sepers & Raymond, 2014; Radi *et al*, 2014; Lee *et al*, 2014; Naia *et al*, 2012).

Mitochondria are essential organelles that control the production of energy *via* adenosine triphosphate (ATP) through OXPHOS, intracellular Ca^{2+} homeostasis, cell metabolism, apoptosis and overall cellular homeostasis (Rosenstock *et al*, 2010). Thus, mitochondrial dysfunction is considered a hallmark of HD pathogenesis since they are major contributors for the increase in generation of ROS, excitotoxicity and

neuronal cell death (Ribeiro *et al*, 2014; Federico *et al*, 2012; Gil & Rego, 2008). Additionally, HD patients demonstrate a marked weight loss in spite of unchanged calorie uptake, decreased brain glucose consumption with consequent elevated lactate production in early stages, prior to pronounced striatal atrophy (Mochel & Haller, 2011; Berent *et al*, 1988). Moreover, ROS production by mitochondria has also been related with increased mitochondrial DNA (mtDNA) damage (Siddiqui *et al*, 2012). As such, mitochondrial function stands for a hallmark of HD pathogenesis and a vast effort has been continuously made to improve it.

1.2.1. Mitochondrial dysfunction – from transcription deregulation to altered calcium handling

Interference of mHTT with nuclear gene transcription may mediate the mitochondrial dysfunction observed in HD. In its soluble form, mHTT interacts with several transcriptional regulators such as CBP, TBP-associated factor (TAF)4/ TAFII130 and peroxisome proliferator-activated receptor γ – PPARγ – coactivator-1α (PGC-1α) (Jin & Johnson, 2010).

mHTT interferes with CREB/TAF4 signaling pathway that regulates various mitochondrial genes, such as β-nicotinamide adenine dinucleotide (NADH) dehydrogenase subunit 5 (ND5) that codes for a subunit of complex I (Steffan *et al*, 2000). PGC-1α is also found repressed in HD in *in vitro* and *in vivo* models, partially due to the direct interaction of mHTT with the signaling pathway mentioned above that regulates its expression, but also by direct binding to its promoter (Cui *et al*, 2006). PGC-1α is a major regulator of mitochondrial function, mediating mitochondrial biogenesis and respiration. Being a transcriptional coactivator, it regulates the expression of nuclear-encoded subunits of each of the electron transport-chain complexes, along with genes involved in antioxidant response (Johri *et al*, 2013). PGC-1α also regulates the nuclear respiratory factor-1/2 (NRF-1/2) and PPARα, PPARδ and PPARγ by forming heteromeric complexes, sharing a role in the expression of genes such as cytochrome *c*, complexes I-V and the mitochondrial

transcription factor A (Tfam) (Jin & Johnson, 2010). The foremost contribution of PGC1-α to HD can be assigned from the neuroprotective effects that come from its restoration in HD transgenic mice (Tsunemi *et al*, 2012).

Mitochondrial function can also be affected by the regulation of nuclear p53 function. p53 has the ability to bind to HTT and regulate it at transcriptional level, by inducing HTT expression (Feng *et al*, 2006). Since p53 responds to different stress stimuli, we can anticipate that many environmental factors would then increase mHTT protein expression levels, by altering p53 activity. Besides this, p53 also regulates the expression of genes involved in metabolism: from glycolysis (e.g.: TP53--induced glycolysis and apoptosis regulator (TIGAR)) to oxidative phosphorylation (e.g.: SCO2 cytochrome *c* oxidase assembly protein), and so it may participate in mitochondrial dysfunction (Wickramasekera & Das, 2014; Bae *et al*, 2005; Nakaso *et al*, 2004). Furthermore, impairment of mitochondrial energy metabolism, with a consequent decrease in ATP levels, can result in induction of p53 expression in the striatum. This will consequently lead to induction of autophagy and neuronal cell death (Zhang *et al*, 2009). In this way, suppression of p53 function can promote stabilization of mitochondria against dysfunction (Lau & Bading, 2009).

Additionally, biochemical studies showed reduced activities of enzymes involved in metabolism such as aconitase – of the tricarboxylic acid cycle and that can be used as an indirect indicator of ROS generation and as thus oxidative stress –, succinate dehydrogenase (complex II), cytochrome *c* oxidase (complex IV), pyruvate dehydrogenase complex, α-ketoglutarate dehydrogenase complex, as detected in caudate and putamen (striatum) tissue derived from symptomatic/advanced HD patients (Solans *et al*, 2006; Benchoua *et al*, 2006; Tabrizi *et al*, 1999). Studies done using mitochondria isolated from human platelets demonstrate that while pre--symptomatic HD patients displayed reduced complex I and citrate synthase activities, symptomatic HD patients presented decreased complex I and increased complex IV activities (Silva *et al*, 2013). Still, there is no relevant deficiency of the respiratory chain complexes in symptomatic patient-derived cybrids or in transgenic mice when expressing full-length mHTT, and thus, these defects can be a secondary feature in the HD pathogenesis (Ferreira *et al*, 2010; Guidetti *et al*, 2001). In accordance, Milakovic and colleagues did not find impairment of mitochondrial

complexes I-IV, but related the presence of mHTT to impaired mitochondrial ATP production (Milakovic & Johnson, 2005). Concordantly, Pickrell and co-authors published some interesting results by showing that the striatum appears to be particularly sensitive to defects in OXPHOS, as they may depend largely on this mechanism and have a higher membrane potential. The authors further suggested that such distinct mitochondrial properties could be due to differential expression of PGC-1α/β (Pickrell *et al*, 2011).

In the presence of mHTT mitochondria have abnormal conformations and morphology as shown in postmortem patient's brain tissue, as well as in human HD lymphoblasts (Napoli *et al*, 2013; Squitieri *et al*, 2006; Goebel *et al*, 1978). Evidence from human HD lymphoblasts, transgenic yeast artificial chromosome (YAC) mice expressing full-length HTT with 72 glutamines, R6/2 and R6/1 mice (expressing exon 1 of human mutant *HTT*), knock-in *Hdh*150 mice (expressing full-length HTT with an expansion of 150 glutamines) and ST*Hdh*$^{Q111/Q111}$ cells that produce N-terminal fragments of mHTT containing the polyQ expansion associate with mitochondria, accumulating at the outer mitochondrial membrane (OMM) (Yu *et al*, 2003; Panov *et al*, 2002). Recently, it was described by Yano and co-authors that the N-terminal of mHTT interacts with mitochondrial import machinery, namely translocase of the inner membrane 23 (TIM23) complex (Yano *et al*, 2014). Furthermore, it was established that this association resulted in the organelle's uncoupling from microtubule-based transport proteins, mitochondrial depolarization with additional impacts on Ca^{2+} homeostasis (Orr *et al*, 2008; Rockabrand *et al*, 2007). Apparently, mHTT interaction with the OMM can destabilize it and in that way increase mitochondrial permeability transition (MPT) pore sensitivity to Ca^{2+} or other stimuli, resulting in apoptosis through the release of cytochrome *c* (Milakovic *et al*, 2006; Panov *et al*, 2005; Choo *et al*, 2004). Meanwhile, recent data obtained with isolated brain synaptic and non-synaptic mitochondria from YAC128 mice suggest that mHTT increases mitochondrial Ca^{2+} uptake, contradictory to the detrimental effect so far documented not only in YAC128 mice, but also in R6/2 and knock-in *Hdh*150 mice (Pellman *et al*, 2015; Zhang *et al*, 2008; Oliveira *et al*, 2007, 2006).

1.2.2. Alterations in mitochondrial dynamics

Mitochondria are dynamic organelles with frequent changes in size, shape, number and even cellular distribution directly related with its function in response to cellular need or to diverse stimuli (Detmer & Chan, 2007). The control of length, shape, size and number of mitochondria is controlled by a wide range of processes – biogenesis, fission/fusion balance, trafficking and mitophagy.

Increasing evidence suggests that unbalanced mitochondrial dynamics take an important role in neurodegeneration, as is the case with HD (Rosenstock & Rego, 2012). The presence of mHTT appears to reduce the number of mitochondria and lead to its fragmentation, with defects in anterograde and retrograde transport and velocity, ultimately causing neuronal cell death (Shirendeb *et al*, 2011).

1.2.2.1. Biogenesis

Mitochondria biogenesis compromises a multistep process, where mtDNA transcription and translation, along with translation of nuclear-encoded mitochondria-related transcripts, mitochondrial protein import and overall assembly into a mitochondrial reticulum must proceed correctly (Zhu *et al*, 2013). NRF1 and NRF2, which are regulated by PGC-1α and PGC-1α itself are considered the major transcriptional regulator of organelle's *de novo* generation (Scarpulla, 2008). NRF (1 and 2) regulate transcription of Tfam, the major transcriptional regulator of mtDNA, while PGC-1α can also command NRFs activity and regulate enzymes such as ATP synthase or superoxide dismutase 2 (SOD2) (Palikaras & Tavernarakis, 2014).

HD patients show reduced levels of Tfam and PGC-1α as disease severity increases, combined with mitochondrial loss (Kim *et al*, 2010b). This was seen not only in brain tissue from HD patients, but also in several animal models and muscle of HD patients and transgenic mice (Shirendeb *et al*, 2012; Chaturvedi *et al*, 2009; Cui *et al*, 2006; Weydt *et al*, 2006).

1.2.2.2. Fission/fusion balance

Both processes of fusion (joining of different mitochondria) and fission (division of a mother mitochondria resulting in two daughter ones) are regulated by members of the dynamin family. In the case of fission, dynamin-related protein 1 (Drp1) takes control of the process. It is largely cytosolic, but can transit towards the OMM upon a fission stimulus, having an effector guanosine triphosphate (GTP)ase domain. Drp1 undergoes complex and numerous post-translational modifications on two main serines (in human, S616 and S637). Phosphorylation at S637 by protein kinase A (PKA) causes a decrease in Drp1 GTPase activity, whilst phosphorylation at S616 by cyclin-dependent kinase 1 (Cdk1)/cyclin B results in translocation of the mitochondrial fission modulator to the effector site. SUMOylation has also been suggested to stabilize and enhance Drp1 binding to the mitochondria (Knott *et al*, 2008).

Drp1 assembles into punctuate spots on mitochondrial tubules, assembling into rings that will constrict the mitochondrial tubule. For the recruitment of Drp1 to the effector site, mitochondrial fission 1 (Fis1), an integral protein of the OMM, is fundamental, binding directly to Drp1 (Chen & Chan, 2004).

While fission modulators are only associated with the OMM, fusion counts with machinery in both the inner mitochondrial membrane (IMM) and OMM. Mitofusins (Mfn) 1 and 2 are also GTPases, located on the OMM, being responsible for the fusion of OMMs of the juxtaposing mitochondria. They form homo- and hetero-oligomeric complexes in the sites that are close together of the opposing mitochondria. Optic atrophy 1 (OPA1) is the regulator for the IMM fusion process, found in the intermembrane space and showing association with IMM. Maintenance of mitochondrial membrane potential ($\Delta\psi_m$) is required for mitochondrial fusion. As such, when there is a dissipation of $\Delta\psi_m$, fusion is inhibited but fission can still occur and mitochondrial fragmentation can become a dominant morphology (van der Bliek *et al*, 2013; Griffin *et al*, 2006; Legros, 2002). In addition to its role in IMM fusion, OPA1 is also connected with maintaining and remodeling cristae junctions and the release of cytochrome *c* (Costa & Scorrano, 2012).

In normal conditions both processes are balanced. Cells that show increased fusion over fission have fewer mitochondria, being long and connected, while cells that show the reversed case have numerous mitochondria, with small and spherical shape, also referred as fragmented mitochondria (Otera & Mihara, 2012; Detmer & Chan, 2007). Fusion and fission control the shape, length and number of mitochondria with functional consequences. They permit the exchange of lipid membranes and intramitochondrial content, mobility of the organelle itself to specific subcellular locations; also, fission facilitates apoptosis by regulating the release of intermembrane space proteins into the cytosol (Detmer & Chan, 2007). In addition, the internal structures also show a dynamic behavior, being linked to the metabolic state of mitochondria: when in low adenosine diphosphate (ADP) conditions, there is limited respiration, with fewer and narrower cristae present; in high ADP and substrate conditions, the inverse situation is seen, with condensed and large cristae (Mannella, 2006).

Fission/fusion balance has been reported to be altered in HD. Altered expression of genes involved in these processes culminates in abnormal mitochondria and consequently in neuronal dysfunction (Reddy & Shirendeb, 2012). Kim and colleagues assessed for the first time altered mitochondrial dynamics in HD. They started by analyzing neostriatal tissues from HD patients by 3D deconvolutional digital imaging using cytochrome *c* oxidase subunit 2 (COX2) for mitochondrial labeling. They observed a visible decrease in the number of mitochondria in HD striatal spiny neurons that appeared to directly correlate with disease severity. Moreover, alterations in size were apparent, with a higher loss of larger and medium-sized mitochondria in the mutant cells. A significant increase in Drp1 expression with a decrease in Mfn1 expression (correlating with overall transcriptional deregulation) showed a preference for fission in HD (Kim *et al*, 2010b). Besides the alterations seen in striatum, increased levels of Drp1 and Fis1 and decreased levels of Mfn1, Mfn2 and OPA1 were also visible in cortex, being specific to disease affected areas (Shirendeb *et al*, 2011).

In addition to the increased expression, Drp1 appears to display an increased GTPase activity due to interaction with mHTT (Song *et al*, 2011). mHTT-induced fragmented mitochondria are found to be localized mainly in the cell body, not being

able to transport to dendrites, axons and synapses, which consequently results in low ATP levels at these sites and in overall synaptic degeneration (Shirendeb *et al*, 2012). On the other hand, along with oxidative stress there is a significant production of nitric oxide (NO), a reactive nitrogen species (RNS), that leads to increasing S-nitrosylation (SNO) of Drp1. SNO-Drp1 was associated with neurotoxic events related with excessive mitochondrial fragmentation, that could be abrogated using NO inhibitors, further suggesting that this mechanism may be a key mediator of mHTT associated toxicity (Haun *et al*, 2013). Additionally, the Ca^{2+}-dependent phosphatase calcineurin displays a higher activity in HD and has been related with activating Drp1 dephosphorylation at S637, resulting in the translocation of the fission modulator to the mitochondria (Ermak *et al*, 2009; Cereghetti *et al*, 2008).

Nuclear factor-erythroid 2-related factor-2 (Nrf2) signaling has a prominent role in the antioxidant response along with regulation of mitochondrial biogenesis (by inducing NRF-1 transcription), and it is found altered in HD. It was reported that this particular signaling pathway can contribute to altered mitochondrial morphology, namely to fragmented mitochondria related with oxidative stress (Jin *et al*, 2013).

Data from lymphoblasts from HD patients, knock-in *Hdh*111 mice and transgenic YAC128 mice show an excessive mitochondrial fragmentation in HD, in accordance with the aforementioned increase in expression of fission-related genes and a decrease in expression of fusion-related genes (Costa *et al*, 2010).

1.2.2.3. Motility

Mitochondria trafficking along the cell allows for the organelle to be present in subcellular compartments that are in need of a higher energy demand. This process is critically important when considering polarized cells, as is the case of neurons, that need energy outside the regular bioenergetic requirements, such as for synaptic transmission. The processes of mitochondrial fusion and fission can be directly related to their motility. Fission allows for smaller mitochondria to be separated from the rest of the network and to be transported along the cell's cytoskeleton –

microtubules and actin filaments – with the aid of dynein, dynactin (retrograde transport) and kinesins motors (anterograde transport) (Zinsmaier *et al*, 2009). Mitochondria enlists motor adaptors such as TRAK1 and TRAK2 that bind Miro (OMM protein) to kynesin motors and ensures targeted and precise trafficking in response to neuronal activity (Lin & Sheng, 2015).

If impaired, mitochondria transport from the cell body to dendrites, axons and synapses will not occur, and damaged mitochondria will be accumulated at these sites (Chen & Chan, 2009).

Impairment in mitochondrial transport along neuronal processes, with slower translocation of the organelle has been associated to HD. Both N-terminal fragments and full-length mHTT can directly affect mitochondria motility in both anterograde and retrograde movement, leading to accumulation of the organelle in close location to mHTT aggregates through destabilization of microtubules in a polyQ expansion--dependent manner. This cytoplasmic dysfunction was suggested to precede transcriptional dysfunction (Shirendeb *et al*, 2012; Orr *et al*, 2008; Trushina *et al*, 2004). Sequestration of mitochondrial transport machinery and blockage by the presence of aggregates may also take place in making impossible for mitochondria to move through narrow neuronal projections, as seen in cortical neurons overexpressing mHTT and in HD striatal neurons (Chang *et al*, 2006; Trushina *et al*, 2004).

1.2.2.4. Mitophagy

Accumulation of damaged mitochondria due to several means – loss of $\Delta\psi_m$, oxidative stress, impaired OXPHOS, excessive fragmentation, decreased biogenesis – occurs in HD cells and can induce apoptosis by cytochrome *c* release and additional neuronal damage (Whitworth & Pallanck, 2009). In these conditions, cells are equipped with specific mechanisms to degrade damaged organelles. Selective mitochondrial degradation by autophagy (hereafter termed mitophagy) ensures mitochondrial quality control and recycling, but must be balanced with organelle's *de novo* synthesis (Twig & Shirihai, 2011). Having been put under the spotlight,

mitophagy has been extensively studied, but its complex dynamics remain to be fully understood. Trying to make some sense of the numerous findings on a wide range of cell and animal models, Lemasters (2014) proposed that the mechanism has several and distinct variants: type 1 mitophagy – phosphatidylinositol-3-kinase (PI3K)--dependent and occurs during nutrient deprivation; type 2 mitophagy – stimulated by mitochondrial damage, counting with autophagic light chain 3 (LC3)-containing vesicles; and type 3 mitophagy – formation of mitochondria-derived vesicles containing oxidized mitochondrial proteins that travel into multivesicular bodies (Lemasters, 2014).

Type 2 mitophagy selectively targets depolarized damaged mitochondria, generated *via* fission events (Buhlman *et al*, 2014; Gomes & Scorrano, 2013; Palikaras & Tavernarakis, 2012; Twig & Shirihai, 2011). Phosphatase and tensin homolog (PTEN)-induced putative kinase 1 (PINK1)/Parkin-dependent mitophagy pathway is the most well characterized type 2 mitophagy pathway, although PINK1/Parkin-independent mitophagy can also occur (Strappazzon *et al*, 2015; Allen *et al*, 2013). PINK1 is a serine/threonine kinase that localizes in the cytosol and, due to its N-terminus, it is also imported through translocase of the outer membrane 40 (TOM40) into IMM where it is degraded by mitochondrial proteases, namely the presenilin-associated rhomboid-like protease (PARL) (cleaves in the transmembrane domain) and mitochondrial processing peptidase (MPP) (cleaves in the N-terminus and mitochondrial targeting sequence) (Okatsu *et al*, 2015; Greene *et al*, 2012; Deas *et al*, 2011a). PINK1 is needed to suppress fusion and autophagy. This kinase appears to sense damage in the mitochondria that results from lesions to mtDNA, oxidative stress and others (Matsuda *et al*, 2013; Gautier *et al*, 2008). When in the presence of damaged mitochondria with loss of $\Delta\psi_m$, PINK1 is stabilized in the OMM, where it induces Parkin translocation to mitochondria and causes phosphorylation of both Parkin and ubiquitin, at serine 65 (S65) (Kazlauskaite *et al*, 2015; Caulfield *et al*, 2014; Narendra *et al*, 2010; Matsuda *et al*, 2010). Parkin on the other hand is a E3 ubiquitin ligase, that ligates ubiquitin chains on OMM proteins, that are recognized by autophagy receptors such as p62 (Narendra *et al*, 2008).

Mitophagy impairment has been associated with several neurodegenerative disorders, including Alzheimer's disease and Parkinson's disease, where mutations in

the multiple genes involved were connected to familial form (Deas *et al*, 2011b; Moreira *et al*, 2007). Meanwhile, a lot was left unsaid in HD and only recently started to change. Although not directly associated with mitophagy, the work by Wong and Holzbaur elegantly proposed that HTT, along with huntingtin-associated protein 1 (HAP1), controlled autophagosome dynamics through regulation of dynein and kinesin, promoting their transport. When considering the expanded polyQ version of HTT, axonal transport of autophagosomes was found impaired. It ultimately ended in inefficient degradation of internalized mitochondria probably due to inhibition of autophagosome/lysosome fusion (Wong & Holzbaur, 2014). Furthermore, wild-type HTT was recently proposed to function in selective autophagy, not just regarding mitochondria, aiding autophagic adaptor p62 to associate with LC3 (present in the autophagosome membrane) and lysine 63 (K63)--linked ubiquitinated substrates (Rui *et al*, 2015).

Using immortalized striatal cells derived from *Hdh*Q111 knock-in mice, it was recently assigned a neuroprotective effect in HD through mitophagy following PINK1 overexpression (Khalil *et al*, 2015). On that same note, Mochly-Rosen group cleverly assayed mitophagy in the same HD cell model and in R6/2 mice. Knowing that in HD, glyceraldehyde-3-phosphate dehydrogenase (GAPDH) is found inactive and associated with damaged mitochondria in a selective way, they used the inactive form to assess mitophagic flux. In the presence of mHTT, GAPDH association with mitochondria became impaired with increased cell death. Interestingly, this effect was counteracted by GAPDH overexpression (Hwang *et al*, 2015). As such, improving mitophagy in HD could prove a successful therapeutic option.

1.3. LYSINE DEACETYLASES AND THEIR ROLE IN NEURODEGENERATION

Lysine (Lys, K) acetylation is a reversible post-translational modification known to target a broad number of proteins in order to manage diverse cellular processes from nutrient adaptation to metabolite homeostasis. It is rapidly reversible, being regulated by lysine acetyltransferases (KATs) and lysine deacetylases (KDACs)

(Karabulut & Frishman, 2015). It has recently emerged as possible therapeutics due to its association with several disorders, from cancer to neurodegenerative diseases (Lu *et al*, 2015b; Xu *et al*, 2014; Yuan *et al*, 2013).

1.3.1. Lysine deacetylases: what are they?

KDACs are present in all organisms, from yeast to mammals. They are mostly known as epigenetic modulators of gene expression by removing acetyl groups from Lys residues found in the N-terminal tails of nucleosomal histone proteins. In this way, chromatin compaction is favored followed by decreased levels of gene transcription. They can be divided in two major families: those with a bound Zn^{2+} ion (histone deacetylases, HDACs) and those dependent on NAD^{+} cofactor (sirtuins, SIRTs). Complementary, when regarding their structural homology, KDACs can also be divided into classes I-IV (see **Table 1.**) (Van Dyke, 2014).

Table 1 | KDACs classification and subcellular localization.
(Adapted from Van Dyke M.W., 2014)

CLASS	KDAC	SUBCELLULAR LOCALIZATION
I	HDAC1	Nucleus
	HDAC2	Nucleus
	HDAC3	Nucleus>cytoplasm
	HDAC8	Nucleus>cytoplasm
II	HDAC4	Nucleus/cytoplasm
	HDAC5	Nucleus/cytoplasm
	HDAC7	Nucleus/cytoplasm
	HDAC9	Nucleus/cytoplasm
	HDAC10	Cytoplasm>Nucleus
	HDAC6	Cytoplasm>Nucleus
III	SIRT1	Nucleus/cytoplasm
	SIRT2	Cytoplasm
	SIRT3	Mitochondria
	SIRT4	Mitochondria
	SIRT5	Mitochondria
	SIRT6	Nucleus
	SIRT7	Nucleolar
IV	HDAC11	Cytoplasm/Nucleus

HDACS are known to function in transcriptional repression through deacetylation of acetyl-L-lysine side chains in histone proteins, although non-histone targets have also been reported (Lombardi *et al*, 2011). Class I KDACs are predominantly nuclear and are ubiquitous, except for HDAC8 that is confined to smooth muscle. Meanwhile, class II KDACs show tissue specificity, being expressed mostly in the brain, heart and muscle. HDAC4, 5 and 7 translocate between nucleus and cytoplasm depending on a phosphorylation stimuli (whilst for HDAC9 this is only true for its splice variant) as HDAC6 and 10 are mostly cytosolic. HDAC11, the only member of class IV, it is largely found in the nucleus, being involved in regulation of immune tolerance (Guedes-Dias & Oliveira, 2013).

HDAC1 can deacetylate all four core histones (H2A, H2B, H3 and H4) but with varying efficiency. HDAC8 was reported to preferentially deacetylate histone H3 and H4, while HDAC11 might deacetylate H3 specifically at K9 and K14. Further studies are still required though to fully comprehend HDACs histone substrate specificity (Seto & Yoshida, 2014). Considering non-histone targets, HDAC8 interacts with α--actin, increasing contractile action (Waltregny, 2005) and HDAC6 is involved in cell motility, cell adhesion and even activation of protein kinases by deacetylation of targets such as α-tubulin and Hsp90, but also participates in clearance of misfolded proteins (Liu *et al*, 2012).

For SIRTs, the case becomes less ambiguous. SIRTs, homologous of yeast silent information regulator 2 (Sir2) that was proven to extend replicative lifespan, are NAD^+-dependent KDACs, resulting in the generation of nicotinamide and –O-acetyl--ADP ribose after substrate deacetylation (Haigis & Guarente, 2006; Tanner *et al*, 2000). Mammals have 7 Sir2 homologs with a highly conserved NAD^+--dependent SIRT core domain, whilst being functionally nonredunctant. They are found in different subcellular locations – SIRT1, 6 and 7 are located mainly in the nucleus, SIRT3, 4 and 5 are mitochondrial and SIRT2 is cytoplasmic –, each containg signal sequences that explain their intracellular localization (Haigis & Sinclair, 2010; Michan & Sinclair, 2007).

SIRT1 and SIRT2 have been reported to deacetylate histones. This may seem contradictory in terms of SIRT2, being mainly cytosolic, but it was observed to localize to chromatin during cell cycle. SIRT2, in the same manner of HDAC6, can deacetylate α-tubulin. SIRT6 has a very low deacetylase activity but has a key role in telomere maintenance and DNA repair, whilst SIRT7 histone deacetylation is involved in cellular transformation in tumorigenesis (Seto & Yoshida, 2014). SIRT1 was found to regulate its own expression, and may also regulate SIRT3 expression, indirectly through regulation of PGC-1α (Bell & Guarente, 2011).

Among the large number of proteins that are known to be acetylated, a high percentage of them are of mitochondrial nature (Kim *et al*, 2006). Although the source for protein acetylation in mitochondria remains relatively unknown, SIRT3 acquired a prominent role in deacetylation of mitochondrial proteins in comparison to SIRT4 and SIRT5 that only show a weak deacetylase activity (Lombard *et al*, 2007).

Mitochondrial SIRTs have not been studied as extensively as SIRT1, but there is a growing interest in them and it has been suggested that they may regulate energy production, signaling and apoptosis (Verdin *et al*, 2010).

Deacetylation of manganese superoxide dismutase (SOD2) on K68 by SIRT3 leads to its activation, generating an antioxidant response and as such, conferring to SIRT3 an antioxidant function (Lu *et al*, 2015a; He *et al*, 2012). Besides this, SIRT3 also facilitates OXPHOS by activating complexes I and II (Finley *et al*, 2011). While SIRT5 and SIRT4 show weak deacetylase activity, demalonylase/desuccinylase and lipoamidase activities have been attributed, respectively (Mathias *et al*, 2014; Guedes-Dias & Oliveira, 2013).

As the most striking characteristic, calorie restriction was shown to correlate with extension of life span through the action of SIRTs. There is an up-regulation of oxidative metabolism, concomitant with a lowering of glycolysis (Qiu *et al*, 2010). This then leads to an increase in the available NAD^+ levels as well as the levels of SIRT1 and SIRT3 (Guarente, 2011). Deacetylation of target proteins by SIRTs can lead to the control of metabolism and to a response against oxidative stress (Guarente, 2011; Rodgers *et al*, 2005). Deacetylation of components of the DNA repair machinery has also been implicated in stress responses. For instance, p53 is a target of SIRT1, keeping the balance between repair and apoptosis (Finkel *et al*, 2009; Haigis & Guarente, 2006).

During nutrient stress there is a shift in metabolism by action of SIRT3, promoting catabolism of acetate and fatty acids via deacetylation of several enzymes, for which, glutamate dehydrogenase (GDH) is one example (Hirschey *et al*, 2010). It has also been suggested that by moving away from the normal carbohydrate metabolism, there might be a decrease in ROS production, decreasing in this way oxidative stress and ameliorating aging (Guarente, 2008). In accordance to its importance, $SIRT3^{-/-}$ mouse embryonic fibroblasts show abnormal mitochondrial morphology, with increases in ROS levels and genomic instability (Kim *et al*, 2010a).

1.3.2. Role of KDACs in Huntington's disease

Epigenetic dysregulation can underline cognition disorders, and thus epigenetics may play an important role in learning and memory processing. As such, epigenetic modulation through KDACs modulation seems promising as a therapy in neurodegeneration (Coppedè, 2014; Jakovcevski & Akbarian, 2012).

Morever, evidence indicates hypoacetylation of H3 at K9 and K14 in HD transgenic mice with a polyQ expansion of 82 glutamines and R6/2 mice (Valor & Guiretti, 2014; McFarland *et al*, 2012). Oal administration of a HDAC inhibitor in R6/2 mice after onset of motor symptoms reduced the marked H3 hypoacetylation, resulting in correction of mRNA expression levels. Additionally, treated mice displayed improved motor performance and body weight (Thomas *et al*, 2008). Further studies showed additional beneficial effects connected to modulation of the ubiquitin-proteasomal and autophagy (Jia *et al*, 2012a). Such effect was later associated by the same group to HDAC1 and HDAC3 preferential inhibition and confirmed on additional HD animal models (Jia *et al*, 2015, 2012b). However, knockdown of HDAC3 in R6/2 mice did not generate physiological or behavior changes with no additional transcriptional effects. As such, the beneficial effects derived from the HDAC1 and HDAC3 inhibitor may not be due to HDAC3 itself (Moumné *et al*, 2012).

Unselective HDAC inhibitors (trichostatin A, TSA and sodium butyrate, SB) improved Ca^{2+} handling after an excitotoxic-like stimuli in primary striatal neuron cultures from YAC128 mice and immortalized HD striatal cells derived from knock-in *Hdh*Q111 mice (Oliveira *et al*, 2006). Additionally, TSA was seen to increase α-tubulin acetylation in HD cell models, further resulting in enhanced vesicle transport and BDNF release (Dompierre *et al*, 2007). Although this effect was justified as HDAC6--derived, its genetic knock-out in R6/2 mice also cause α-tubulin deacetylation, while it did not in increased BDNF transport, or additional changes on behavior or physiology assessments (Bobrowska *et al*, 2011).

mHTT was described to interact with HDAC4. Interestingly, when HDAC4 knockdown was achieved in R6/2 and *Hdh*Q150 mice, mHTT aggregation was delayed in cytoplasm, with no changes occurring in the nucleus. Meanwhile, reduced

HDAC4 levels led to restoration of membrane electrophysiological properties of MSN and corticostriatal synaptic transmission (Mielcarek *et al*, 2013).

When it comes to SIRTs modulation in HD, the data becomes more puzzling. Overall, SIRTs pharmacological inhibition using nicotinamide (NAM) in B6.HDR6/1 transgenic mice (that display human *HTT* exon 1 with 1 kB of the endogenous promoter) resulted in increased expression of BDNF and PGC-1α, with additional beneficial motor effects (Hathorn *et al*, 2011). Meanwhile, beneficial effects were also reported after SIRTs activation. Using *Caenorhabditis elegans* as an early phase HD model with 128Q, Parker and colleagues correlated increased Sir2 levels with neuronal rescue and reduced axonal aggregation. The authors went further, and tested SIRTs activator resveratrol on ST*Hdh*$^{Q111/Q111}$ cells, achieving decreased cell death (Parker *et al*, 2005). The use of resveratrol was also seen to improve gene expression of genes involved in OXPHOS and mitochondrial biogenesis, the latter through an increase in PGC-1α activity subsequent of decreased acetylation, thus promoting overall mitochondrial function (Lagouge *et al*, 2006).

Resveratrol effects have been associated with SIRT1 activation, although it lacks complete specificity. A large focus has been made in regards to the possible neuroprotection derived from increased SIRT1 activation (Naia & Rego, 2015). Overexpression of SIRT1 in cortical neurons overexpressing 120Q HTT prevented mitochondrial loss, although the effect was achieved after co-transfection with PGC--1α/β (Wareski *et al*, 2009). Furthermore, it appeared to cause autophagy activation in SH-SY5Y cells transfected with HTT exon 1 with 97Q, resulting in reduced polyQ aggregation (Shin *et al*, 2013). The observed neuroprotection was proposed to occur at the transcriptional level, namely through the activation of transcriptional factor forkhead box O3A (FOXO3a) and CREB-regulated transcription coactivator 1 (TORC1), and subsequent modulation of CREB activity (Jiang *et al*, 2011; Jeong *et al*, 2011).

Meanwhile, inhibition of SIRT2 was reported as a possible neuroprotective strategy for HD. Inhibition of SIRT2 in HD *Drosophila melanogaster*, *C. elegans* and R6/2 mice increased neuronal viability, which was accounted for by alterations in sterol biosynthesis pathway (Luthi-Carter *et al*, 2010). This was quickly challenged by Cattaneo's group as the previous authors did not show data regarding sterol biosynthesis in all models and in equivalent conditions, with their hypothesis being

contradictory to the decreased levels of sterol and cholesterol shown already in several HD models (Valenza & Cattaneo, 2010). With the additional report by Bobrowska and colleagues showing no visible effects on tubulin acetylation or even in sterol biosynthesis after SIRT2 inhibition in R6/2 mice, modulation of SIRT2 in HD should be further investigated (Bobrowska *et al*, 2012).

So far, the role of SIRT3 in HD has only been assessed in one study. Fu and colleagues showed decreased levels and activity of SIRT3 in ST*Hdh*$^{Q111/Q111}$ cells. They went further and showed that the use of a resveratrol dimer could attenuate the effects caused by mHTT on SIRT3 levels and activity, by activating of AMP-activated kinase (AMPK) and by replenishing NAD^+ levels (Fu *et al*, 2012). Recent evidence indicates that, along with the already recognized role for SIRT3 in the regulation of metabolic enzymes, this class III KDAC can also be involved in regulating mitochondrial dynamics and thus promote mitochondrial function (Tseng *et al*, 2013). On this perspective, it was found that OPA1 activity can be regulated through (de)acetylation during stress responses and that SIRT3 is capable of deacetylating and increasing its activity, preserving mitochondrial network (Samant *et al*, 2014). In this way, modulating SIRT3 levels in HD models may ameliorate toxic effects generated from the presence of mHtt. If this is proved correctly, then SIRT3 can be thought as a new possible target for the treatment of HD.

1.4. MAIN GOALS

Mitochondrial dysfunction has long been implicated in HD pathogenesis and constitutes a large focus of research, namely in HD therapeutic pursuit. Considering that abnormalities in mitochondrial dynamics have been reported in HD, attempting to restore it could prove a successful strategy to improve mitochondrial function and capacity to respond to stress. Although affected mitochondrial dynamics have been characterized in several HD models (biogenesis, fission/fusion balance, trafficking), one important process in the life cycle of mitochondria remained forgotten – mitophagy. In the present study we aimed to assure the relevance of altered mitochondrial dynamics in HD using immortalized striatal cells derived from HD knock-in mice expressing full-length mutant Htt with 111 glutamines (ST*Hdh*$^{Q111/Q111}$ or mutant cells) under endogenous regulation *versus* wild-type striatal cells (ST*Hdh*$^{Q7/Q7}$). Because intracellular accumulation of damaged mitochondria has been suggested to evoke changes in biogenesis of mitochondrial components, morphology or motility, therapeutical strategies based on degradation of damaged organelles may be more effective. In this study we also intended to shed some light on mitophagy, by studying the better understood PINK1 and Parkin dependent pathway.

KDACs modulation has been largely used in neurodegenerative diseases as possible therapeutics. SIRT3 in particular, due to its unique localization in mitochondria poses as an intriguing target for rescuing mitochondrial dysfunction. Meanwhile, its effects on HD remain largely unexplored. Therefore, herein we also explored the hypothesis of a possible neuroprotective effect of SIRT3 in HD cells, focusing on the processes of fission/fusion and mitophagy after SIRT3 overexpression in both HD and wild-type mouse striatal cells.

CHAPTER II – MATERIAL & METHODS

2.1. MATERIALS

OPTIMEM (GIBCO 22600), fetal bovine serum (FBS) and antibiotics were purchased from GIBCO (Paisley, UK). Hoechst 33342 nucleic acid stain and Lipofectamine® 3000 were purchased from Invitrogen/Molecular Probes (Life Technologies Corporation, Carlsbad, CA, USA). Dulbecco's Modified Eagle's Medium (DMEM) culture medium (SIGMA D5648), trypsin, protease cocktail inhibitors and other analytical grade reagents were purchased from Sigma Chemical and Co. (St.Louis, MO, USA). Western Blot PVDF membrane and BioRad Protein Assay were purchased from BioRad Laboratories, Inc. (Munich, Germany). Bovine serum albumin (BSA) was purchased from Santa Cruz Biotechnology (Santa Cruz Biotechnology, Inc., TX, USA). ECF substrate was purchased from GE Healthcare (GE Healthcare Bio-Sciences, PA, USA). The antibodies used for Western Blotting and immunocytochemistry are listed in **Table 2.**

Table 2 | Antibody information used in this study.

	Host	Dilution	Reference/Supplier
Primary antibodies			
β actin	Mouse	1:5 000 (WB)	Sigma A5316 (Sigma (St. Louis, MO, USA)
Complex II (70 kDa subunit)	Mouse	1:1 000 (WB)	Molecular Probes A11142 (Molecular Probes—Invitrogen (Eugene, OR, USA)
Drp1	Mouse	1:500 (WB) / 1:300 (ICC)	BD biosciences 611112 (BD Biosciences, Franklin Lakes, NJ, USA)
Phospho-Drp1 (S616)	Rabbit	1:500 (WB)	Cell signalling #3455S (Cell Signalling, Danvers, MA, USA)
FIS1 (TTC11)	Rabbit	1:1 000 (WB)	Novus NB100-56646 (Novus Biologicals, LLC, CO, USA)
LC3 A/B	Rabbit	1:1 000 (WB) / 1:300 (ICC)	Cell Signaling #12741 (Cell Signalling, Danvers, MA, USA)
Mfn2	Rabbit	1:1 000 (WB) / 1:450 (ICC)	Sigma M6319 (Sigma (St. Louis, MO, USA)
OPA1	Mouse	1:500 (WB)	BD Biosciences 612606 (BD Biosciences, Franklin Lakes, NJ, USA)
Parkin	Rabbit	1:1 000 (WB) / 1:300 (ICC)	Abcam ab15954 (Abcam, Cambridge, UK)
Phospho-Parkin (S65)	Rabbit	1:500 (WB)	Abcam ab154995 (Abcam, Cambridge, UK)
PINK1	Rabbit	1:500 (WB)	Abcam ab23707 (Abcam, Cambridge, UK)
p62	Rabbit	1:500 (WB)	#AP2183B (Biomol GmbH, Hamburg)

Secondary antibodies			
Alexa Fluor-647 donkey anti-mouse	Donkey	1:300	#A31571 (Molecular Probes—Invitrogen, Eugene, OR, USA)
Alexa Fluor-647 donkey anti-rabbit	Donkey	1:300	#A31573 (Molecular Probes—Invitrogen, Eugene, OR, USA)
Anti-mouse (H+L), Alkaline Phosphatase Conjugated	Goat	1:20 000	Thermo Scientific Pierce #31320 (Pierce Thermo Fisher Scientific, Rockford, IL, USA)
Anti-rabbit (H+L), Alkaline Phosphatase Conjugated	Goat	1:20 000	Thermo Scientific Pierce #31340 (Pierce Thermo Fisher Scientific, Rockford, IL, USA)

2.2. CELL CULTURE

Striatal cells derived from knock-in mice expressing full-length humanized HTT with 7 glutamines (ST*Hdh*$^{Q7/Q7}$ or wild-type cells; ref: CHDI-9000073) or homozygous mutant cells derived from knock-in mice, expressing full-lengt mHTT with 111 glutamines (ST*Hdh*$^{Q111/Q111}$ or mutant cells; ref: CHDI-9000071) were obtained from Coriell Institute for Medical Research (New Jersey, USA). Cells were cultured in DMEM culture medium supplemented with 10% inactivated FBS, 1% penicillin/streptomycin, 400 µg/mL geneticin (G418; #11811-031, GIBCO), and maintained in a humidified atmosphere at 5% CO_2, 33^{o}C, as described previously (Trettel *et al*, 2000). Striatal cells were plated on 16-mm-diameter uncoated glass coverslips, multiple well chambers, 100-mm petri dishes or flasks until the desired confluence was achieved. ST*Hdh*$^{Q7/Q7}$ cells were plated at a density between 6-25×10^4 cells/mL and ST*Hdh*$^{Q111/Q111}$ cells between 8-30×10^4 cells/mL.

2.3. CONSTRUCTS, TRANSFECTION AND INCUBATIONS

2.3.1. Constructs

Plasmids used for transfection were: GFP-tagged human SIRT3 (SIRT3-GFP; ref: RG217770) and pCMV-AC-GFP (GFP; ref: PS100010) obtained from Origene (MD, USA), and pDsRed2-Mito (MitoDsRed; ref: 632421) from Clontech (CA, USA).

2.3.2. Bacteria transformation

The whole procedure was done in sterile conditions. 1 µg of plasmid DNA was added to competent DH5α *Escherichia coli* cells and mixed by tapping. The cells were incubated 25 minutes on ice, followed by a heat shock of 30 seconds at 42°C and returned to ice for 3 more minutes. Pre-warmed Lennox L Broth (LB) (Invitrogen, Eugene, OR, USA) was added to the transformed *E. coli* cells and incubated at 37°C for 5 hours under 220 rpm. The cells were centrifuged at 6 000×*g* for 10 minutes and plated onto LB-Agar plates, prepared with the respective antibiotic (100 µg/mL carbenicillin for SIRT3-GFP and GFP, 30 µg/mL kanamycin for MitoDsRed), and left overnight at 37°C.

2.3.3. Plasmid DNA extraction

An isolated colony was picked from the LB-Agar plates and was grown overnight, at 37°C, under 220 rpm, in LB with the respective antibiotic. Cells were centrifuged at 4000×*g* for 10 minutes and the medium was discarded. PureLink® HiPure Plasmid Filter DNA Purification kit (Invitrogen, Eugene, OR, USA) was used for plasmid DNA extraction. Plasmid DNA quantification was done using NanoDrop® 2000 (Pierce Thermo Fisher Scientific, Rockford, IL, USA).

*2.3.4. Transfection of ST*Hdh$^{(Q111/Q111)}$ *and ST*Hdh$^{(Q7/Q7)}$ *striatal cells*

Striatal cells were transiently transfected with SIRT3-GFP, GFP and MitoDsRed plasmid DNA using Lipofectamine®3000 (Invitrogen), 48 hours before experiments, according to the manufacturer's protocol. OPTIMEN media (with 28.5 mM $NaHCO_3$) was replaced with fresh DMEM culture media 4 hours after transfection.

*2.3.5. Analysis of Autophagy flux in untransfected ST*Hdh$^{(Q111/Q111)}$ *and ST*Hdh$^{(Q7/Q7)}$ *striatal cells*

Cell culture medium was replaced with fresh one 24h before collecting the samples, in order to avoid autophagy-like responses derived from energy deprivation (Zhu *et al*, 2014). Cells were then treated with 50 nM bafilomycin A1 (Ref: B1793, Sigma, St. Louis, MO, USA) for 8h prior to sample collection for Western Blotting. Additionally, cells were incubated with viral particles containing a RFP-GFP-LC3B construct (Ref: P36239, Molecular Probes—Invitrogen, Eugene, OR, USA) according to the manufacturer's protocol, and treated with 80 µM chloroquine diphosphate (Chloroquine; Ref: P36239, Molecular Probes—Invitrogen, Eugene, OR, USA) for 4h prior to immunocytochemistry.

2.4. SAMPLE PREPARATION AND WESTERN BLOTTING

2.5.1. *Subcellular fractionation*

Cells were washed twice with ice-cold phosphate-buffered saline (PBS) 1x. Cells were scratched in ice-cold sucrose buffer (250 mM sucrose, 20 mM HEPES, 10 mM KCl, 1.5 mM $MgCl_2$, 1 mM EDTA, 1 mM EGTA – pH 7.4), supplemented with 1 mM dithiothreitol (DTT), 1 µM TSA, 1 µg/mL protease inhibitor cocktail (chymostation, pepstatin A, leupeptin and atipain), 1 mM phenylmethylsulfonyl fluoride (PMSF), 1 mM sodium ortovanadate, 10 mM nicotinamide, 180 nM okadaic acid. Lysates were homogenized using a potter with 40 strokes, at 280 rpm, and later centrifuged at 1300×*g* for 12 minutes (4^{o}C). The nuclear/cell debris pellet was discarded, and the supernatant was centrifuged again at 11 900×*g* for 20 minutes (4^{o}C). The mitochondrial pellet was resuspended in ice-cold supplemented sucrose buffer. Trichloroacetic acid (TCA) at 15% was used to precipitate cytosolic proteins from the cytosolic supernatant and centrifuged at 16 300×*g* for 10 minutes (4^{o}C). Cytosolic pellet was resuspended in ice-cold supplemented sucrose buffer, and brought to pH 7 with 10 M KOH.

2.5.2. *Total protein extracts*

Cells were washed twice with ice-cold PBS 1x. Cells were scratched in ice-cold lysis buffer (20 mM Tris, 2mM EDTA, 2 mM EGTA, 100 mM NaCl, 0.1% Triton X-100), supplemented in the same manner as the sucrose buffer described in the previous section. The homogenates were then frozen/thawed three times in liquid nitrogen and centrifuged for 10 minutes at 20 800×*g* (4^{o}C), to remove cell debris, where the supernatant was collected.

2.5.3. *Western Blotting*

Protein content from each sample was determined by the BioRad protein assay reagent, using the Bradford assay procedure. Equivalent amounts of protein were then subjected to denaturation in 50 mM Tris-HCL pH 6.8, 2% SDS, 5% glycerol, 100 mM DTT and 0.01% bromophenol blue, at 95^{o}C, for 5 minutes. Protein separation was achieved by electrophoresis on 7.5-15% SDS-PAGE gels, transferred onto PVDF membranes. Membranes were then blocked with 5% (w/v) BSA in Tris Buffered Saline with 0.1% Tween-20 (TBS-T), for 1h at room temperature and later incubated with primary antibodies (see **Table 2.**), overnight at 4^{o}C. TBS-T was used as a membrane washing solution, and incubation with secondary antibodies was done, for 1h at room temperature. All antibodies were prepared in 5% (w/v) BSA in TBS-T. Immunoreactive bands were visualized using VersaDoc Imaging System (BioRad, Hercules, USA) and quantification was done using QuantityOne software.

2.5. IMMUNOCYTOCHEMISTRY

Cells were washed twice with warm PBS 1x, fixed with 4% paraformaldehyde (pre-warmed at 37^{o}C) for 20 minutes, permeabilized in 0.1% Triton X-100 in PBS 1x for 2 minutes and blocked for 1 hour, at room temperature in 3% (w/v) BSA in PBS 1x. In particular, for LC3 A/B labeling, permeabilization was replaced with subsequent ice-cold methanol fixation, for 20 minutes, at -20^{o}C. Incubation with primary antibodies occurred overnight, at 4^{o}C. Then, cells were incubated for 1 hour,

at room temperature, with secondary antibodies. All antibodies were prepared in 3% (w/v) BSA in PBS 1x. Finally, cells were incubated with Hoechst 33342 (4 µg/mL) for 20 minutes and mounted using Mowiol 40-88 (Sigma Chemical and Co., St.Louis, MO, USA). Confocal images were obtained using a Plan-Apochromat/1.4NA 63x lens on an Axio Observer.Z1 confocal microscope (Zeiss Microscopy, Germany) with Zeiss LSM 710 software.

2.6. IMAGE ANALYSIS

Mitochondrial morphology and protein co-localization analysis was achieved using Macros designed by Doctor Jorge Valero (Center for Neuroscience and Cell Biology – University of Coimbra, presently at Achucarro – Basque Center for Neuroscience, Spain) in Fiji (ImageJ, National Institute of Health, USA) (see **Attachment 1.2.**). Firstly, each cell to be considered in the analysis was delineated as a Region of Interest (ROI) (see **Attachment 1.1.**). Image background was normalized using the function *Subtract Background*, included in Fiji (rolling ball radius: 10 µm for mitochondria and proteins involved in mitochondrial dynamics; 30 µm for SIRT3-GFP/GFP, for 8 bit images). For mitochondrial morphology analysis, the cells were transfected with mitochondria-targeting MitoDsRed. Images were extracted to grayscale. *FindFoci* function was then used to allow the identification of peak intensity regions (Herbert *et al*, 2014) in order to show mitochondria-specific fluorescence. A threshold was applied to optimally resolve individual mitochondria. Mitochondrial outlines were traced through *Analyze Particles* function (see **Fig. 2**). Aspect ratio (the ratio between the major and minor axis of mitochondria) was used as an index of mitochondrial length alongside Roundness (a relation between the area of mitochondria and its major axis) (see **Table 3**). For proteins involved in mitochondrial dynamics a threshold was set similarly to the one described above and *Set Measurements* function was employed to obtain Integrated Density (product of Area and Mean Gray Value) (see **Table 3**) and later normalized to cellular area using the designed ROI area as an approximation. To obtain information about protein co--localization in mitochondria, selection of mitochondrial ROIs was done, and the

respective Integrated Density inside the ROIs was considered. SIRT3-GFP and GFP were analyzed in the same way, considering also the value of Integrated Density inside the nuclei. Each value derived represents a single cell.

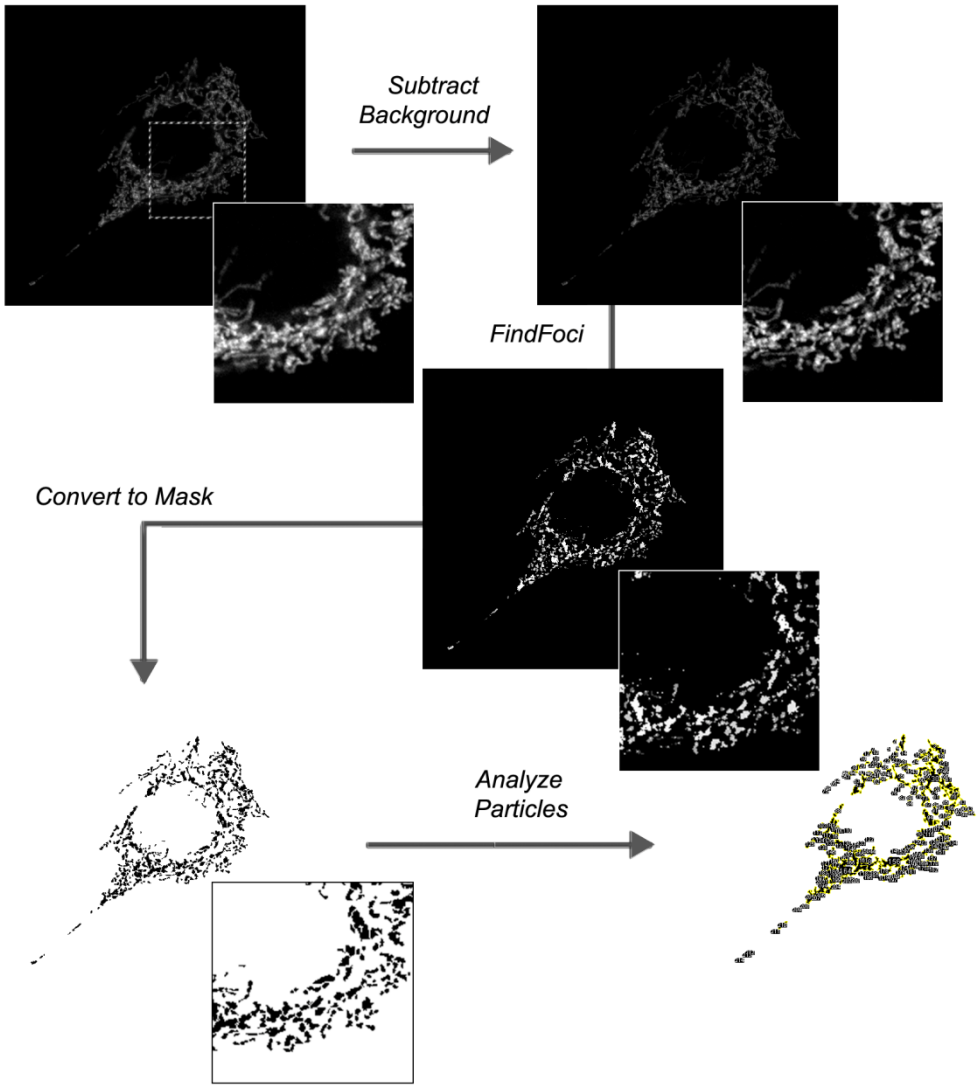

Fig. 2 | Visual representation of mitochondrial morphology analysis done in Image J.

Table 3 | Variables used in the study of mitochondrial morphology and protein quantification by immunocytochemistry.

Variable	Equation
Aspect Ratio (AR)	$\frac{\textbf{Major Axis}}{\textbf{Minor Axis}}$ **(length)**
Roundness (Round)	$\mathbf{4} \times \frac{\textbf{Area}}{\boldsymbol{\pi} \times \textbf{(Major Axis)}^{\mathbf{2}}}$
Integrated Density (Int. Den.)	**Area × Mean Grey Value**

2.7. STATISTICAL ANALYSIS

Statistical analyses were performed using GraphPad Prism 5 (GraphPad Software, Sand Diego, CA, USA). Data is presented as the mean ± SEM of the number of experiments indicated and analyzed using two-way ANOVA followed by Bonferroni *post hoc* test for multiple groups or by Student's *t* test for comparison between two Gaussian populations, as described in the figure legends. Significance was accepted at $P<0.05$.

CHAPTER III – RESULTS

3.1. HD STRIATAL CELLS SHOW INCREASED SIRT3-GFP ACCUMULATION IN MITOCHONDRIA

In the present study we were interested in exploring the effect of SIRT3 on mitochondrial dynamics, overexpression of human SIRT3 was performed using a plasmid with a GFP tag to its C-terminus. In this regard, it has been reported that SIRT3 overexpression (SIRT3OE) results not only in deacetylation of mitochondrial targets, but also of cytosolic and nuclear proteins (Webster *et al*, 2013). SIRT3-GFP cellular distribution was thus evaluated through immunocytochemistry in both ST*Hdh*$^{Q7/Q7}$ and ST*Hdh*$^{Q111/Q111}$ cells taking into account the Integrated Density present in the area occupied by the mitochondrial network (transfection with cytochrome *c* oxidase subunit VIII-targeted DsRed or MitoDsRed) and nuclei (stained with nucleic acid dye Hoechst 33342). Values for the cytoplasmic fraction were considered as the remainder of percentage between the mitochondrial and nuclear fraction.

No differences were found considering the cell's genotype in the control condition using the same expression vector without the SIRT3 sequence (GFP). Curiously, HD striatal cells showed an increased accumulation of SIRT3-GFP in the mitochondria, with a decrease in the nuclear fraction, in comparison to wild-type cells (**Fig. 3**).

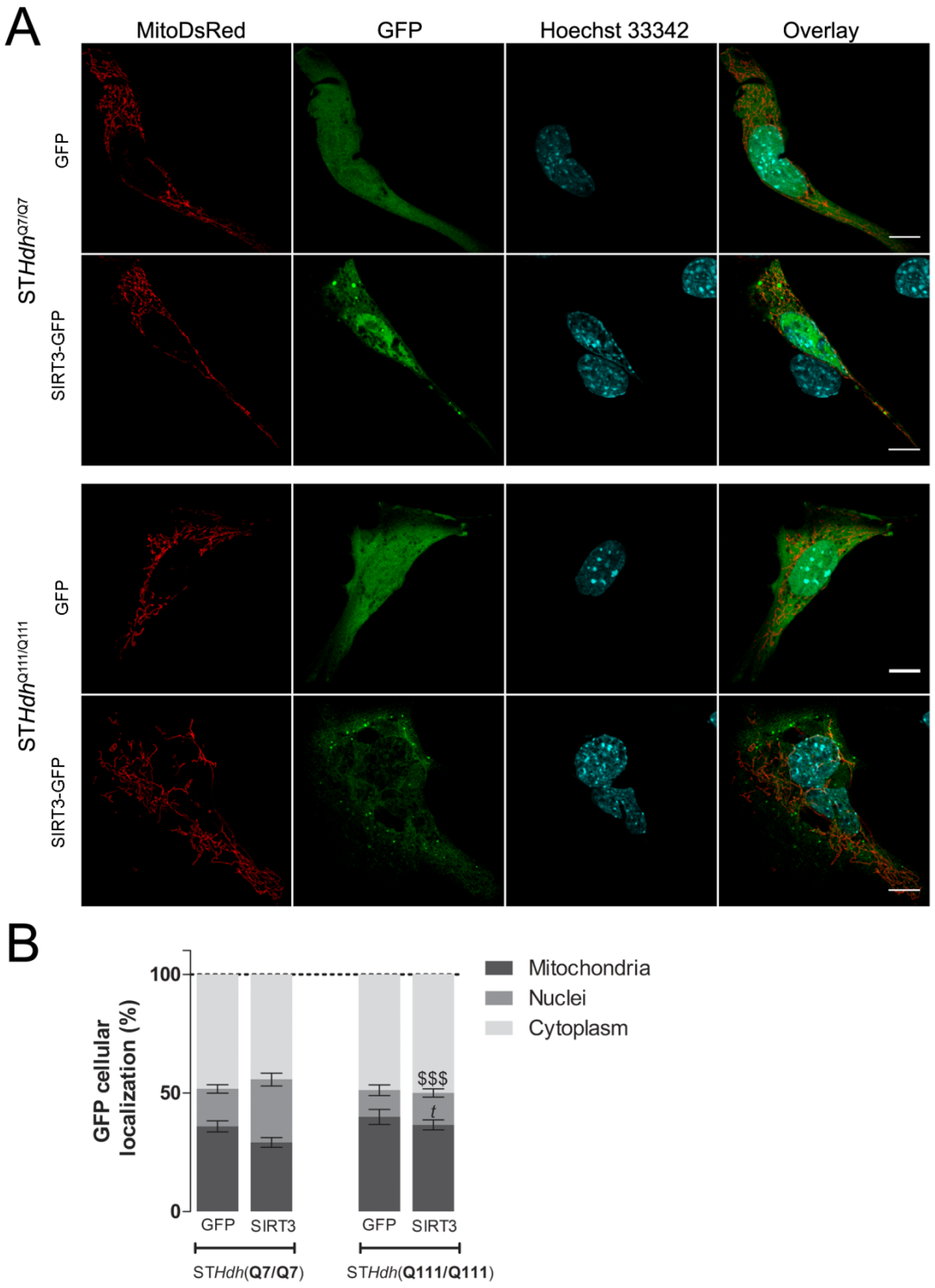

Fig. 3 | Overexpressed SIRT3-GFP accumulates more in the mitochondria of ST*Hdh*$^{Q111/Q111}$ cells.
A) Confocal images obtained with a 63x objective, NA=1.4 on a Zeiss LSM 710 inverted microscope. Striatal cells were transfected with either GFP/SIRT3-GFP. Mitochondria were labeled using targeted DsRed and nuclei were visualized by Hoechst stain. Scale bar: 10 µm. **B)** SIRT3-GFP and GFP cellular localization were quantified in Image J. Data is presented as the mean ± SEM of 4 independent experiments considering ~20 cells/condition. Statistical significance: ^{t}P<0.05 versus ST*Hdh*$^{Q7/Q7}$ mitochondria (%) (two-tailed Student's *t*-test), $^{\$\$\$}P$<0.001 *versus* ST*Hdh*$^{Q7/Q7}$ nuclei (%) (two-way ANOVA, followed by Bonferroni *post-hoc* test).

3.2. FISSION IS REDUCED UPON SIRT3 OVEREXPRESSION IN HD STRATAL CELLS THROUGH DECREASED DRP1 ACCUMULATION IN MITOCHONDRIA AND FIS1 TOTAL PROTEIN LEVELS

To initiate the study of mitochondrial dynamics, we examined the levels of proteins involved in maintaining mitochondrial morphology, namely those involved in the fission/fusion balance.

Significantly lower Drp1 levels were seen by Western Blot in mutant cells (**Fig. 4 *F, G.***). In addition, while in wild-type cells Drp1 was shown to be mostly cytosolic, in mutant cells it was found similarly distributed between mitochondrial-enriched and cytosolic fractions (**Fig. 4 *C***). In previous studies, only about 3% of total Drp1 was demonstrated to localize in mitochondria (Smirnova *et al*, 2001). Interestingly, we observed that HD striatal cells had increased Drp1 accumulation in mitochondria when compared to wild-type cells (**Fig. 4 *B***). Drp1 phosphorylated at S616 was then analyzed, although no significant changes were observed in untransfected cells (**Fig. 4 *D, E, G.***). Phosphorylation of Drp1 at S616 is regularly studied as an activating signal. When this post-translational modification occurs by Cdk1, it allows Drp1 to translocate to mitochondria (Bossy *et al*, 2010). Meanwhile, Drp1 goes through a complex and complicated network of post-translational modifications, many dependent on the type of stimuli (Santel & Frank, 2008). As such, processes that might result in Drp1 phosphorylation at S616 may not be the ones responsible for its accumulation in mitochondria. On another level, Fis1 levels were significantly increased in ST*Hdh*$^{Q111/Q111}$ cells (**Fig. 4 *H***).

Further immunocytochemistry analyses demonstrated that SIRT3OE decreased Drp1 accumulation in mitochondria in mutant cells (**Fig. 4 *B***). In addition, it resulted in a slight increase in Drp1 phosphorylation at S616 in wild-type cells (**Fig. 4 *E, G***). SIRT3OE also led to a decrease in Drp1 total protein levels in ST*Hdh*$^{Q7/Q7}$ cells, although this was accompanied by a similar decrease after GFP transfection alone and could thus be an effect of the transfection procedure and not of SIRT3OE (**Fig. 4 F, *G***). Furthermore, SIRT3OE reduced protein levels of Fis1 in both ST*Hdh*$^{Q7/Q7}$ and ST*Hdh*$^{Q111/Q111}$ cells (**Fig. 4 *H***), diminishing fission in HD striatal cells.

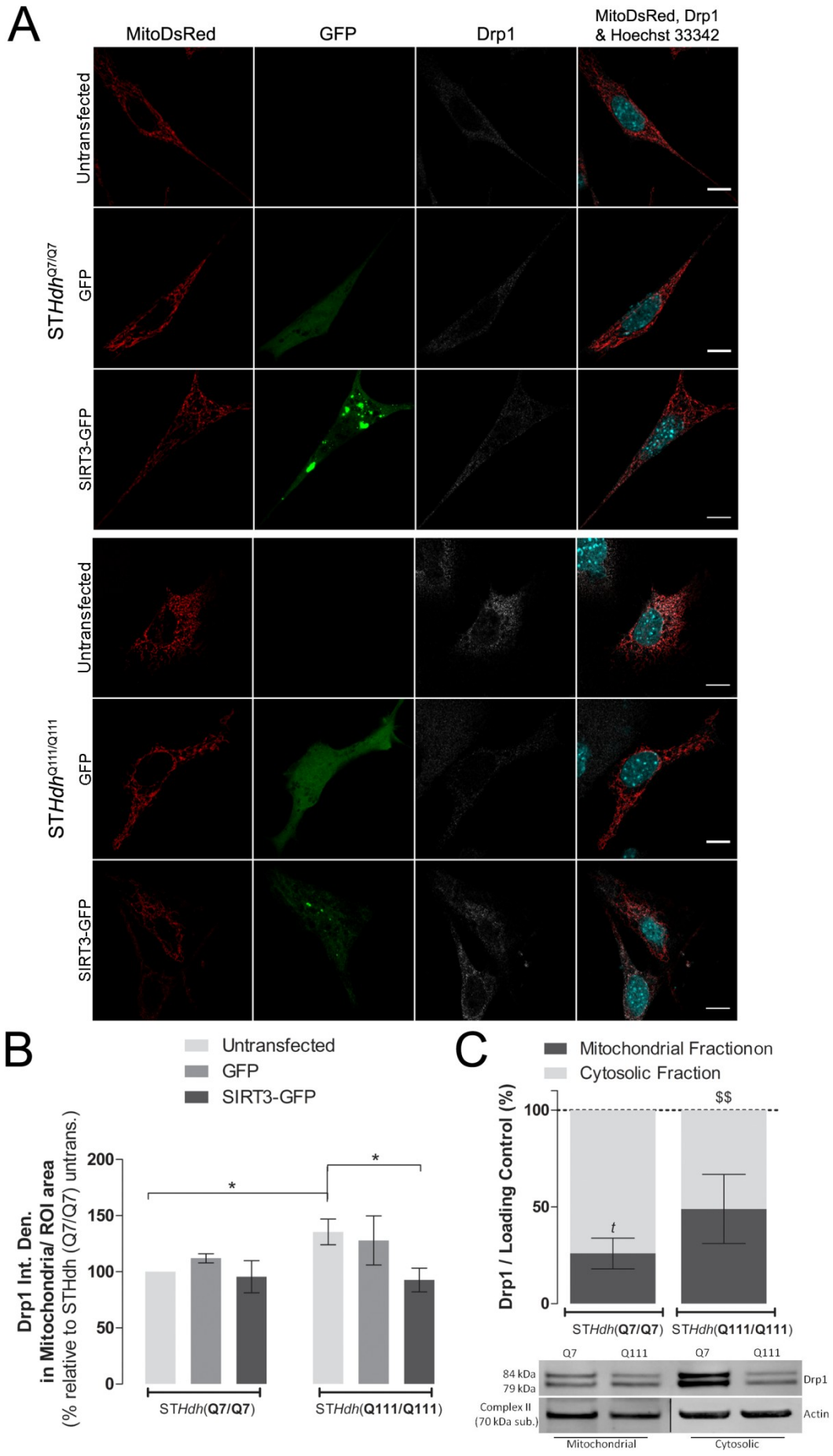
A
MitoDsRed
GFP
Drp1
MitoDsRed, Drp1 & Hoechst 33342
Untransfected
GFP
SIRT3-GFP
STHdhQ7/Q7
STHdhQ111/Q111
B
Untransfected
GFP
SIRT3-GFP
Drp1 Int. Den. in Mitochondria/ ROI area (% relative to STHdh (Q7/Q7) untrans.)
200
150
100
50
0
*
*
STHdh(Q7/Q7)
STHdh(Q111/Q111)
C
Mitochondrial Fraction
Cytosolic Fraction
Drp1 / Loading Control (%)
100
50
0
$$
t
STHdh(Q7/Q7)
STHdh(Q111/Q111)
Q7
Q111
Q7
Q111
84 kDa
79 kDa
Drp1
Complex II (70 kDa sub.)
Actin
Mitochondrial
Cytosolic

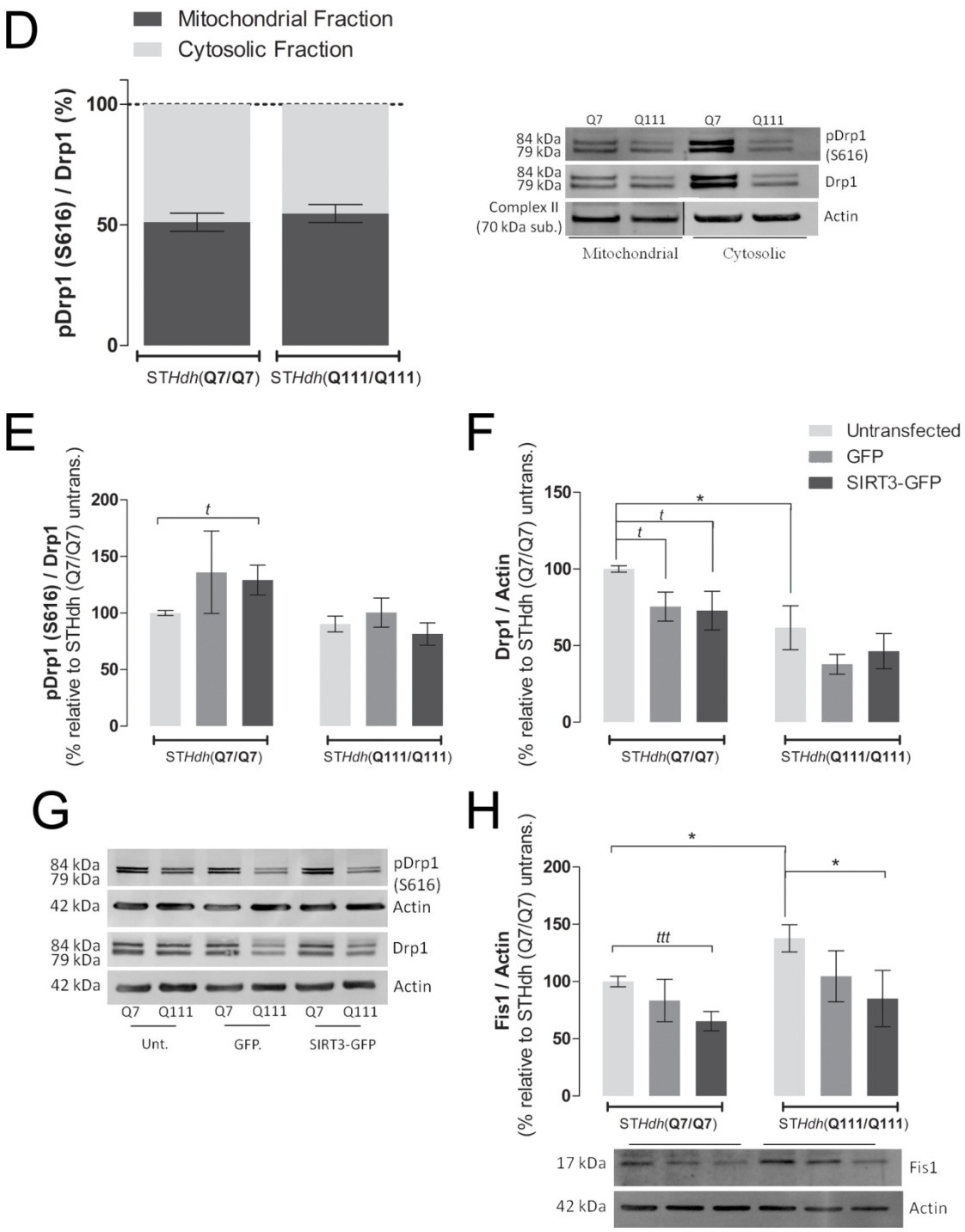

Fig. 4 | Drp1 accumulation in mitochondria and increased Fis1 protein levels in HD striatal cells are rescued by SIRT3 overexpression.

A) Confocal images obtained with a 63x objective, NA=1.4 on a Zeiss LSM 710 inverted microscope. Scale bar: 10 µm. Striatal cells were transfected with either GFP/SIRT3-GFP. Mitochondria were labeled using targeted DsRed and nuclei were visualized by Hoechst stain. Drp1 was immunostained with a specific antibody. **B)** Drp1 cellular localization was quantified in Image J. A total of 3 independent experiments were made, considering ~20 cells/condition. **C-D)** Protein levels of Drp1 and pDrp1 were assessed in mitochondrial-enriched and cytosolic fractions by Western Blotting in untransfected cells. **E-H)** Protein levels of pDrp1, Drp1 and Fis1 were assessed in total protein extracts by Western Blotting. Data is presented as the mean ± SEM of at least 3 independent experiments. Statistical significance: $^{t}P<0.05$ *versus* ST*Hdh*$^{Q7/Q7}$ mitochondria (%) and untransfected ST*Hdh*$^{Q7/Q7}$ cells (two-tailed Student's *t*-test), $^{\$\$}P<0.01$ *versus* ST*Hdh*$^{Q7/Q7}$ cytosolic fraction, $^{*}P<0.05$ (two-way ANOVA, followed by Bonferroni *post-hoc* test) and $^{ttt}P<0.001$ (two-tailed Student's *t*-test).

3.3. MITOCHONDRIAL FUSION-RELATED PROTEIN LEVELS ARE DECREASED IN HD STRIATAL CELLS AND REMAIN UNALTERED AFTER SIRT3 OVEREXPRESSION

To further explore the study of mitochondrial dynamics in HD striatal cells, proteins involved in mitochondrial fusion were then investigated, namely Mfn2 and OPA1. Mfn1 was not explored as it shares a redunctant fusion-related function with Mfn2, with the latter displaying a higher GTPase activity.

ST*Hdh*$^{Q111/Q111}$ cells exhibited lower protein levels of Mfn2 and OPA1 than ST*Hdh*$^{Q7/Q7}$ cells. Unlike what is seen with fission modulators, SIRT3OE did not affect Mfn2 or OPA1 protein levels (**Fig. 5 *B-D***). These data indicate that the changes seen in fission/fusion modulators after SIRT3OE in HD striatal cells would result in diminished mitochondrial fragmentation.

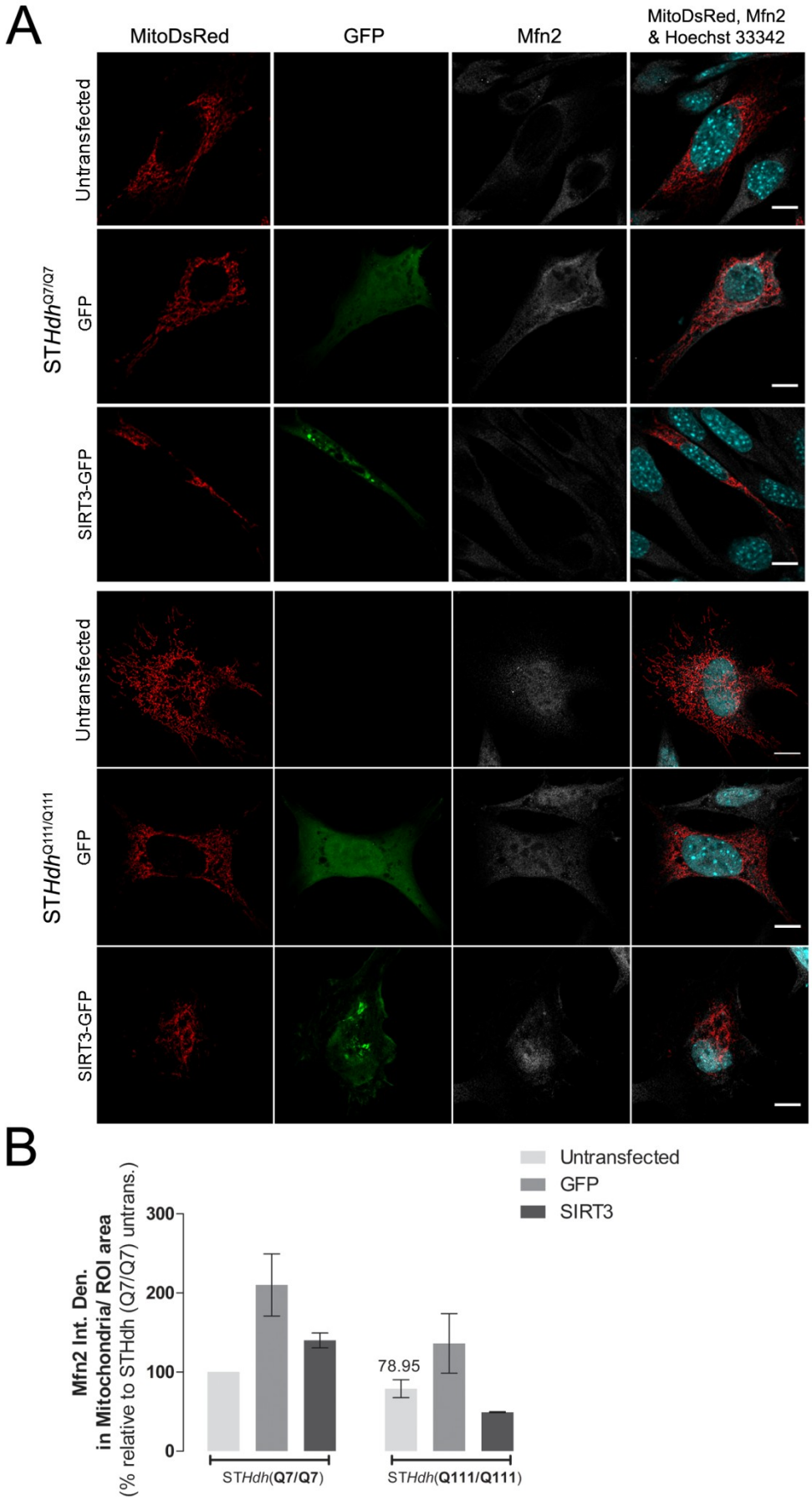
A
MitoDsRed
GFP
Mfn2
MitoDsRed, Mfn2 & Hoechst 33342
Untransfected
GFP
SIRT3-GFP
STHdhQ7/Q7
STHdhQ111/Q111
B
Untransfected
GFP
SIRT3
Mfn2 Int. Den. in Mitochondria/ ROI area (% relative to STHdh (Q7/Q7) untrans.)
300
200
100
0
78.95
STHdh(Q7/Q7)
STHdh(Q111/Q111)

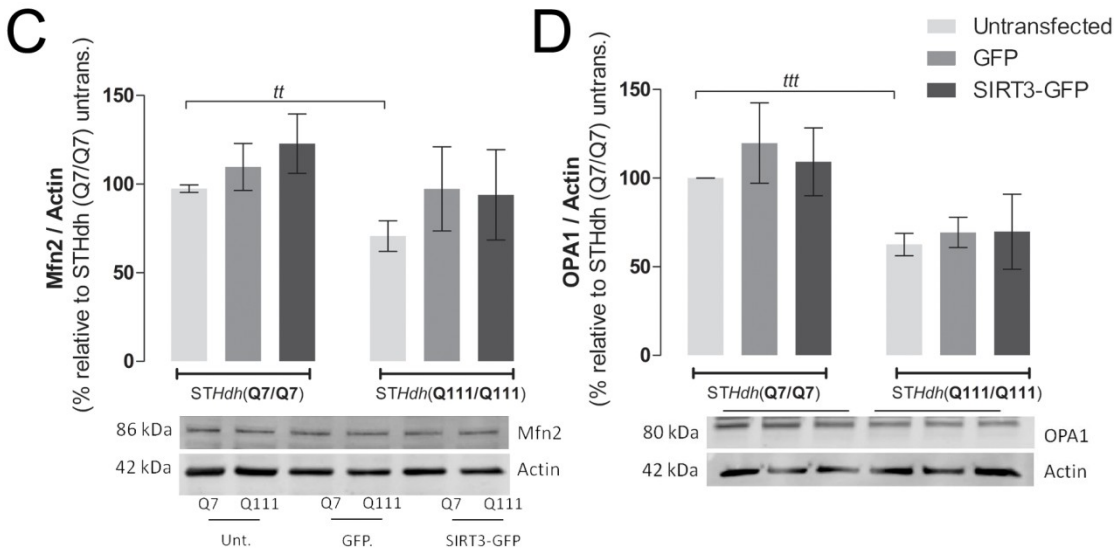

Fig. 5 | ST*Hdh*$^{Q111/Q111}$ cells show decreased levels of fusion proteins, Mfn2 and OPA1, that are not recovered after SIRT3 overexpression.

A) Confocal images obtained with a 63x objective, NA=1.4 on a Zeiss LSM 710 inverted microscope. Mitochondria were labeled using targeted DsRed and nuclei were visualized by Hoechst stain. Mfn2 was immunostained with a specific antibody. Scale bar: 10 µm. **B)** Mfn2 cellular localization was quantified in Image J. Data is presented as the mean ± SEM of 2 independent experiments, considering ~20 cells/condition. **C-D)** Protein levels of Mfn2 and OPA1 were assessed in total protein extracts by Western Blotting. Data is presented as the mean ± SEM of at least 4 independent experiments. Statistical significance: ^{tt}P<0.01, ^{ttt}P<0.001 (two-tailed Student's *t*-test).

3.4. SIRT3 OVEREXPRESSION APPEARS TO RESTORE MITOCHONDRIAL MORPHOLOGY IN MUTANT CELLS

Mitochondrial morphology was evaluated through immunocytochemistry using two variables: Aspect Ratio, positively correlated with length, and Roundness, correlated with the degree of circularity.

No differences were seen regarding Aspect Ratio or Roundness between ST*Hdh*$^{Q7/Q7}$ and ST*Hdh*$^{Q111/Q111}$ cells when considering the raw values generated after automated image analysis (*data not shown*). However, different studies have shown that mitochondrial morphology is altered in HD (Kim *et al*, 2010b; Shirendeb *et al*, 2011), where fragmented mitochondria are dominant. Thus, the cells were visually categorized into the four categories vastly reported in literature: mainly tubular, mixed, fragmented and swollen mitochondria. Data showed that less than 10% of ST*Hdh*$^{Q111/Q111}$ cells presented mainly tubular mitochondria, with ~20% showing fragmented mitochondria, while ST*Hdh*$^{Q7/Q7}$ cells showed a higher percentage of cells displaying a tubular mitochondrial network (higher than 30%), with only a small percentage showing fragmented mitochondria (less than 10%) (**Fig. S1 *A***). In this regard, ST*Hdh*$^{Q111/Q111}$ cells presented a significantly higher percentage of cells with fragmented mitochondria than wild-type cells. Nevertheless, it relied on the visual classification of a cell's mitochondrial network by a single observer, thus presenting a high level of subjectivity. The variables (Aspect Ratio and Roundness) were then evaluated for their trustworthiness. A cell showing notoriously fragmented mitochondria was analyzed versus one showing a tubular mitochondrial network, and the values of each mitochondrion were considered (**Fig. S1 *B***). The cell with fragmented mitochondria showed a lower Aspect Ratio and higher Roundness (in accordance with a reduced length and more circular mitochondria) than the one displaying tubular mitochondria. The variables seemed to recognize both extremes of categorization, but this could be lost when values were being considered per cell instead of per mitochondrion. Therefore, cells previously categorized as showing mainly tubular or fragmented mitochondria were analyzed independently (**Fig. S1 *C***). For cells displaying the same mitochondrial morphology, independently of genotype,

an equivalent value of either Aspect Ratio or Roundness was obtained whilst the reverse was seen when considering opposite morphology.

What could then solve the initial conundrum that arisen when each value per cell was considered? As it was already described (Jin *et al*, 2013) and consistently with what was obtained after visual classification of mitochondrial morphology (**Fig. S1 A**), around 60% of cells from both genotypes demonstrated the same mixed mitochondrial morphology (with short tubular mitochondria) that could be masking the characteristics of cells with tubular or fragmented mitochondria.

Considering the previous data, cells were divided into the following categories: mainly tubular, mixed and fragmented (**Fig. 6**). Of note, cells displaying swollen mitochondria were discarded from this analysis, since they represented a minority of the whole population for either genotype.

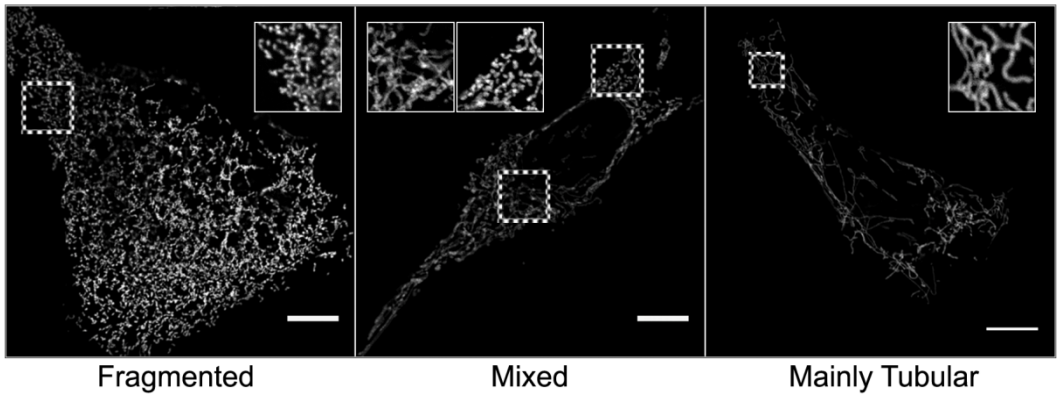

Fig. 6 | Categorization of mitochondrial morphology.
Confocal images obtained with a 63x objective, NA=1.4 on a Zeiss LSM 710 inverted microscope. Scale bar: 10 µm. Mitochondria-targeted DsRed was transfected in the striatal cells to visualize their mitochondrial network, being later assigned to one of the three categories considered for mitochondrial morphology (fragmented, mixed and mainly tubular). Cells considered having fragmented mitochondria show small, round and numerous mitochondria, whereas cells considered as having a mainly tubular mitochondrial network show a highly connected network, with long mitochondria. Cells assigned for a mixed morphology show aspects of both fragmented and tubular morphology.

Given that the variables were proven to be consistent between extremes of classification and regardless of genotype, SPSS software (IBM® SPSS® Statistics, New York, USA) was used to analyze *Percentiles* for each variable. More than 4 independent experiences were considered to assure the strength of each parameter as well as both genotypes. Values for the Percentile of 25% and 75% were taken into consideration and used as demonstrated on **Table 4**. Cells were then counted for each category and results are displayed as the percentage of the total number of cells.

Table 4 | Thresholds used for mitochondrial morphology evaluation.

	Aspect Ratio	**Roundness**
Mainly tubular	$x > 2.43$	$x < 0.5$
Mixed	$2.07 \leq x \leq 2.43$	$0.5 \leq x \leq 0.55$
Fragmented	$x < 2.07$	$x > 0.55$

The resulting analysis confirmed what was observed by visual classification in a more robust manner: ~30% of the cell population of mutant cells having fragmented mitochondria *versus* less than 10% of the wild-type cells and ~30% of ST*Hdh*$^{Q7/Q7}$ cells displaying tubular mitochondria *versus* ~15% of ST*Hdh*$^{Q111/Q111}$ cells, with the maintenance of ~60% of the cell population from both genotypes exhibiting a mixed morphology. Interestingly, following SIRT3OE, the percentage of HD striatal cells with tubular mitochondria increased dramatically to more than 40%, higher than what was seen in untransfected wild-type cells, with a consequent decrease in the percentage of mutant cells with fragmented mitochondria (less than 10%) (**Fig. 7 *B***). In addition, mitochondrial mass was quantified as the percentage of a cell's area that was occupied by DsRed labeling. Mutant cells were shown to have lower mitochondrial mass than wild-type counterparts, without significant alterations after SIRT3OE (**Fig. 7 *C***).

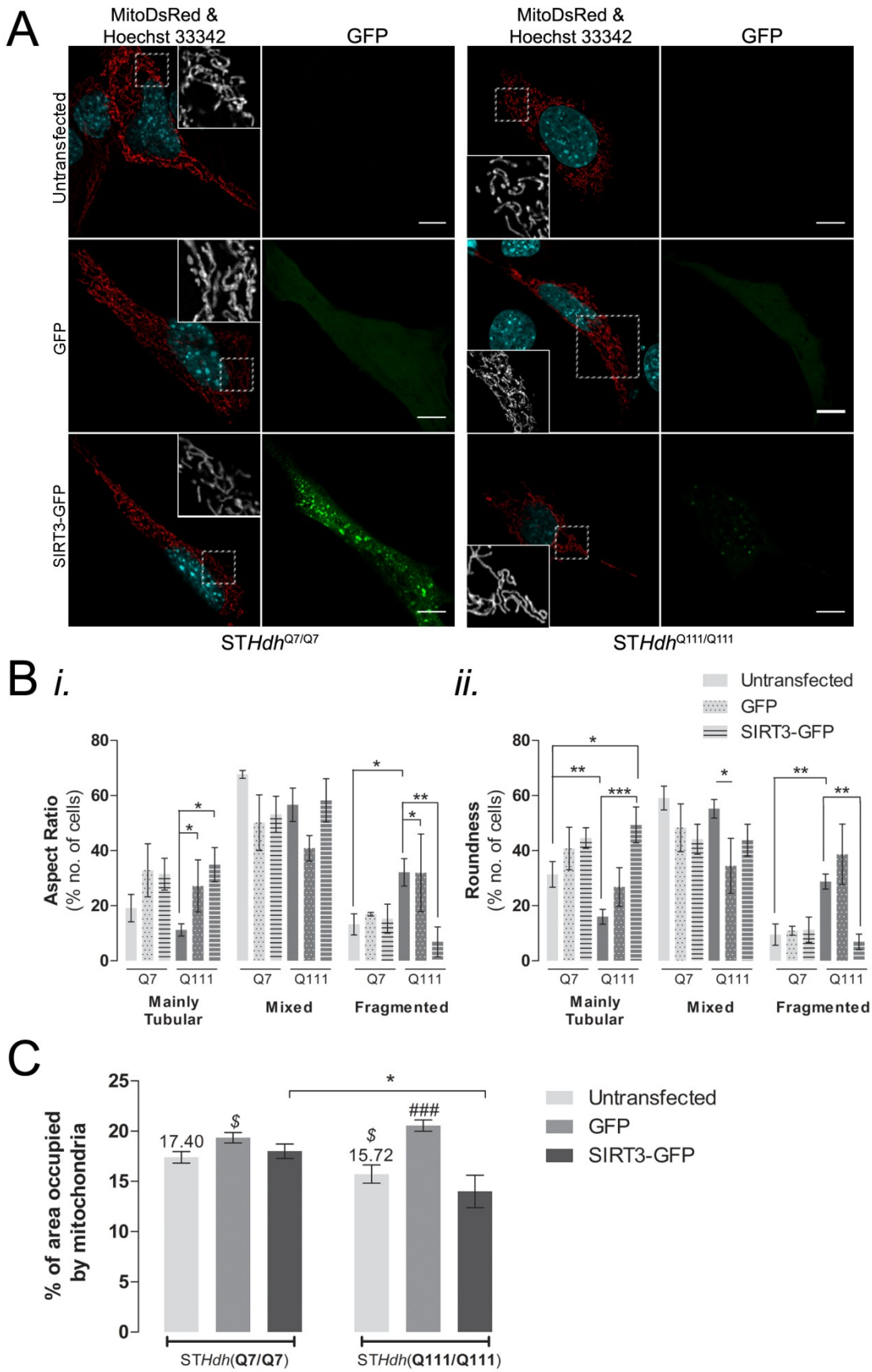
A
MitoDsRed & Hoechst 33342
GFP
MitoDsRed & Hoechst 33342
GFP
Untransfected
GFP
SIRT3-GFP
STHdhQ7/Q7
STHdhQ111/Q111
B i.
ii.
Untransfected
GFP
SIRT3-GFP
Aspect Ratio (% no. of cells)
Roundness (% no. of cells)
Q7
Q111
Mainly Tubular
Mixed
Fragmented
C
% of area occupied by mitochondria
17.40
15.72
STHdh(Q7/Q7)
STHdh(Q111/Q111)

Fig. 7 | Mutant cells display more fragmented mitochondria with decreased percentage of the cellular area occupied by the mitochondrial network than wild-type cells and the former is counteracted upon SIRT3 overexpression.

A) Confocal images obtained with a 63x objective, NA=1.4 on a Zeiss LSM 710 inverted microscope. Mitochondria were labeled using targeted DsRed and nuclei were visualized by Hoechst stain. Scale bar: 10 µm. **B)** Image analysis was done in Image J. Data is presented as the mean ± SEM of 3 independent experiments, considering ~20 cells/condition. **C)** Percentage of cellular area occupied by mitochondria was quantified in Image J. Data is presented as the mean ± SEM of 4 independent experiments, considering ~20 cells/condition. Statistical significance: $^{\$}P<0.05$ *versus* untransfected ST*Hdh*$^{Q7/Q7}$ cells(two-tailed Student's *t*-test), $^{\#\#\#}P<0.001$ *versus* untransfected ST*Hdh*$^{Q111/Q111}$ cells and $^{*}P<0.05$, $^{**}P<0.01$ and $^{***}P<0.01$ (two-way ANOVA, followed by Bonferroni *post-hoc* test).

3.5. SIRT3 OVEREXPRESSION MIGHT ACTIVATE MACROAUTOPHAGY BUT NOT PARKIN-DEPENDENT MITOPHAGY IN MUTANT CELLS

Dysfunctional mitochondria tend to accumulate in HD, a process detected in the cell model used in this study (Quintanilla *et al*, 2013; Siddiqui *et al*, 2012; Quintanilla *et al*, 2008; Milakovic *et al*, 2006; Milakovic & Johnson, 2005). Having found differences in regards to mitochondrial morphology and mass, we further explored the selective degradation of dysfunctional mitochondrial in ST*Hdh*$^{Q7/Q7}$ and ST*Hdh*$^{Q111/Q111}$ cells. Although of critical importance for cellular homeostasis, neuronal mitophagy has remained an elusive subject until recently (Shaltouki *et al*, 2015; Ashrafi & Schwarz, 2015; Ashrafi *et al*, 2014; Amadoro *et al*, 2014), being even more obscure when it comes to HD pathogenesis (Hwang *et al*, 2015; Rui *et al*, 2015; Khalil *et al*, 2015). Therefore, basic regulators involved in mitophagy were firstly investigated.

ST*Hdh*$^{Q111/Q111}$ cells demonstrated strikingly low levels of Parkin (62% less than wild-type cells) (**Fig. 8 *C i.***). Meanwhile, immunocytochemistry analyses seem to indicate that Parkin localization in mitochondria from HD striatal cells is not significantly different from wild-type cells (**Fig. 8 *A, B***). It is also necessary to bear in mind that quantification of images derived from its normalization to cellular area (ROI area) and not to mitochondrial area. In fact, ST*Hdh*$^{Q111/Q111}$ cells show decreased mitochondria mass (**Fig. 7 *C***). To settle the question if the low levels seen could be the result of over-activation or impairment of mitophagy, PINK1 levels were evaluated as well as the activated form of Parkin, namely its PINK1-dependent phosphorylation at S65. No significant differences in phosphorylated Parkin (S65) were found in HD striatal cells, when compared to ST*Hdh*$^{Q7/Q7}$ cells (**Fig. 8 *C ii.***), but decreased levels of PINK1 were observed in HD striatal cells. As such, mitophagy dependent on PINK1/Parkin may be impaired in HD striatal cells. No differences were seen in ST*Hdh*$^{Q111/Q111}$-SIRT3 cells in either case, whilst SIRT3OE appears to decrease Parkin and PINK1 levels in ST*Hdh*$^{Q7/Q7}$ cells.

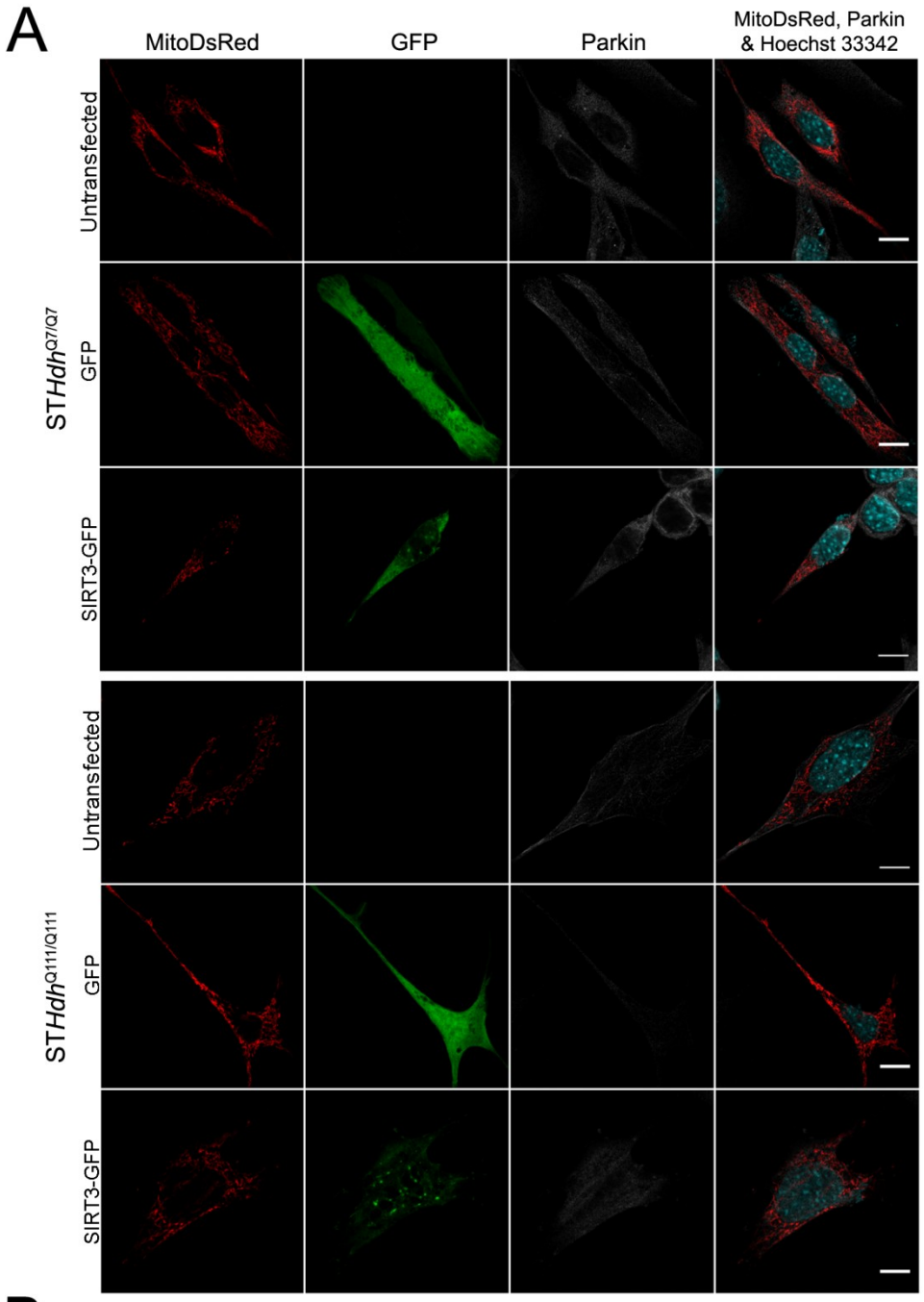
A
MitoDsRed
GFP
Parkin
MitoDsRed, Parkin & Hoechst 33342
Untransfected
GFP
SIRT3-GFP
STHdhQ7/Q7
STHdhQ111/Q111

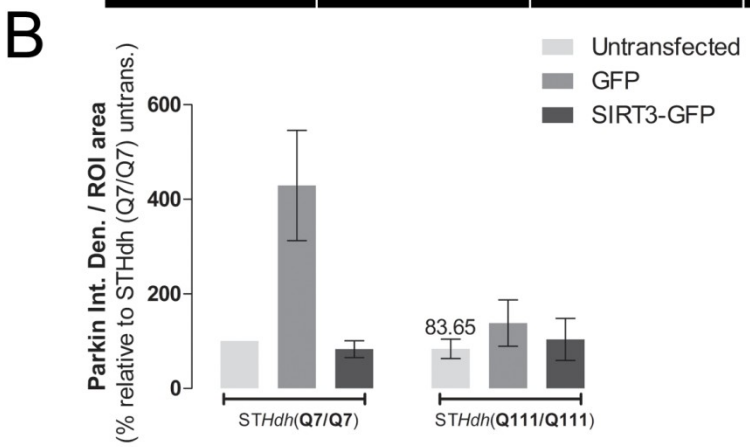
B
Untransfected
GFP
SIRT3-GFP
Parkin Int. Den. / ROI area
(% relative to STHdh (Q7/Q7) untrans.)
600
400
200
0
83.65
STHdh(Q7/Q7)
STHdh(Q111/Q111)

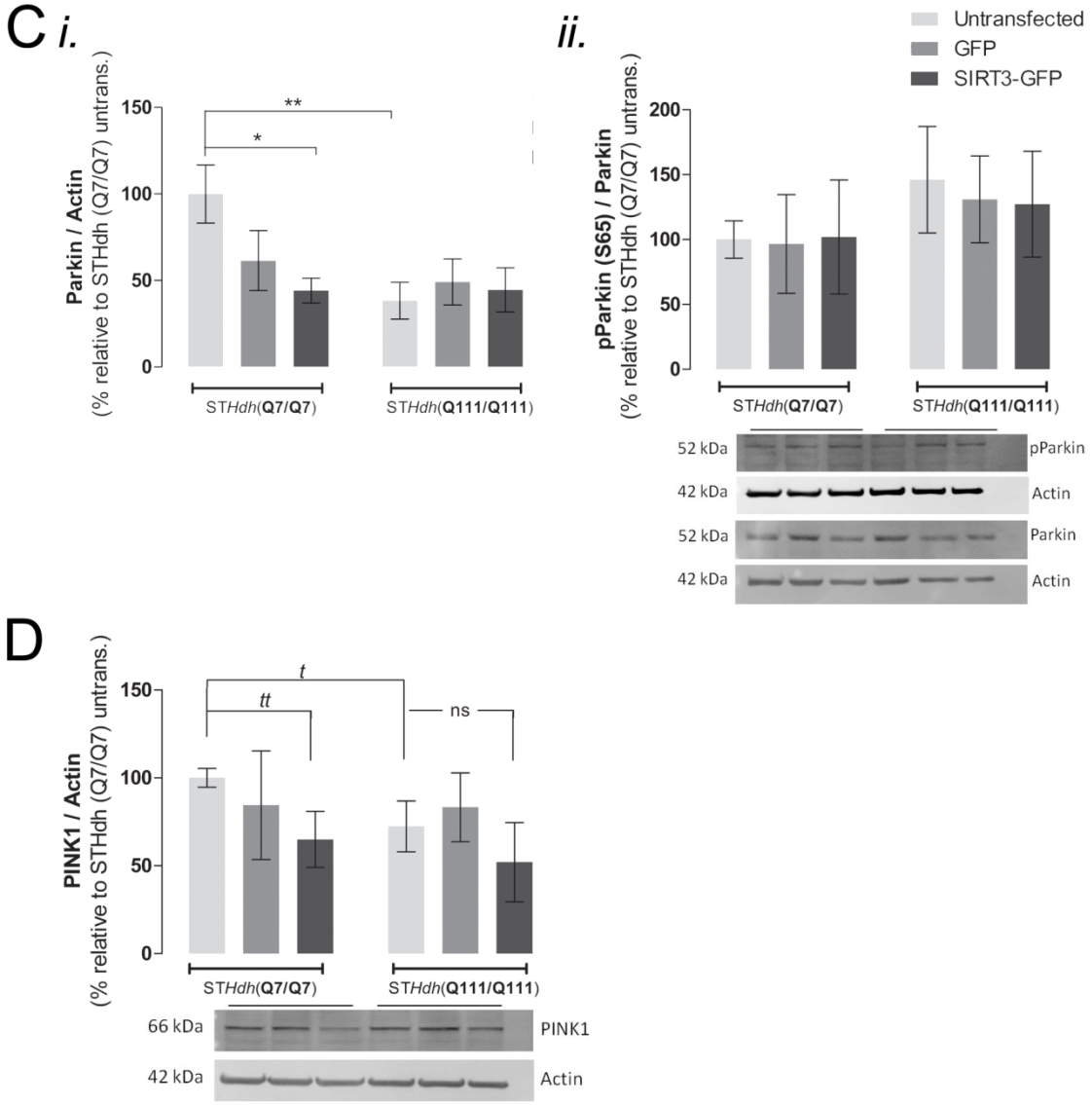

Fig. 8 | Analysis of mitophagy in HD striatal cells – Decreased levels of Parkin were maintained after SIRT3OE, with no additional changes in Parkin phosphorylation (at S65) and PINK1.
A) Confocal images obtained with a 63x objective, NA=1.4 on a Zeiss LSM 710 inverted microscope. Mitochondria were labeled using targeted DsRed and nuclei were visualized by Hoechst stain. Mfn2 was immunostained with a specific antibody. Scale bar: 10 µm. **B)** Parkin cellular localization was quantified in Image J. Data is presented as the mean ± SEM of 4 independent experiments, considering ~20 cells/condition. **C-D)** Protein levels of Parkin, pParkin and PINK1 were assessed in total protein extracts fractions by Western Blotting. Data is presented as the mean ± SEM of 3-4 experiments. Statistical significance: $^{t}P<0.05$, $^{tt}P<0.01$ (two-tailed Student's *t*-test), $^{*}P<0.05$, $^{**}P<0.01$ (two-way ANOVA, followed by Bonferroni *post-hoc* test).

Autophagosome formation and cargo recognition were analyzed through LC3 and adaptor p62 protein levels, respectively. Of interest, HD striatal cells presented a higher increase of LC3-II/I ratio in relation to wild-type cells, showing an increased association of the truncated form of LC3 (LC3-I) with phosphatidylethanolamine (PE)

(LC3-II), found in the autophagosome membrane (**Fig. 9 *B***). This becomes obvious in **Fig. 9 *A***, where mutant cells displayed a higher number of LC3 aggregates, whereas wild-type cells showed more sporadic aggregates. One could assume that the reason why wild-type cells did not display more LC3 labeling was due to enhanced autophagosome degradation. Inhibitors of autophagy flux, such as bafilomycin A1 (BafA1), a vacuolar H^+-ATPase inhibitor, impairing autophagosome-lysosome fusion (late phase of autophagy) and chloroquine that accumulates in lysosomes and prevents its acidification, further inhibiting lysosomal enzymes and content degradation, could enlighten these questions. BafA1 (50 nM) was added to ST*Hdh* cells 8h prior to total protein extracts performance. Additionally, cell culture medium was changed to fresh medium 24h earlier in order to avoid starvation-derived effects. Under such conditions, LC3-II/I ratio did not differ between ST*Hdh*$^{Q7/Q7}$ and ST*Hdh*$^{Q111/Q111}$ cells, increasing after BafA1 addition in both cells (**Fig. 9 *D***). Under these conditions, HD striatal cells may not need to turn to autophagy to meet energy requirements. Additionally, autophagosome formation and fusion with lysosomes was evaluated through RFP-GFP-LC3B in untransfected cells. LC3 has 3 human isoforms – A, B and C. Isoform B has a known role in autophagy by associating with autophagosome membranes, however recently LC3A was seen to co-localize in autophagosomes in a pattern similar to LC3B (Bai *et al*, 2012). With GFP being acid--sensitive unlike RFP, in acidic conditions such as those within lysosomes, GFP fluorescence is quenched and only RFP fluorescence is observed. Thus, this construct allows to distinguish between an autophagosome (neutral pH, fluorescence obtained from RFP and GFP) and an autolysosome (acidic pH, fluorescence obtained only from RFP). In both cells, punctuate LC3B emitting only red fluorescence could be seen, indicative of lysosome fusion with autophagosome, with autophagosome accumulation after 4h treatment with chloroquine (80 µM) (**Fig. 9 *C***). These data demonstrate that ST*Hdh*$^{Q111/Q111}$ cells do not show lysosomal impairment and are capable of autophagosome degradation.

p62 was found to be decreased in mutant striatal cells (**Fig. 9 *E***), which could also be a result of autophagy activation, being degraded alongside autophagosomes.

SIRT3OE led to a more pronounced effect on LC3-II/I ratio, without affecting p62 levels in ST*Hdh*$^{Q111/Q111}$ cells (**Fig. 9 *A***, ***B***). Meanwhile, there was a decrease in

p62 levels in ST*Hdh*$^{Q7/Q7}$ cells after SIRT3OE. Together, data suggest that SIRT3OE may be increasing macroautophagy signaling but not evoking changes in selective mitochondria autophagy, considering at least the Parkin-dependent pathway.

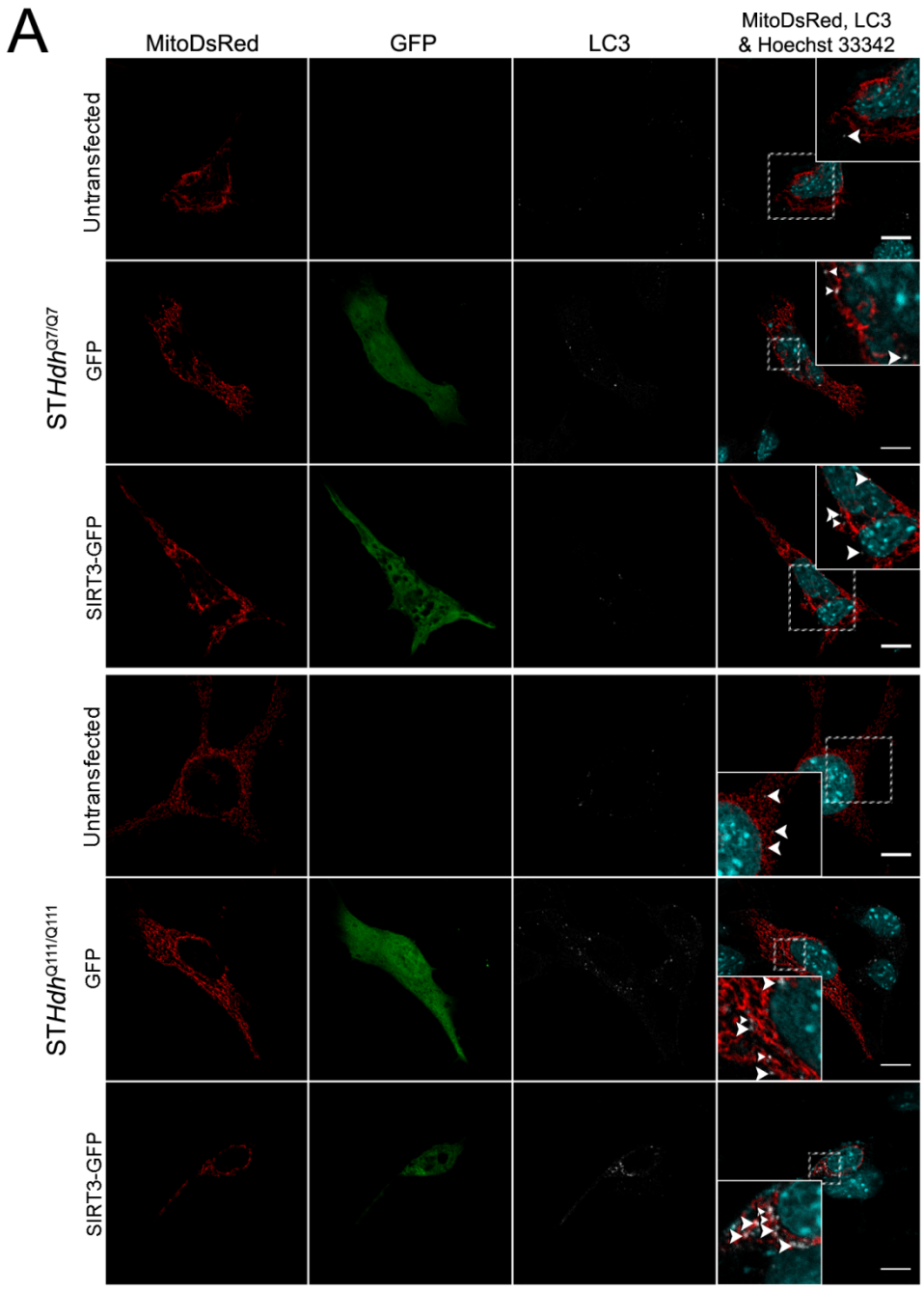
A
MitoDsRed
GFP
LC3
MitoDsRed, LC3
& Hoechst 33342
STHdhQ7/Q7
Untransfected
GFP
SIRT3-GFP
STHdhQ111/Q111
Untransfected
GFP
SIRT3-GFP

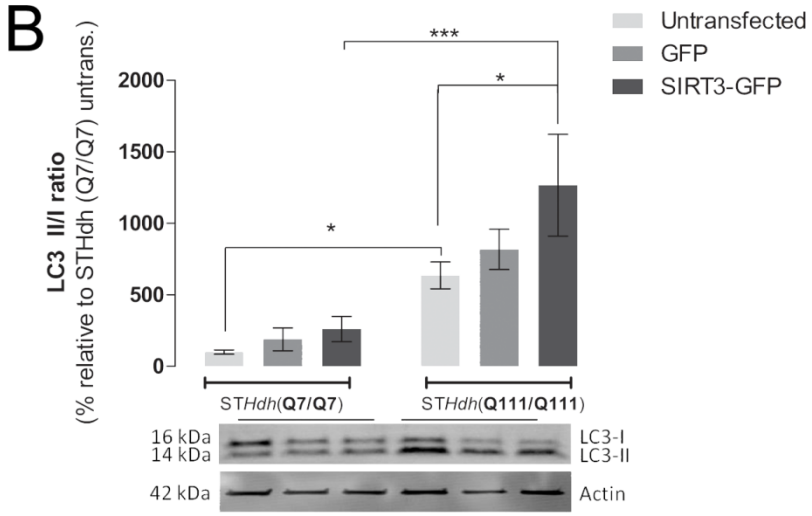
B
Untransfected
GFP
SIRT3-GFP
LC3 II/I ratio
(% relative to STHdh (Q7/Q7) untrans.)
2000
1500
1000
500
0
***
*
*
STHdh(Q7/Q7)
STHdh(Q111/Q111)
16 kDa
14 kDa
LC3-I
LC3-II
42 kDa
Actin

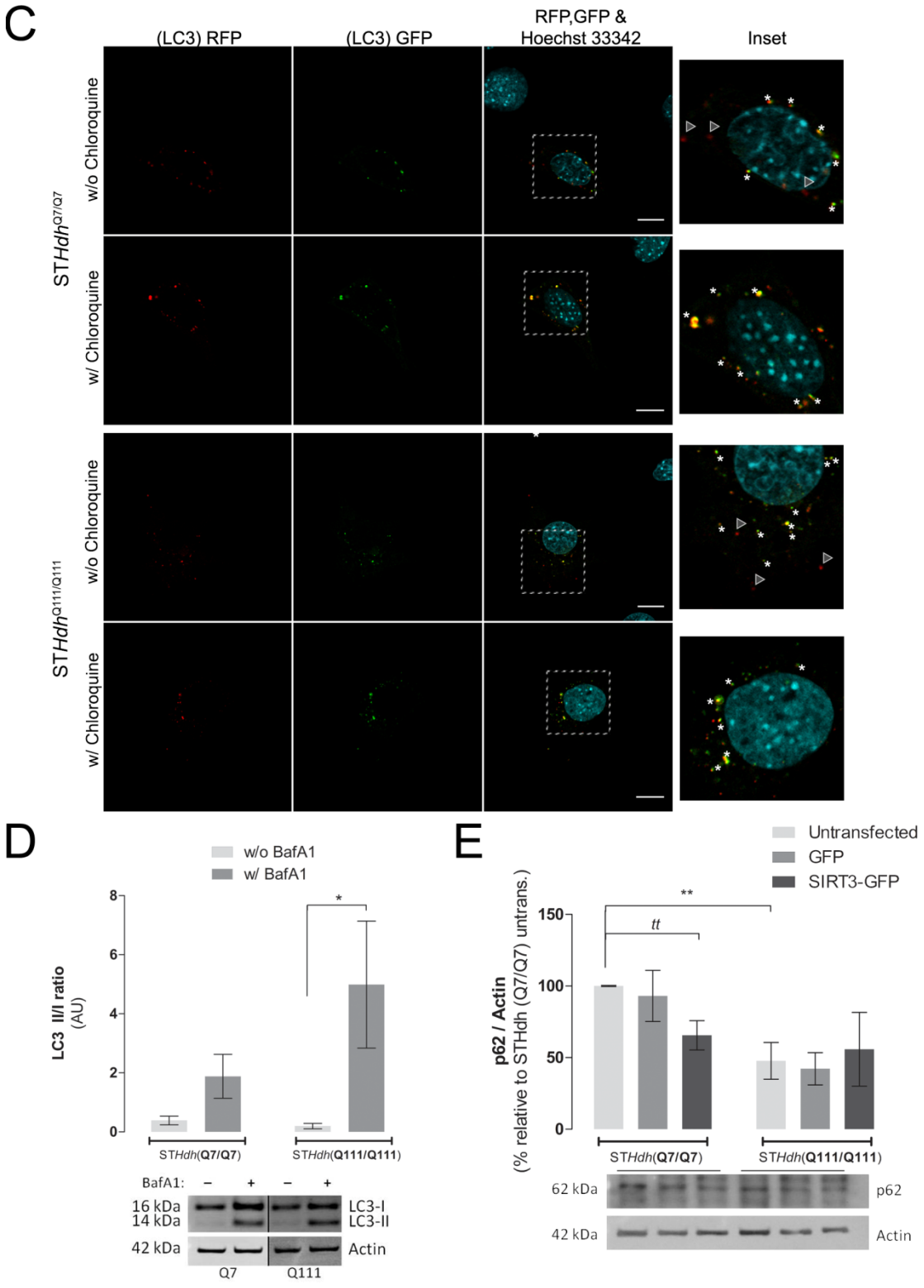

Fig. 9 | Apparent activation of macroautophagy upon SIRT3 overexpression in ST*Hdh*$^{Q111/Q111}$ cells.
A, C) Confocal images obtained with a 63x objective, NA=1.4 on a Zeiss LSM 710 inverted microscope. Scale bar: 10 µm. White arrows in **A** were used to demonstrate LC3 labelling, with smaller ones representing colocalization with mitochondria. In **C**, grey arrows were used to demonstrate only RFP fluorescence while, ***** was used to demonstrate RFP and GFP colocalization of RFP-GFP-LC3B. **B, D, E)** Protein levels of LC3 and p62 were assessed in total protein extracts by Western Blotting. Data is presented as the mean ± SEM of 3-4 independent experiments. Statistical significance: $^{tt}P<0.01$ (two-tailed Student's *t*-test), $^{*}P<0.05$, $^{**}P<0.01$, $^{***}P<0.001$ (two-way ANOVA, followed by Bonferroni *post-hoc* test).

CHAPTER IV – DISCUSSION & CONCLUSIONS

4.1. DISCUSSION

Mitochondrial dysfunction has long been associated with the pathogenesis of HD, hence a part of research focused on searching targets that could ameliorate it (Costa & Scorrano, 2012). KDACS have demonstrated to be promising targets, not only for HD but for a large spectrum of neurodegenerative disorders (Guedes-Dias & Oliveira, 2013).

Several parameters play a role in modulating mitochondrial function to ensure proper cellular homeostasis as well as capacity to respond to different stress factors. One of such factors is the maintenance of the balance between mitochondrial fusion and fission that is found altered in HD (Reddy, 2014). Several studies using distinct models (e.g., postmortem neostriatal and frontal cortex tissue specimens from HD patients, human lymphoblasts and fibroblasts, striatal neurons from YAC128 mice, BACHD mice, ST*Hdh*$^{Q111/Q111}$ cells, HeLa cells expressing Htt-fusion proteins) have shown that the presence of mHTT leads to extensive mitochondrial fragmentation, culminating in the disruption of mitochondrial dynamics and progressing to neuronal cell death. They report an increase in the expression of fission modulators Fis1 and Drp1 with a concomitant decrease in the expression of fusion-related Mfn1, Mfn2 and OPA1 (Shirendeb *et al*, 2012; Song *et al*, 2011; Kim *et al*, 2010b; Costa *et al*, 2010; Wang *et al*, 2009). Overall our findings reinforce the relevance of altered mitochondrial dynamics in HD.

In accordance to a previous report by Jin and collaborators, more than a half of the cell population of both genotypes displayed a mixed mitochondrial morphology; ST*Hdh*$^{Q111/Q111}$ cells showed a higher proportion of fragmented mitochondria, whilst there was a higher percentage of ST*Hdh*$^{Q7/Q7}$ cells exhibiting tubular mitochondrial network (**Fig. 7**). Jin related the increased mitochondrial fragmentation seen in mutant cells to a decrease in OPA1 protein levels alone, not having seen significant changes in the protein levels of Mfn2 (Jin *et al*, 2013). Herein we demonstrated that despite total protein levels of Drp1 were found decreased in HD striatal cells when compared to ST*Hdh*$^{Q7/Q7}$ cells (**Fig. 4 *F, G***), it was vastly found in mitochondria of mutant cells than in wild-type cells (**Fig. 4 *B-C***). In addition to Fis1 total protein levels

also being increased in HD striatal cells (**Fig. 4 *H***), we observed reduced protein levels of both OPA1 and Mfn2 (**Fig. 5**). Thus an increase in fission and reduced fusion could generate mitochondrial fragmentation in HD.

Cells are equipped with special mechanisms to deal with damaged organelles in a specific manner that separates it from bulk degradation processes related with macroautophagy. Being an organelle of extreme importance, namely for neuronal cells that have a high energy demand, mitophagy has rapidly been placed under the spotlight. It has gained a special relevance in regards to neurodegeneration (Lionaki *et al*, 2015).

In the present study, we detected low protein levels of Parkin and PINK1 in ST*Hdh*$^{Q111/Q111}$ cells (**Fig. 8 *A***, ***B***, ***C ii***) that combined with unchanged levels of Parkin's active form, phoshorylated at S65 by PINK1 (**Fig. 8 *C i***, ***D***), suggesting that mitophagy by PINK1/Parkin pathway could be inactive in this HD cell model. At the same time, recent data indicate a role of Mfn2 in PINK1/Parkin-mediated mitophagy. It would appear that PINK1-phosphorylated Mfn2 serves as a receptor for Parkin in damaged mitochondria (Chen & Dorn, 2013) before being ubiquitinated for degradation. Decreased levels of Mfn2 seen in HD cells would then impede mitophagy to proceed. This would also imply that the reduced mitochondrial mass observed in mutant cells (**Fig. 7 *C***) would not resort from increased mitophagy but from decreased biogenesis (*Naia* et al*, unpublished data*).

Still, one needs to be aware that the studies were conducted using cultured cells under basal conditions. In fact, it was recently reported that only a minority of mitochondria are degraded by mitophagy under these conditions. Namely the PINK1/Parkin pathway can only be reproduced in limited conditions, requiring the use of expression vectors in certain cell lines due to low expression levels of mitophagy players before mitophagy induction (Hirota *et al*, 2015). In addition, the continuous discovery of alternative mitophagy pathways leads not only to controversial findings (Devireddy *et al*, 2015; Ashrafi & Schwarz, 2015; Van Laar *et al*, 2011), but also to an increased difficulty in connecting what is being developed in research with what is physiological viable.

Sequentially, we observed a significant increase in LC3-II/I ratio (**Fig. 9 *B***), with increased autophagosome formation in mutant cells (**Fig. 9 *A***). ST*Hdh*$^{Q111/Q111}$ cells

also presented reduced p62 proteins levels (**Fig. 9 *E***), which could indicate an increase in autophagic clearance in these cells. Meanwhile, increased expression and further accumulation of p62 protein levels have been reported in other models (Rué *et al*, 2013; Heng *et al*, 2010) in agreement with autophagy impairment characteristic of HD (Martinez-Vicente *et al*, 2010). Care must be taken when assessing such results, as the models differ not only in the different forms of mHTT expressed (full-length *versus* truncated N-terminal), but also in genetic background (homozygous/heterozygous). Using a homozygous cell line may not always represent a feasible disease event, and thus discrepancies may arise between different models. As a result, oxidative stress manifested in HD and already described in ST*Hdh*$^{Q111/Q111}$ cells (Ribeiro *et al*, 2013) may lead to oxidative damage to the promoter region of p62, as reported by Du and co-authors (Du *et al*, 2009). While Rué and collaborators observed an increase in p62 mRNA levels in R6/1 mice striatum and cortex, Jin and colleagues reported the same decrease in p62 protein levels that we observed in ST*Hdh*$^{Q111/Q111}$ cells with no significant changes in mRNA levels, combined with a compromised response to oxidative stress in HD striatal cells (Rué *et al*, 2013; Jin *et al*, 2013).

What could this mean for mitophagy? Using the same striatal cell model, Khalil and colleagues focused on the induction of the PINK1/Parkin pathway with the protonophore carbonyl cyanide *m*-chlorophenyl hydrazone (CCCP), overexpressing Parkin and PINK1. Apparently the presence of mHTT did not affect the capacity of Parkin to translocate to mitochondria upon a depolarization stimulus or the ubiquitination rate, but the number of mitochondria that were degraded by mitophagy was lower in mutant cells than in ST*Hdh*$^{Q7/Q7}$ cells. Overexpression of PINK1 increased mitophagy, but levels in mutant cells remained lower than in wild-type counterparts (Khalil *et al*, 2015). Recently, Cuervo's lab brilliantly proposed that HTT acts as a scaffold protein for selective autophagy, including mitophagy, by assisting p62 recognition of K63 poly-Ub chains on modified targets. More importantly, polyQ expansion could compromise the role of HTT in selective autophagy (Rui *et al*, 2015). In accordance, an accumulation of empty autophagic vesicles that fail to engulf cytosolic cargo in HD cells has been reported, along with defective autophagosome transport (Wong & Holzbaur, 2014; Martinez-Vicente *et*

al, 2010). Therefore, although an accumulation of damaged and fragmented mitochondria due to an increase in fission, a pre-requisite for mitophagy, would favor their removal, the reduced capacity of HD cells to recognize cytosolic cargo makes any upregulation of macroautophagy futile.

Acetylation plays a preponderant role in modulating mitochondrial dynamics and homeostasis (Webster *et al*, 2014), being a rapidly reversible post-translational modification. As such, having established altered mitochondrial dynamics in HD cells, we next explored the effect that SIRT3, the major mitochondrial lysine deacetylase, could exert.

SIRT3 exists under two forms, both enzimatically active: a nuclear full-length and a processed form localized in mitochondria. Upon cellular stress, SIRT3 translocates from the nucleus to the mitochondria, being processed along the way (Scher *et al*, 2007). As it was the case, after SIRT3OE ST*Hdh*$^{Q111/Q111}$ cells exhibited a higher accumulation of SIRT3-GFP in mitochondria in relation to ST*Hdh*$^{Q7/Q7}$ cells (**Fig. 3**).

SIRT3OE was able to restore mitochondrial morphology in HD striatal cells, leading to a higher number of cells with a tubular mitochondrial network than untransfected wild-type cells (**Fig. 7 *A*-*B***). Because no changes in the proteins levels of fusion-related proteins (**Fig. 5**) or in the overall mitochondrial mass (**Fig. 7 *C***), could be observed in SIRT3OE mutant cells, enhanced tubular morphology could be accounted to decreased Drp1 accumulation in mitochondria (**Fig. 4 *A*-*C***) coupled with a reduction in Fis1 protein levels (**Fig. 4 *H***).

We also detected increased autophagosome formation in ST*Hdh*$^{Q111/Q111}$-SIRT3 cells (**Fig. 9 *A*-*B***), suggesting an increase turnover of autophagosomes. However, any colocalization seen through confocal microscopy between LC3 and mitochondria (**Fig. 9 *A***) may not be of any particular relevance.

Even though diffused labeling was not included in quantification (derived from LC3-I and background noise) in order to consider only the PE-associated form, because ST*Hdh*$^{Q111/Q111}$-SIRT3 cells display mainly a tubular mitochondrial network, their degradation by autophagosomes would be physically conflicting. It is our understanding that increased LC3 levels would more likely be related with an increase in macroautophagy, possibly as an attempt to increase ATP levels in a

bioenergetic deficient cell, even in untransfected cells (*Naia* et al*, unpublished data*; Morán *et al*, 2014). Concordantly, untransfected HD striatal cells did not display lysosomal impairment, with no apparent difference in LC3 II/I ratio in ST*Hdh*$^{Q111/Q111}$ cells replenished with fresh medium 24h prior to harvesting (**Fig. 9** ***C, D***).

Even though it would seem like SIRT3OE would paint an almost perfect picture for HD, it displayed a darker side. Not only did it decreased cell viability but also increased oxidative damage through ROS production, in particular hydrogen peroxide (H_2O_2) and superoxide anion radical ($O_2^{\bullet-}$), and reduced $\Delta\psi_m$ in both ST*Hdh*$^{Q7/Q7}$ and ST*Hdh*$^{Q111/Q111}$ cells. Strikingly, untransfected HD striatal cells showed higher mitochondrial SIRT3 levels (mRNA and protein) and activity than untransfected wild-type cells, which can underlie a compensatory mechanism that could overwhelm mutant cells upon overexpression (*Naia* et al*, unpublished data*). This seems contradictory to what was reported by Fu and colleagues in 2012, having described lower levels of the processed mitochondrial form of SIRT3 in ST*Hdh*$^{Q111/Q111}$ cells with SIRT3-dependent neuroprotection by trans-(–)-ε-viniferin (viniferin) (Fu *et al*, 2012). Such may be explained considering the technical differences – we analyzed mitochondrial SIRT3 levels in mitochondrial-enriched fractions and additionally measured mRNA levels through qPCR, and further detected SIRT3 deacetylase activity directly using a fluorometric assay and by evaluating the levels of SOD2 acetylation at K68, one of its main targets; Fu *et al*, on the other hand, quantified the mitochondrial form using total protein extracts and after serum deprivation and assumed SIRT3 activity by also evaluating the levels of acetylation of SOD2. Concordantly with our data showing increased SIRT3 activity, our group has previously established increased activity levels of SOD2 in ST*Hdh*$^{Q111/Q111}$ cells related with decreased levels of acetylated SOD2 (Ribeiro *et al*, 2014). In addition, we directly induced an increase of SIRT3 levels by overexpressing SIRT3, while Fu and colleagues studied the effect of a naturally occurring compound. Although the authors connected the neuroprotective effect of viniferin to increased SIRT3 levels and activity, activation of other signaling pathways could still be at play. In fact, viniferin could be increasing upstream molecules that could aid on the SIRT3 neuroprotective response, which would likely remain unchanged by SIRT3OE alone. ST*Hdh*$^{Q111/Q111}$ cells also displayed reduced NAD^+/NADH ratio which was ameliorated

by viniferin (Fu *et al*, 2012). Being NAD^+-dependent, after serum deprivation SIRT3 activity could be found decreased due to a restrict pool of NAD^+; therefore SIRT3OE could even further diminish the NAD^+/NADH ratio in HD striatal cells and cause cell death (Yang *et al*, 2007).

Drp1 inhibition has been vastly describing in ameliorating several disorders by restoring mitochondrial morphology and function (Rappold *et al*, 2014; Guo *et al*, 2013; Su & Qi, 2013) but also raised important questions concerning long-term effects on cellular viability, namely in neurons. Prevention of mitochondrial fission has also been associated with excessively fused mitochondria, oxidative damage, and accumulation of ubiquitin and mitophagy markers and loss of respiratory functions (Berthet *et al*, 2014; Kageyama *et al*, 2014; Malena *et al*, 2009; Möpert *et al*, 2009; Parone *et al*, 2008). It all comes down to *aurea mediocritas*, as the roman poet Horacio proclaimed. Efforts should be made in order to achieve an adequate equilibrium between both processes of mitochondrial fission and fusion (Reddy, 2014). Consequently, by decreasing fission modulators in mitochondria, but not being able to affect the mutant cells capacity to maintain functional mitochondria, damaged mitochondria displaying decreased $\Delta\psi_m$ would not be separated from the remaining functional network. The resulting damage dissipation throughout the mitochondrial network could then worsen mitochondrial function in HD cells after SIRT3OE.

Wang and co-authors found that after camptothecin-derived genotoxic stress, cultured postnatal mouse cortical neurons presented a more tubular mitochondrial morphology in contrast to the fragmentation seen upon the same treatment in fibroblasts that could be traced to p53-dependent declines in expression of Drp1 and Parkin (Wang *et al*, 2013). ST*Hdh*$^{Q111/Q111}$ cells also showed increased levels of p53 (Trettel *et al*, 2000), which has been associated with increased cell death signaling in HD (Tsoi & Chan, 2013; Illuzzi *et al*, 2011). Besides induction of apoptosis, p53 regulates a wide range of parameters regarding mitochondrial function, including mitochondrial dynamics (Wang *et al*, 2014). A study by Guo and colleagues implicated an interaction between p53 and Drp1 resorting to several HD models, including ST*Hdh*$^{Q7/Q7}$ and ST*Hdh*$^{Q111/Q111}$ cells. They suggested that while Drp1 accumulation in mitochondria does not depend on p53, this protein is required for

Drp1-mediated mitochondrial dysfunction (Guo *et al*, 2013). Interestingly, the Drp1--p53 complex may also include mHTT, interacting not only with Drp1 (Song *et al*, 2011) but also with p53 (Ryan *et al*, 2006).

When it comes to mitochondrial SIRTs and their connection with apoptosis, curiously little is known despite mitochondria's critical role (Verdin *et al*, 2010). SIRT3 has a more known cytoprotective effect (Song *et al*, 2013; Magnifico *et al*, 2013; Li *et al*, 2010) although a pro-apoptotic function has been implicated in Bcl2--p53- and JNK-dependent apoptosis (Pfister *et al*, 2008; Allison & Milner, 2007). SIRT3 has also been more explored in cancer, being suggested as a potential tumor suppressor due to reduced levels found in human breast cancers, with *SIRT3*$^{-/-}$ knock-out mice developing mammary tumors (Kim *et al*, 2010a)

Further studies are thus required to ultimately explore the possibility of SIRT3 exerting a pro-apoptotic effect and if it can be related with increased levels, as those generated through overexpression. In addition, investigating a possible interplay between SIRT3, p53 and Drp1 and what the presence of mHTT could implicate may also elucidate what lies behind some of our most intriguing results.

Taken as a whole, our findings indicate that modulation of SIRT3 levels in an HD striatal precursor cell model mitigates excessive mitochondrial fragmentation derived from the presence of mHTT by decreasing the presence of fission modulators in mitochondria, increasing additionally macroautophagy signaling. It failed however to improve overall mitochondrial function and turnover. Efforts should be made to comprehend possible signaling pathways that could increase mitophagy (not only PINK1/Parkin-dependent) and lead to the consequential degradation of damaged mitochondria (Hwang *et al*, 2015). Looking for new adaptor molecules other than p62 that could efficiently deliver damaged mitochondria or aggregation prone polyQ proteins to autophagosomes (Lazarou *et al*, 2015; Lu *et al*, 2014) could be an ideal therapeutical strategy.

4.2. CONCLUSIONS

HD is a neurodegenerative disease caused by expanded polyQ in HTT, resulting in general cytotoxicity and neuronal cell death. The presence of mHTT causes mitochondrial dysfunction, with consequent bioenergetic deficit, increased ROS production, decreased Ca^{2+} buffering capacity and release of proapototic molecules such as cytochrome *c.* Mitochondrial dynamics (biogenesis, fission/fusion balance, trafficking, mitophagy) are required to maintain proper mitochondrial function and have been reported to be impaired in HD. Thus, attempting to restore some of these processes could help restore mitochondrial function and ameliorate HD pathogenesis. We herein explored the effect of increased SIRT3 levels on mitochondrial morphology, fission/fusion balance and mitophagy in a HD cell model.

We confirmed the presence of increased mitochondrial fragmentation in HD striatal cells, with increased Drp1 accumulation in mitochondria, increased protein levels of Fis1 along with reduced levels of fusion-related proteins (Mfn2, OPA1).

In addition, we explored PINK1/Parkin-dependent mitophagy in ST*Hdh* cells. The reduced protein levels of Parkin and PINK1 in mutant cells along with unchanged levels of activating Parkin phosphorylation (S65), when compared to wild-type cells, suggested that this particular mitophagy pathway is impaired in HD striatal cells. Corroborating these data, reduced levels of autophagy adaptor p62 were found in ST*Hdh*$^{Q111/Q111}$ cells. Indeed, impaired cargo recognition by autophagososmes has been described in HD models. Further studies are needed to assess the veracity of these findings, as specific mitophagy changes could be easier to identify upon induction. To do so, mitophagy should be induced, using ionophore CCCP, for instance, to destabilize $\Delta\psi_m$. Inhibitors of autophagy flux should also be considered to unravel the origin of reduced protein levels, namely inhibitors that act at the level of post-sequestration into autophagosomes or at the autolysosomes, such as bafilomycin A1 and chloroquine. Additionally, PINK1/Parkin-independent pathways should be explored.

We found that SIRT3OE was capable to restore mitochondrial morphology in ST*Hdh*$^{Q111/Q111}$ cells, increasing the number of cells presenting a tubular mitochondrial morphology with a marked decreased in the number of cells with

fragmented mitochondria. We credited this effect to reduction of Fis1 protein levels and decreased Drp1 accumulation in mitochondria. Macroautophagy also appears to be activated and could be related to a cellular response to nutrient deficiency.

AS SIRT3OE failed to ameliorate mitochondrial function (*Naia* et al*, unpublished data*) regardless of restored mitochondrial morphology, the results implicate that a decrease in excessive fragmentation by reduction of fission alone may not serve as a therapeutic strategy without improvement of other processes involved in mitochondrial dynamics and/or degradation.

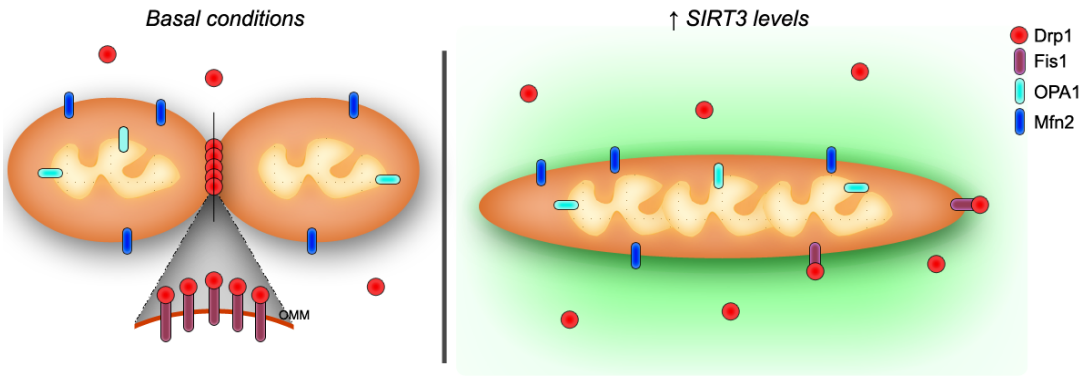

Fig. 10 | Schematic representation of fission/fusion-related protein localization in untransfected and in ST*Hdh*$^{Q111/Q111}$ cells overexpressing SIRT3.
HD striatal cells show a predisposition towards fission, with increased Fis1 levels and increased Drp1 accumulation in mitochondria along with decreased levels of proteins involved in mitochondrial fusion (Mfn2, OPA1). As such, fragmented mitochondria are a key feature in mutant cells. Upon SIRT3 overexpression, a higher percentage of ST*Hdh*$^{Q111/Q111}$ cells display tubular mitochondria, with reduced Fis1 levels and decreased Drp1 accumulation in mitochondria. Fusion-related proteins are not significantly affected under these conditions.

REFERENCES

Allen GFG, Toth R, James J & Ganley IG (2013) Loss of iron triggers PINK1/Parkin-independent mitophagy. *EMBO reports* **14:** 1127–35

Allison SJ & Milner J (2007) SIRT3 is pro-apoptotic and participates in distinct basal apoptotic pathways. *Cell Cycle* **6:** 2669–2677

Amadoro G, Corsetti V, Florenzano F, Atlante A, Bobba A, Nicolin V, Nori SL & Calissano P (2014) Morphological and bioenergetic demands underlying the mitophagy in post-mitotic neurons: The pink-parkin pathway. *Frontiers in Aging Neuroscience* **6:** 18

Andrade MA, Petosa C, O'Donoghue SI, Müller CW & Bork P (2001) Comparison of ARM and HEAT protein repeats. *Journal of Molecular Biology* **309:** 1–18

Appl T, Kaltenbach L, Lo DC & Terstappen GC (2012) Targeting mutant huntingtin for the development of disease-modifying therapy. *Drug Discovery Today* **17:** 1217–1223

Ashrafi G, Schlehe JS, LaVoie MJ & Schwarz TL (2014) Mitophagy of damaged mitochondria occurs locally in distal neuronal axons and requires PINK1 and Parkin. *The Journal of Cell Biology* **206:** 655–670

Ashrafi G & Schwarz TL (2015) PINK1- and PARK2-mediated local mitophagy in distal neuronal axons. *Autophagy* **11:** 187–9

Atwal RS, Xia J, Pinchev D, Taylor J, Epand RM & Truant R (2007) Huntingtin has a membrane association signal that can modulate huntingtin aggregation, nuclear entry and toxicity. *Human Molecular Genetics* **16:** 2600–2615

Ayala-Peña S (2013) Role of oxidative DNA damage in mitochondrial dysfunction and Huntington's disease pathogenesis. *Free Radical Biology and Medicine* **62:** 102–110

Bae B II, Xu H, Igarashi S, Fujimuro M, Agrawal N, Taya Y, Hayward SD, Moran TH, Montell C, Ross CA, Snyder SH & Sawa A (2005) p53 mediates cellular dysfunction and behavioral abnormalities in Huntington's disease. *Neuron* **47:** 29–41

Bai H, Inoue J, Kawano T & Inazawa J (2012) A transcriptional variant of the LC3A gene is involved in autophagy and frequently inactivated in human cancers. *Oncogene* **31:** 4397–4408

Bano D, Zanetti F, Mende Y & Nicotera P (2011) Neurodegenerative processes in Huntington's disease. *Cell Death and Disease* **2:** e228

Bell EL & Guarente L (2011) The SirT3 Divining Rod Points to Oxidative Stress. *Molecular Cell* **42:** 561–568

Benchoua A, Trioulier Y, Zala D, Gaillard M-C, Lefort N, Dufour N, Saudou F, Elalouf J-M, Hirsch E, Hantraye P, Déglon N & Brouillet E (2006) Involvement of mitochondrial

complex II defects in neuronal death produced by N-terminus fragment of mutated huntingtin. *Molecular Biology of the Cell* **17:** 1652–1663

Berent S, Giordani B, Lehtinen S, Markel D, Penney JB, Buchtel HA, Starosta-Rubinstein S, Hichwa R & Young AB (1988) Positron emission tomographic scan investigations of Huntington's disease: cerebral metabolic correlates of cognitive function. *Annals of Neurology* **23:** 541–546

Berthet A, Margolis EB, Zhang J, Hsieh I, Zhang J, Hnasko TS, Ahmad J, Edwards RH, Sesaki H, Huang EJ & Nakamura K (2014) Loss of mitochondrial fission depletes axonal mitochondria in midbrain dopamine neurons. *The Journal of Neuroscience* **34:** 14304–17

Van der Bliek AM, Shen Q & Kawajiri S (2013) Mechanisms of Mitochondrial Fission and Fusion. *Cold Spring Harbor Perspectives in Biology* **5:** a011072–a011072

Bobrowska A, Donmez G, Weiss A, Guarente L & Bates G (2012) SIRT2 Ablation Has No Effect on Tubulin Acetylation in Brain, Cholesterol Biosynthesis or the Progression of Huntington's Disease Phenotypes In Vivo. *PLoS ONE* **7:** e34805

Bobrowska A, Paganetti P, Matthias P & Bates GP (2011) Hdac6 Knock-Out Increases Tubulin Acetylation but Does Not Modify Disease Progression in the R6/2 Mouse Model of Huntington's Disease. *PLoS ONE* **6:** e20696

Borrell-Pagès M, Zala D, Humbert S & Saudou F (2006) Huntington's disease: From huntingtin function and dysfunction to therapeutic strategies. *Cellular and Molecular Life Sciences* **63:** 2642–2660

Bossy B, Petrilli A, Klinglmayr E, Chen J, Lütz-Meindl U, Knott AB, Masliah E, Schwarzenbacher R & Bossy-Wetzel E (2010) S-nitrosylation of DRP1 does not affect enzymatic activity and is not specific to Alzheimer's disease. *Journal of Alzheimer's Disease* **20:** 1–22

Brandstaetter H, Kruppa AJ & Buss F (2014) Huntingtin is required for ER-to-Golgi transport and for secretory vesicle fusion at the plasma membrane. *Disease Models & Mechanisms* **7:** 1335–1340

Buhlman L, Damiano M, Bertolin G, Ferrando-Miguel R, Lombès A, Brice A & Corti O (2014) Functional interplay between Parkin and Drp1 in mitochondrial fission and clearance. *Biochimica et Biophysica Acta (BBA) - Molecular Cell Research* **1843:** 2012–2026

Carroll JB, Warby SC, Southwell AL, Doty CN, Greenlee S, Skotte N, Hung G, Bennett CF, Freier SM & Hayden MR (2011) Potent and Selective Antisense Oligonucleotides Targeting Single-Nucleotide Polymorphisms in the Huntington Disease Gene / Allele-Specific Silencing of Mutant Huntingtin. *Molecular Therapy* **19:** 2178–2185

Cattaneo E (2003) Dysfunction of Wild-Type Huntingtin in Huntington disease. *Physiology* **18:** 34–37

Cattaneo E, Zuccato C & Tartari M (2005) Normal huntingtin function: an alternative approach to Huntington's disease. *Nature Reviews Neuroscience Neuroscience* **6:** 919–30

Caulfield TR, Fiesel FC, Moussaud-Lamodière EL, Dourado DFAR, Flores SC & Springer W (2014) Phosphorylation by PINK1 Releases the UBL Domain and Initializes the Conformational Opening of the E3 Ubiquitin Ligase Parkin. *PLoS Computational Biology* **10:** e1003935

Caviston JP & Holzbaur ELF (2009) Huntingtin as an essential integrator of intracellular vesicular trafficking. *Trends in Cell Biology* **19:** 147–155

Cereghetti GM, Stangherlin A, Martins de Brito O, Chang CR, Blackstone C, Bernardi P & Scorrano L (2008) Dephosphorylation by calcineurin regulates translocation of Drp1 to mitochondria. *Proceedings of the National Academy of Sciences of the United States of America* **105:** 15803–15808

Chang DTW, Rintoul GL, Pandipati S & Reynolds IJ (2006) Mutant huntingtin aggregates impair mitochondrial movement and trafficking in cortical neurons. *Neurobiology of Disease* **22:** 388–400

Chaturvedi RK, Adhihetty P, Shukla S, Hennessy T, Calingasan N, Yang L, Starkov A, Kiaei M, Cannella M, Sassone J, Ciammola A, Squitieri F & Beal MF (2009) Impaired PGC-1 function in muscle in Huntington's disease. *Human Molecular Genetics* **18:** 3048–3065

Chen H & Chan DC (2004) Mitochondrial Dynamics in Mammals. *Current Topics in Developmental Biology* **59:** 119–144

Chen H & Chan DC (2009) Mitochondrial dynamics-fusion, fission, movement, and mitophagy-in neurodegenerative diseases. *Human Molecular Genetics* **18:** R169–R176

Chen Y & Dorn GW (2013) PINK1-Phosphorylated Mitofusin 2 Is a Parkin Receptor for Culling Damaged Mitochondria. *Science* **340:** 471–475

Choo YS, Johnson GVW, MacDonald M, Detloff PJ & Lesort M (2004) Mutant huntingtin directly increases susceptibility of mitochondria to the calcium-induced permeability transition and cytochrome c release. *Human Molecular Genetics* **13:** 1407–1420

Cicchetti F, Lacroix S, Cisbani G, Vallières N, Saint-Pierre M, St-Amour I, Tolouei R, Skepper JN, Hauser RA, Mantovani D, Barker RA & Freeman TB (2014) Mutant huntingtin is present in neuronal grafts in huntington disease patients. *Annals of Neurology* **76:** 31–42

Coppedè F (2014) The potential of epigenetic therapies in neurodegenerative diseases. *Frontiers in Genetics* **5:** 220

Cornett J, Cao F, Wang C-E, Ross CA, Bates GP, Li S-H & Li X-J (2005) Polyglutamine expansion of huntingtin impairs its nuclear export. *Nature Genetics* **37:** 198–204

Costa M do C, Magalhães P, Ferreirinha F, Guimarães L, Januário C, Gaspar I, Loureiro L, Vale J, Garrett C, Regateiro F, Magalhães M, Sousa A, Maciel P & Sequeiros J (2003) Molecular diagnosis of Huntington disease in Portugal: implications for genetic counselling and clinical practice. *European Journal of Human Genetics* **11:** 872–878

Costa V, Giacomello M, Hudec R, Lopreiato R, Ermak G, Lim D, Malorni W, Davies KJA, Carafoli E & Scorrano L (2010) Mitochondrial fission and cristae disruption increase the response of cell models of Huntington's disease to apoptotic stimuli. *EMBO Molecular Medicine* **2:** 490–503

Costa V & Scorrano L (2012) Shaping the role of mitochondria in the pathogenesis of Huntington's disease. *The EMBO Journal* **31:** 1853–1864

Cui L, Jeong H, Borovecki F, Parkhurst CN, Tanese N & Krainc D (2006) Transcriptional Repression of PGC-1α by Mutant Huntingtin Leads to Mitochondrial Dysfunction and Neurodegeneration. *Cell* **127:** 59–69

Deas E, Plun-Favreau H, Gandhi S, Desmond H, Kjaer S, Loh SHY, Renton AEM, Harvey RJ, Whitworth AJ, Martins LM, Abramov AY & Wood NW (2011a) PINK1 cleavage at position A103 by the mitochondrial protease PARL. *Human Molecular Genetics* **20:** 867–879

Deas E, Wood NW & Plun-Favreau H (2011b) Mitophagy and Parkinson's disease: The PINK1–parkin link. *Biochimica et Biophysica Acta (BBA) - Molecular Cell Research* **1813:** 623–633

Desmond CR, Atwal RS, Xia J & Truant R (2012) Identification of a Karyopherin 1/ 2 Proline-Tyrosine Nuclear Localization Signal in Huntingtin Protein. *Journal of Biological Chemistry* **287:** 39626–39633

Detmer SA & Chan DC (2007) Functions and dysfunctions of mitochondrial dynamics. *Nature Reviews Molecular Cell Biology* **8:** 870–879

Devireddy S, Liu A, Lampe T & Hollenbeck PJ (2015) The Organization of Mitochondrial Quality Control and Life Cycle in the Nervous System In Vivo in the Absence of PINK1. *Journal of Neuroscience* **35:** 9391–9401

Dompierre JP, Godin JD, Charrin BC, Cordelieres FP, King SJ, Humbert S & Saudou F (2007) Histone Deacetylase 6 Inhibition Compensates for the Transport Deficit in Huntington's Disease by Increasing Tubulin Acetylation. *Journal of Neuroscience* **27:** 3571–3583

Du Y, Wooten MC & Wooten MW (2009) Oxidative damage to the promoter region of SQSTM1/p62 is common to neurodegenerative disease. *Neurobiology of Disease* **35:** 302–310

Van Dyke MW (2014) Lysine Deacetylase (KDAC) Regulatory Pathways: an Alternative Approach to Selective Modulation. *ChemMedChem* **9:** 511–522

Ermak G, Hench KJ, Chang KT, Sachdev S & Davies KJA (2009) Regulator of Calcineurin (RCAN1-1L) Is Deficient in Huntington Disease and Protective against Mutant Huntingtin Toxicity in Vitro. *Journal of Biological Chemistry* **284:** 11845–11853

Federico A, Cardaioli E, Da Pozzo P, Formichi P, Gallus GN & Radi E (2012) Mitochondria, oxidative stress and neurodegeneration. *Journal of the Neurological Sciences* **322:** 254–262

Feng Z, Jin S, Zupnick A, Hoh J, de Stanchina E, Lowe S, Prives C & Levine AJ (2006) p53 tumor suppressor protein regulates the levels of huntingtin gene expression. *Oncogene* **25:** 1–7

Ferreira IL, Nascimento M V., Ribeiro M, Almeida S, Cardoso SM, Grazina M, Pratas J, Santos MJ, Januário C, Oliveira CR & Rego AC (2010) Mitochondrial-dependent apoptosis in Huntington's disease human cybrids. *Experimental Neurology* **222:** 243–255

Finkel T, Deng C-X & Mostoslavsky R (2009) Recent progress in the biology and physiology of sirtuins. *Nature* **460:** 587–591

Finley LWS, Haas W, Desquiret-Dumas V, Wallace DC, Procaccio V, Gygi SP & Haigis MC (2011) Succinate Dehydrogenase Is a Direct Target of Sirtuin 3 Deacetylase Activity. *PLoS ONE* **6:** e23295

Fu J, Jin J, Cichewicz RH, Hageman S a., Ellis TK, Xiang L, Peng Q, Jiang M, Arbez N, Hotaling K, Ross C a. & Duan W (2012) Trans-(-)-ε-viniferin increases mitochondrial sirtuin 3 (SIRT3), activates AMP-activated Protein Kinase (AMPK), and protects cells in models of huntington disease. *Journal of Biological Chemistry* **287:** 24460–24472

Fukata Y & Fukata M (2010) Protein palmitoylation in neuronal development and synaptic plasticity. *Nature Reviews Neuroscience* **11:** 161–175

Gautier CA, Kitada T & Shen J (2008) Loss of PINK1 causes mitochondrial functional defects and increased sensitivity to oxidative stress. *Proceedings of the National Academy of Sciences* **105:** 11364–11369

Gervais FG, Singaraja R, Xanthoudakis S, Gutekunst C-A, Leavitt BR, Metzler M, Hackam AS, Tam J, Vaillancourt JP, Houtzager V, Rasper DM, Roy S, Hayden MR & Nicholson DW (2002) Recruitment and activation of caspase-8 by the Huntingtin-interacting protein Hip-1 and a novel partner Hippi. *Nature Cell Biology* **4:** 95–105

Ghavami S, Shojaei S, Yeganeh B, Ande SR, Jangamreddy JR, Mehrpour M, Christoffersson J, Chaabane W, Moghadam AR, Kashani HH, Hashemi M, Owji AA & Łos MJ (2014) Autophagy and apoptosis dysfunction in neurodegenerative disorders. *Progress in Neurobiology* **112:** 24–49

Gil JM & Rego AC (2008) Mechanisms of neurodegeneration in Huntington's disease. *European Journal of Neuroscience* **27:** 2803–2820

Goebel HH, Heipertz R, Scholz W, Iqbal K & Tellez-Nagel I (1978) Juvenile Huntington chorea: Clinical, ultrastructural, and biochemical studies. *Neurology* **28:** 23–23

Gomes LC & Scorrano L (2013) Mitochondrial morphology in mitophagy and macroautophagy. *Biochimica et Biophysica Acta (BBA) - Molecular Cell Research* **1833:** 205–212

Greene AW, Grenier K, Aguileta MA, Muise S, Farazifard R, Haque ME, McBride HM, Park DS & Fon EA (2012) Mitochondrial processing peptidase regulates PINK1 processing, import and Parkin recruitment. *EMBO reports* **13:** 378–385

Griffin EE, Detmer SA & Chan DC (2006) Molecular mechanism of mitochondrial membrane fusion. *Biochimica et Biophysica Acta (BBA) - Molecular Cell Research* **1763:** 482–489

Gu X, Greiner ER, Mishra R, Kodali R, Osmand A, Finkbeiner S, Steffan JS, Thompson LM, Wetzel R & Yang XW (2009) Serines 13 and 16 Are Critical Determinants of Full-Length Human Mutant Huntingtin Induced Disease Pathogenesis in HD Mice. *Neuron* **64:** 828–840

Guarente L (2008) Mitochondria-A Nexus for Aging, Calorie Restriction, and Sirtuins? *Cell* **132:** 171–176

Guarente L (2011) Sirtuins, Aging, and Metabolism. *Cold Spring Harbor Symposia on Quantitative Biology* **76:** 81–90

Guedes-Dias P & Oliveira JMA (2013) Lysine deacetylases and mitochondrial dynamics in neurodegeneration. *Biochimica et Biophysica Acta (BBA) - Molecular Basis of Disease* **1832:** 1345–1359

Guidetti P, Charles V, Chen E-Y, Reddy PH, Kordower JH, Whetsell WO, Schwarcz R & Tagle D a (2001) Early Degenerative Changes in Transgenic Mice Expressing Mutant Huntingtin Involve Dendritic Abnormalities but No Impairment of Mitochondrial Energy Production. *Experimental Neurology* **169:** 340–350

Guo X, Disatnik M-H, Monbureau M, Shamloo M, Mochly-Rosen D & Qi X (2013) Inhibition of mitochondrial fragmentation diminishes Huntington's disease–associated neurodegeneration. *Journal of Clinical Investigation* **123:** 5371–5388

Haigis MC & Guarente LP (2006) Mammalian sirtuins - Emerging roles in physiology, aging, and calorie restriction. *Genes and Development* **20:** 2913–2921

Haigis MC & Sinclair DA (2010) Mammalian Sirtuins: Biological Insights and Disease Relevance. *Annual Review of Pathology: Mechanisms of Disease* **5:** 253–295

Harjes P & Wanker EE (2003) The hunt for huntingtin function: Interaction partners tell many different stories. *Trends in Biochemical Sciences* **28:** 425–433

Hathorn T, Snyder-Keller A & Messer A (2011) Nicotinamide improves motor deficits and upregulates PGC-1α and BDNF gene expression in a mouse model of Huntington's disease. *Neurobiology of Disease* **41:** 43–50

Haun F, Nakamura T, Shiu AD, Cho D-H, Tsunemi T, Holland EA, La Spada AR & Lipton SA (2013) S-Nitrosylation of Dynamin-Related Protein 1 Mediates Mutant Huntingtin-Induced Mitochondrial Fragmentation and Neuronal Injury in Huntington's Disease. *Antioxidants & Redox Signaling* **19:** 1173–1184

He W, Newman JC, Wang MZ, Ho L & Verdin E (2012) Mitochondrial sirtuins: Regulators of protein acylation and metabolism. *Trends in Endocrinology and Metabolism* **23:** 467–476

Heng MY, Detloff PJ, Paulson HL & Albin RL (2010) Early alterations of autophagy in Huntington disease-like mice. *Autophagy* **6:** 1206–1208

Herbert AD, Carr AM & Hoffmann E (2014) FindFoci: A Focus Detection Algorithm with Automated Parameter Training That Closely Matches Human Assignments, Reduces Human Inconsistencies and Increases Speed of Analysis. *PLoS ONE* **9:** e114749

Hipp MS, Patel CN, Bersuker K, Riley BE, Kaiser SE, Shaler TA, Brandeis M & Kopito RR (2012) Indirect inhibition of 26S proteasome activity in a cellular model of Huntington's disease. *The Journal of Cell Biology* **196:** 573–587

Hirota Y, Yamashita S, Kurihara Y, Jin X, Aihara M, Saigusa T, Kang D & Kanki T (2015) Mitophagy is primarily due to alternative autophagy and requires the MAPK1 and MAPK14 signaling pathways. *Autophagy* **11:** 332–43

Hirschey MD, Shimazu T, Goetzman E, Jing E, Schwer B, Lombard DB, Grueter CA, Harris C, Biddinger S, Ilkayeva OR, Stevens RD, Li Y, Saha AK, Ruderman NB, Bain JR, Newgard CB, Farese R V, Alt FW, Kahn CR & Verdin E (2010) SIRT3 regulates mitochondrial fatty-acid oxidation by reversible enzyme deacetylation. *Nature* **464:** 121–125

Humbert S, Bryson EA, Cordelières FP, Connors NC, Datta SR, Finkbeiner S, Greenberg ME & Saudou F (2002) The IGF-1/Akt pathway is neuroprotective in Huntington's disease and involves huntingtin phosphorylation by Akt. *Developmental Cell* **2:** 831–837

Hwang S, Disatnik M-H & Mochly-Rosen D (2015) Impaired GAPDH-induced mitophagy contributes to the pathology of Huntington's disease. *EMBO Molecular Medicine* **7:** 1307–1326

Illuzzi JL, Vickers CA & Kmiec EB (2011) Modifications of p53 and the DNA damage response in cells expressing mutant form of the protein huntingtin. *Journal of Molecular Neuroscience* **45:** 256–268

Ismailoglu I, Chen Q, Popowski M, Yang L, Gross SS & Brivanlou AH (2014) Huntingtin protein is essential for mitochondrial metabolism, bioenergetics and structure in murine embryonic stem cells. *Developmental Biology* **391:** 230–240

Jakovcevski M & Akbarian S (2012) Epigenetic mechanisms in neurological disease. *Nature Medicine* **18:** 1194–1204

Jana NR (2001) Altered proteasomal function due to the expression of polyglutamine-expanded truncated N-terminal huntingtin induces apoptosis by caspase activation through mitochondrial cytochrome c release. *Human Molecular Genetics* **10:** 1049–1059

Jeong H, Cohen DE, Cui L, Supinski A, Savas JN, Mazzulli JR, Yates JR, Bordone L, Guarente L & Krainc D (2011) Sirt1 mediates neuroprotection from mutant huntingtin by activation of the TORC1 and CREB transcriptional pathway. *Nature Medicine* **18:** 159–165

Jia H, Kast RJ, Steffan JS & Thomas EA (2012a) Selective histone deacetylase (HDAC) inhibition imparts beneficial effects in Huntington's disease mice: Implications for the ubiquitin-proteasomal and autophagy systems. *Human Molecular Genetics* **21:** 5280–5293

Jia H, Morris CD, Williams RM, Loring JF & Thomas EA (2015) HDAC inhibition imparts beneficial transgenerational effects in Huntington's disease mice via altered DNA and histone methylation. *Proceedings of the National Academy of Sciences* **112:** E56–E64

Jia H, Pallos J, Jacques V, Lau A, Tang B, Cooper A, Syed A, Purcell J, Chen Y, Sharma S, Sangrey GR, Darnell SB, Plasterer H, Sadri-Vakili G, Gottesfeld JM, Thompson LM, Rusche JR, Marsh JL & Thomas EA (2012b) Histone deacetylase (HDAC) inhibitors targeting HDAC3 and HDAC1 ameliorate polyglutamine-elicited phenotypes in model systems of Huntington's disease. *Neurobiology of Disease* **46:** 351–361

Jiang M, Wang J, Fu J, Du L, Jeong H, West T, Xiang L, Peng Q, Hou Z, Cai H, Seredenina T, Arbez N, Zhu S, Sommers K, Qian J, Zhang J, Mori S, Yang XW, Tamashiro KLK, Aja S, et al (2011) Neuroprotective role of Sirt1 in mammalian models of Huntington's disease through activation of multiple Sirt1 targets. *Nature Medicine* **18:** 153–158

Jin YN & Johnson GVW (2010) The interrelationship between mitochondrial dysfunction and transcriptional dysregulation in Huntington disease. *Journal of Bioenergetics and Biomembranes* **42:** 199–205

Jin YN, Yu Y V., Gundemir S, Jo C, Cui M, Tieu K & Johnson GVW (2013) Impaired Mitochondrial Dynamics and Nrf2 Signaling Contribute to Compromised Responses to Oxidative Stress in Striatal Cells Expressing Full-Length Mutant Huntingtin. *PLoS ONE* **8:** e57932

Johri A, Chandra A & Beal MF (2013) PGC-1α mitochondrial dysfunction, and Huntington's disease. *Free Radical Biology and Medicine* **62:** 37–46

Kageyama Y, Hoshijima M, Seo K, Bedja D, Sysa-Shah P, Andrabi SA, Chen W, Hoke A, Dawson VL, Dawson TM, Gabrielson K, Kass DA, Iijima M & Sesaki H (2014) Parkin-independent mitophagy requires Drp1 and maintains the integrity of mammalian heart and brain. *The EMBO Journal* **33:** 2798–2813

Kalchman MA, Graham RK, Xia G, Brook Koide H, Graeme Hodgson J, Graham KC, Paul Goldberg Y, Dan Gietz R, Pickart CM & Hayden MR (1996) Huntingtin is ubiquitinated and interacts with a specific ubiquitin- conjugating enzyme. *Journal of Biological Chemistry* **271:** 19385–19394

Karabulut NP & Frishman D (2015) Tissue-specific sequence and structural environments of lysine acetylation sites. *Journal of Structural Biology* **191:** 39–48

Kazlauskaite A, Martínez-Torres RJ, Wilkie S, Kumar A, Peltier J, Gonzalez A, Johnson C, Zhang J, Hope AG, Peggie M, Trost M, van Aalten DM, Alessi DR, Prescott AR, Knebel A, Walden H & Muqit MM (2015) Binding to serine 65-phosphorylated ubiquitin primes Parkin for optimal PINK1-dependent phosphorylation and activation. *EMBO reports* **16:** 939–54

Khalil B, El Fissi N, Aouane a, Cabirol-Pol M-J, Rival T & Liévens J-C (2015) PINK1-induced mitophagy promotes neuroprotection in Huntington's disease. *Cell Death and Disease* **6:** e1617

Kim HS, Patel K, Muldoon-Jacobs K, Bisht KS, Aykin-Burns N, Pennington JD, van der Meer R, Nguyen P, Savage J, Owens KM, Vassilopoulos A, Ozden O, Park SH, Singh KK, Abdulkadir SA, Spitz DR, Deng CX & Gius D (2010a) SIRT3 Is a Mitochondria-Localized Tumor Suppressor Required for Maintenance of Mitochondrial Integrity and Metabolism during Stress. *Cancer Cell* **17:** 41–52

Kim J, Moody JP, Edgerly CK, Bordiuk OL, Cormier K, Smith K, Flint Beal M & Ferrante RJ (2010b) Mitochondrial loss, dysfunction and altered dynamics in Huntington's disease. *Human Molecular Genetics* **19:** 3919–3935

Kim SC, Sprung R, Chen Y, Xu Y, Ball H, Pei J, Cheng T, Kho Y, Xiao H, Xiao L, Grishin N V., White M, Yang XJ & Zhao Y (2006) Substrate and Functional Diversity of Lysine Acetylation Revealed by a Proteomics Survey. *Molecular Cell* **23:** 607–618

Knott AB, Perkins G, Schwarzenbacher R & Bossy-Wetzel E (2008) Mitochondrial fragmentation in neurodegeneration. *Nature Reviews Neuroscience* **9:** 505–518

Kumar A, Vaish M & Ratan RR (2014) Transcriptional dysregulation in Huntington's disease: A failure of adaptive transcriptional homeostasis. *Drug Discovery Today* **19:** 956–962

Van Laar VS, Arnold B, Cassady SJ, Chu CT, Burton EA & Berman SB (2011) Bioenergetics of neurons inhibit the translocation response of Parkin following rapid mitochondrial depolarization. *Human Molecular Genetics* **20:** 927–940

Lagouge M, Argmann C, Gerhart-Hines Z, Meziane H, Lerin C, Daussin F, Messadeq N, Milne J, Lambert P, Elliott P, Geny B, Laakso M, Puigserver P & Auwerx J (2006) Resveratrol improves mitochondrial function and protects against metabolic disease by activating SIRT1 and PGC-1alpha. *Cell* **127:** 1109–22

Lau D & Bading H (2009) Synaptic Activity-Mediated Suppression of p53 and Induction of Nuclear Calcium-Regulated Neuroprotective Genes Promote Survival through Inhibition of Mitochondrial Permeability Transition. *Journal of Neuroscience* **29:** 4420–4429

Lazarou M, Sliter DA, Kane LA, Sarraf SA, Wang C, Burman JL, Sideris DP, Fogel AI & Youle RJ (2015) The ubiquitin kinase PINK1 recruits autophagy receptors to induce mitophagy. *Nature* **524:** 309–314

Lee J, Hwang YJ, Ryu H, Kowall NW & Ryu H (2014) Nucleolar dysfunction in Huntington's disease. *Biochimica et Biophysica Acta (BBA) - Molecular Basis of Disease* **1842:** 785–790

Legros F (2002) Mitochondrial Fusion in Human Cells Is Efficient, Requires the Inner Membrane Potential, and Is Mediated by Mitofusins. *Molecular Biology of the Cell* **13:** 4343–4354

Leitman J, Barak B, Benyair R, Shenkman M, Ashery U, Hartl FU & Lederkremer GZ (2014) ER stress-induced eIF2-alpha phosphorylation underlies sensitivity of striatal neurons to pathogenic huntingtin. *PLoS ONE* **9:** e90803

Leitman J, Ulrich Hartl F & Lederkremer GZ (2013) Soluble forms of polyQ-expanded huntingtin rather than large aggregates cause endoplasmic reticulum stress. *Nature Communications* **4:** 2753

Lemasters JJ (2014) Variants of mitochondrial autophagy: Types 1 and 2 mitophagy and micromitophagy (Type 3). *Redox Biology* **2:** 749–754

Levine B & Kroemer G (2008) Autophagy in the Pathogenesis of Disease. *Cell* **132:** 27–42

Li S, Banck M, Mujtaba S, Zhou M-M, Sugrue MM & Walsh MJ (2010) p53-Induced Growth Arrest Is Regulated by the Mitochondrial SirT3 Deacetylase. *PLoS ONE* **5:** e10486

Li SH & Li XJ (2004) Huntingtin-protein interactions and the pathogenesis of Huntington's disease. *Trends in Genetics* **20:** 146–154

Lin M-Y & Sheng Z-H (2015) Regulation of mitochondrial transport in neurons. *Experimental Cell Research* **334:** 35–44

Lionaki E, Markaki M, Palikaras K & Tavernarakis N (2015) Mitochondria, autophagy and age-associated neurodegenerative diseases: New insights into a complex interplay. *Biochimica et Biophysica Acta (BBA) - Bioenergetics* **1847:** 1412–1423

Liu Y, Peng L, Seto E, Huang S & Qiu Y (2012) Modulation of histone deacetylase 6 (HDAC6) nuclear import and tubulin deacetylase activity through acetylation. *Journal of Biological Chemistry* **287:** 29168–29174

Lombard DB, Alt FW, Cheng H-L, Bunkenborg J, Streeper RS, Mostoslavsky R, Kim J, Yancopoulos G, Valenzuela D, Murphy A, Yang Y, Chen Y, Hirschey MD, Bronson RT,

Haigis M, Guarente LP, Farese R V, Weissman S, Verdin E & Schwer B (2007) Mammalian Sir2 Homolog SIRT3 Regulates Global Mitochondrial Lysine Acetylation. *Molecular and Cellular Biology* **27:** 8807–8814

Lombardi PM, Cole KE, Dowling DP & Christianson DW (2011) Structure, mechanism, and inhibition of histone deacetylases and related metalloenzymes. *Current Opinion in Structural Biology* **21:** 735–743

Lu J, Cheng K, Zhang B, Xu H, Cao Y, Guo F, Feng X & Xia Q (2015a) Novel mechanisms for superoxide-scavenging activity of human manganese superoxide dismutase determined by the K68 key acetylation site. *Free Radical Biology and Medicine* **85:** 114–126

Lu K, Psakhye I & Jentsch S (2014) A new class of ubiquitin-Atg8 receptors involved in selective autophagy and polyQ protein clearance. *Autophagy* **10:** 2381–2

Lu X, Wang L, Yu C, Yu D & Yu G (2015b) Histone Acetylation Modifiers in the Pathogenesis of Alzheimerâ€™s Disease. *Frontiers in Cellular Neuroscience* **9:** 226

Lu X-H & Yang XW (2012) 'Huntingtin holiday': progress toward an antisense therapy for Huntington's disease. *Neuron* **74:** 964–6

Luo S, Vacher C, Davies JE & Rubinsztein DC (2005) Cdk5 phosphorylation of huntingtin reduces its cleavage by caspases: Implications for mutant huntingtin toxicity. *Journal of Cell Biology* **169:** 647–656

Luthi-Carter R, Taylor DM, Pallos J, Lambert E, Amore A, Parker A, Moffitt H, Smith DL, Runne H, Gokce O, Kuhn A, Xiang Z, Maxwell MM, Reeves SA, Bates GP, Neri C, Thompson LM, Marsh JL & Kazantsev AG (2010) SIRT2 inhibition achieves neuroprotection by decreasing sterol biosynthesis. *Proceedings of the National Academy of Sciences of the United States of America* **107:** 7927–7932

Ben M'Barek K, Pla P, Orvoen S, Benstaali C, Godin JD, Gardier AM, Saudou F, David DJ & Humbert S (2013) Huntingtin Mediates Anxiety/Depression-Related Behaviors and Hippocampal Neurogenesis. *Journal of Neuroscience* **33:** 8608–8620

Magnifico S, Saias L, Deleglise B, Duplus E, Kilinc D, Miquel M-C, Viovy J-L, Brugg B & Peyrin J-M (2013) NAD+ acts on mitochondrial SirT3 to prevent axonal caspase activation and axonal degeneration. *The FASEB Journal* **27:** 4712–4722

Maiuri T, Woloshansky T, Xia J & Truant R (2013) The huntingtin N17 domain is a multifunctional CRM1 and Ran-dependent nuclear and cilial export signal. *Human Molecular Genetics* **22:** 1383–1394

Malena A, Loro E, Di Re M, Holt IJ & Vergani L (2009) Inhibition of mitochondrial fission favours mutant over wild-type mitochondrial DNA. *Human Molecular Genetics* **18:** 3407–3416

Mannella CA (2006) Structure and dynamics of the mitochondrial inner membrane cristae. *Biochimica et Biophysica Acta (BBA) - Molecular Cell Research* **1763:** 542–548

Martin DDO, Ladha S, Ehrnhoefer DE & Hayden MR (2015) Autophagy in Huntington disease and huntingtin in autophagy. *Trends in Neurosciences* **38:** 26–35

Martinez-Vicente M, Talloczy Z, Wong E, Tang G, Koga H, Kaushik S, de Vries R, Arias E, Harris S, Sulzer D & Cuervo AM (2010) Cargo recognition failure is responsible for inefficient autophagy in Huntington's disease. *Nature Neuroscience* **13:** 567–576

Mathias RA, Greco TM, Oberstein A, Budayeva HG, Chakrabarti R, Rowland EA, Kang Y, Shenk T & Cristea IM (2014) Sirtuin 4 is a lipoamidase regulating pyruvate dehydrogenase complex activity. *Cell* **159:** 1615–25

Matsuda N, Sato S, Shiba K, Okatsu K, Saisho K, Gautier CA, Sou Y -s., Saiki S, Kawajiri S, Sato F, Kimura M, Komatsu M, Hattori N & Tanaka K (2010) PINK1 stabilized by mitochondrial depolarization recruits Parkin to damaged mitochondria and activates latent Parkin for mitophagy. *The Journal of Cell Biology* **189:** 211–221

Matsuda S, Kitagishi Y & Kobayashi M (2013) Function and Characteristics of PINK1 in Mitochondria. *Oxidative Medicine and Cellular Longevity* **2013:** 1–6

McFarland KN, Das S, Sun TT, Leyfer D, Xia E, Sangrey GR, Kuhn A, Luthi-Carter R, Clark TW, Sadri-Vakili G & Cha J-HJ (2012) Genome-Wide Histone Acetylation Is Altered in a Transgenic Mouse Model of Huntington's Disease. *PLoS ONE* **7:** e41423

McKinnon C & Tabrizi SJ (2014) The Ubiquitin-Proteasome System in Neurodegeneration. *Antioxidants & Redox Signaling* **21:** 2302–2321

Michan S & Sinclair D (2007) Sirtuins in mammals: insights into their biological function. *Biochemical Journal* **404:** 1–13

Mielcarek M, Landles C, Weiss A, Bradaia A, Seredenina T, Inuabasi L, Osborne GF, Wadel K, Touller C, Butler R, Robertson J, Franklin SA, Smith DL, Park L, Marks PA, Wanker EE, Olson EN, Luthi-Carter R, van der Putten H, Beaumont V, et al (2013) HDAC4 Reduction: A Novel Therapeutic Strategy to Target Cytoplasmic Huntingtin and Ameliorate Neurodegeneration. *PLoS Biology* **11:** e1001717

Milakovic T & Johnson GVW (2005) Mitochondrial Respiration and ATP Production Are Significantly Impaired in Striatal Cells Expressing Mutant Huntingtin. *Journal of Biological Chemistry* **280:** 30773–30782

Milakovic T, Quintanilla R a & Johnson GVW (2006) Mutant Huntingtin Expression Induces Mitochondrial Calcium Handling Defects in Clonal Striatal Cells: FUNCTIONAL CONSEQUENCES. *Journal of Biological Chemistry* **281:** 34785–34795

Mochel F & Haller RG (2011) Energy deficit in Huntington disease: why it matters. *Journal of Clinical Investigation* **121:** 493–499

Möpert K, Hajek P, Frank S, Chen C, Kaufmann J & Santel A (2009) Loss of Drp1 function alters OPA1 processing and changes mitochondrial membrane organization. *Experimental Cell Research* **315:** 2165–2180

Morán M, Delmiro A, Blázquez A, Ugalde C, Arenas J & Martín MA (2014) Bulk autophagy, but not mitophagy, is increased in cellular model of mitochondrial disease. *Biochimica et Biophysica Acta (BBA) - Molecular Basis of Disease* **1842:** 1059–1070

Moreira PI, Siedlak SL, Wang X, Santos MS, Oliveira CR, Tabaton M, Nunomura A, Szweda LI, Aliev G, Smith MA, Zhu X & Perry G (2007) Autophagocytosis of Mitochondria Is Prominent in Alzheimer Disease. *Journal of Neuropathology and Experimental Neurology* **66:** 525–532

Morreale MK (2015) Huntington's Disease: Looking Beyond the Movement Disorder. In *Advances in Psychosomatic Medicine* pp 135–142.

Moumné L, Betuing S & Caboche J (2013) Multiple Aspects of Gene Dysregulation in Huntington's Disease. *Frontiers in Neurology* **4:** 127

Moumné L, Campbell K, Howland D, Ouyang Y & Bates GP (2012) Genetic Knock-Down of Hdac3 Does Not Modify Disease-Related Phenotypes in a Mouse Model of Huntington's Disease. *PLoS ONE* **7:** e31080

Naia L & Rego AC (2015) Sirtuins: double players in Huntington's disease. *Biochimica et Biophysica Acta (BBA) - Molecular Basis of Disease* **1852:** 2183–2194

Naia L, Ribeiro MJ & Rego AC (2012) Mitochondrial and metabolic-based protective strategies in Huntington's disease: the case of creatine and coenzyme Q. *Reviews in the Neurosciences* **23:** 13–28

Nakaso K, Yoshimoto Y, Yano H, Takeshima T & Nakashima K (2004) p53-mediated mitochondrial dysfunction by proteasome inhibition in dopaminergic SH-SY5Y cells. *Neuroscience Letters* **354:** 213–216

Napoli E, Wong S, Hung C, Ross-Inta C, Bomdica P & Giulivi C (2013) Defective mitochondrial disulfide relay system, altered mitochondrial morphology and function in Huntington's disease. *Human Molecular Genetics* **22:** 989–1004

Narendra D, Tanaka A, Suen D-F & Youle RJ (2008) Parkin is recruited selectively to impaired mitochondria and promotes their autophagy. *The Journal of Cell Biology* **183:** 795–803

Narendra DP, Jin SM, Tanaka A, Suen D-F, Gautier C a, Shen J, Cookson MR & Youle RJ (2010) PINK1 is selectively stabilized on impaired mitochondria to activate Parkin. *PLoS Biology* **8:** e1000298

Neuwald AF & Hirano T (2000) HEAT repeats associated with condensins, cohesins, and other complexes involved in chromosome-related functions. *Genome Research* **10:** 1445–1452

Nguyen GD, Gokhan S, Molero AE & Mehler MF (2013) Selective Roles of Normal and Mutant Huntingtin in Neural Induction and Early Neurogenesis. *PLoS ONE* **8:** e64368

Okatsu K, Kimura M, Oka T, Tanaka K & Matsuda N (2015) Unconventional PINK1 localization to the outer membrane of depolarized mitochondria drives Parkin recruitment. *Journal of Cell Science* **128:** 964–978

Oliveira JMA, Chen S, Almeida S, Riley R, Goncalves J, Oliveira CR, Hayden MR, Nicholls DG, Ellerby LM & Rego AC (2006) Mitochondrial-Dependent Ca2+ Handling in Huntington's Disease Striatal Cells: Effect of Histone Deacetylase Inhibitors. *Journal of Neuroscience* **26:** 11174–11186

Oliveira JMA, Jekabsons MB, Chen S, Lin A, Rego AC, Gonçalves J, Ellerby LM & Nicholls DG (2007) Mitochondrial dysfunction in Huntington's disease: The bioenergetics of isolated and in situ mitochondria from transgenic mice. *Journal of Neurochemistry* **101:** 241–249

Orr AL, Li S, Wang C-E, Li H, Wang J, Rong J, Xu X, Mastroberardino PG, Greenamyre JT & Li X-J (2008) N-Terminal Mutant Huntingtin Associates with Mitochondria and Impairs Mitochondrial Trafficking. *Journal of Neuroscience* **28:** 2783–2792

Otera H & Mihara K (2012) Mitochondrial Dynamics: Functional Link with Apoptosis. *International Journal of Cell Biology* **2012:** 1–10

Palikaras K & Tavernarakis N (2012) Mitophagy in neurodegeneration and aging. *Frontiers in Genetics* **3:** 297

Palikaras K & Tavernarakis N (2014) Mitochondrial homeostasis: The interplay between mitophagy and mitochondrial biogenesis. *Experimental Gerontology* **56:** 182–188

Panov A V, Gutekunst C-A, Leavitt BR, Hayden MR, Burke JR, Strittmatter WJ & Greenamyre JT (2002) Early mitochondrial calcium defects in Huntington's disease are a direct effect of polyglutamines. *Nature Neuroscience* **5:** 731–736

Panov A V., Lund S & Greenamyre JT (2005) Ca2+-induced permeability transition in human lymphoblastoid cell mitochondria from normal and Huntington's disease individuals. *Molecular and Cellular Biochemistry* **269:** 143–152

Parker JA, Arango M, Abderrahmane S, Lambert E, Tourette C, Catoire H & Néri C (2005) Resveratrol rescues mutant polyglutamine cytotoxicity in nematode and mammalian neurons. *Nature Genetics* **37:** 349–350

Parone PA, Da Cruz S, Tondera D, Mattenberger Y, James DI, Maechler P, Barja F & Martinou J-C (2008) Preventing Mitochondrial Fission Impairs Mitochondrial Function and Leads to Loss of Mitochondrial DNA. *PLoS ONE* **3:** e3257

Pellman JJ, Hamilton J, Brustovetsky T & Brustovetsky N (2015) Ca 2+ handling in isolated brain mitochondria and cultured neurons derived from the YAC128 mouse model of Huntington's disease. *Journal of Neurochemistry* **134:** 652–667

Pfister JA, Ma C, Morrison BE & D'Mello SR (2008) Opposing Effects of Sirtuins on Neuronal Survival: SIRT1-Mediated Neuroprotection Is Independent of Its Deacetylase Activity. *PLoS ONE* **3:** e4090

Pickrell AM, Fukui H, Wang X, Pinto M & Moraes CT (2011) The Striatum Is Highly Susceptible to Mitochondrial Oxidative Phosphorylation Dysfunctions. *Journal of Neuroscience* **31:** 9895–9904

Qiu X, Brown K, Hirschey MD, Verdin E & Chen D (2010) Calorie Restriction Reduces Oxidative Stress by SIRT3-Mediated SOD2 Activation. *Cell Metabolism* **12:** 662–667

Quintanilla R a, Jin YN, von Bernhardi R & Johnson GV (2013) Mitochondrial permeability transition pore induces mitochondria injury in Huntington disease. *Molecular Neurodegeneration* **8:** 45

Quintanilla RA, Jin YN, Fuenzalida K, Bronfman M & Johnson GVW (2008) Rosiglitazone Treatment Prevents Mitochondrial Dysfunction in Mutant Huntingtin-expressing Cells: POSSIBLE ROLE OF PEROXISOME PROLIFERATOR-ACTIVATED RECEPTOR- (PPAR) IN THE PATHOGENESIS OF HUNTINGTON DISEASE. *Journal of Biological Chemistry* **283:** 25628–25637

Quintanilla RA & Johnson GVW (2009) Role of mitochondrial dysfunction in the pathogenesis of Huntington's disease. *Brain Research Bulletin* **80:** 242–247

Radi E, Formichi P, Battisti C & Federico A (2014) Apoptosis and oxidative stress in neurodegenerative diseases. *Journal of Alzheimer's disease: JAD* **42:** S125–52

Rappold PM, Cui M, Grima JC, Fan RZ, de Mesy-Bentley KL, Chen L, Zhuang X, Bowers WJ & Tieu K (2014) Drp1 inhibition attenuates neurotoxicity and dopamine release deficits in vivo. *Nature Communications* **5:** 5244

Reddy PH (2014) Increased mitochondrial fission and neuronal dysfunction in Huntington's disease: Implications for molecular inhibitors of excessive mitochondrial fission. *Drug Discovery Today* **19:** 951–955

Reddy PH & Shirendeb UP (2012) Mutant huntingtin, abnormal mitochondrial dynamics, defective axonal transport of mitochondria, and selective synaptic degeneration in Huntington's disease. *Biochimica et Biophysica Acta (BBA) - Molecular Basis of Disease* **1822:** 101–110

Ribeiro M, Rosenstock TR, Oliveira AM, Oliveira CR & Rego AC (2014) Insulin and IGF-1 improve mitochondrial function in a PI-3K/Akt-dependent manner and reduce mitochondrial generation of reactive oxygen species in Huntington's disease knock-in striatal cells. *Free Radical Biology and Medicine* **74:** 129–144

Ribeiro M, Silva AC, Rodrigues J, Naia L & Rego AC (2013) Oxidizing effects of exogenous stressors in Huntington's disease knock-in striatal cells-protective effect oflcystamine and creatine. *Toxicological Sciences* **136:** 487–499

Rigamonti D, Bauer JH, De-Fraja C, Conti L, Sipione S, Sciorati C, Clementi E, Hackam A, Hayden MR, Li Y, Cooper JK, Ross CA, Govoni S, Vincenz C & Cattaneo E (2000) Wild-type huntingtin protects from apoptosis upstream of caspase-3. *Journal of Neuroscience* **20:** 3705–3713

Rockabrand E, Slepko N, Pantalone A, Nukala VN, Kazantsev A, Marsh JL, Sullivan PG, Steffan JS, Sensi SL & Thompson LM (2007) The first 17 amino acids of Huntingtin modulate its sub-cellular localization, aggregation and effects on calcium homeostasis. *Human Molecular Genetics* **16:** 61–77

Rodgers JT, Lerin C, Haas W, Gygi SP, Spiegelman BM & Puigserver P (2005) Nutrient control of glucose homeostasis through a complex of PGC-1alpha and SIRT1. *Nature* **434:** 113–118

Rosas H, Salat D, Lee S & Zaleta A (2008) Cerebral cortex and the clinical expression of Huntington's disease: complexity and heterogeneity. *Brain* **131:** 1057–1068

Rosenstock T & Rego A (2012) Modified mitochondrial dynamics, turnover and function in neurodegeneration: a focus on Huntington's Disease. In *Cellular Bioenergetics in Health and Diseases: New Perspectives in Mitochondrial Biology* pp 149–194.

Rosenstock TR, Duarte AI & Rego AC (2010) Mitochondrial-associated metabolic changes and neurodegeneration in Huntington's disease - from clinical features to the bench. *Current Drug Targets* **11:** 1218–1236

Ross CA & Tabrizi SJ (2011) Huntington's disease: From molecular pathogenesis to clinical treatment. *The Lancet Neurology* **10:** 83–98

Rubinsztein DC (2006) The roles of intracellular protein-degradation pathways in neurodegeneration. *Nature* **443:** 780–786

Rué L, López-Soop G, Gelpi E, Martínez-Vicente M, Alberch J & Pérez-Navarro E (2013) Brain region- and age-dependent dysregulation of p62 and NBR1 in a mouse model of Huntington's disease. *Neurobiology of Disease* **52:** 219–228

Rui Y-N, Xu Z, Patel B, Chen Z, Chen D, Tito A, David G, Sun Y, Stimming EF, Bellen HJ, Cuervo AM & Zhang S (2015) Huntingtin functions as a scaffold for selective macroautophagy. *Nature Cell Biology* **17:** 262–275

Ryan AB, Zeitlin SO & Scrable H (2006) Genetic interaction between expanded murine Hdh alleles and p53 reveal deleterious effects of p53 on Huntington's disease pathogenesis. *Neurobiology of Disease* **24:** 419–427

Sakahira H, Breuer P, Hayer-Hartl MK & Hartl FU (2002) Molecular chaperones as modulators of polyglutamine protein aggregation and toxicity. *Proceedings of the National Academy of Sciences* **99:** 16412–16418

Samant SA, Zhang HJ, Hong Z, Pillai VB, Sundaresan NR, Wolfgeher D, Archer SL, Chan DC & Gupta MP (2014) SIRT3 Deacetylates and Activates OPA1 To Regulate Mitochondrial Dynamics during Stress. *Molecular and Cellular Biology* **34:** 807–819

Santel A & Frank S (2008) Shaping mitochondria: The complex posttranslational regulation of the mitochondrial fission protein DRP1. *IUBMB Life* **60:** 448–455

Scarpulla RC (2008) Nuclear Control of Respiratory Chain Expression by Nuclear Respiratory Factors and PGC-1-Related Coactivator. *Annals of the New York Academy of Sciences* **1147:** 321–334

Schaffar G, Breuer P, Boteva R, Behrends C, Tzvetkov N, Strippel N, Sakahira H, Siegers K, Hayer-Hartl M & Hartl FU (2004) Cellular toxicity of polyglutamine expansion proteins: Mechanism of transcription factor deactivation. *Molecular Cell* **15:** 95–105

Scher MB, Vaquero A & Reinberg D (2007) SirT3 is a nuclear NAD+-dependent histone deacetylase that translocates to the mitochondria upon cellular stress. *Genes and Development* **21:** 920–928

Sepers MD & Raymond LA (2014) Mechanisms of synaptic dysfunction and excitotoxicity in Huntington's disease. *Drug Discovery Today* **19:** 990–996

Seto E & Yoshida M (2014) Erasers of Histone Acetylation: The Histone Deacetylase Enzymes. *Cold Spring Harbor Perspectives in Biology* **6:** a018713–a018713

Shaltouki A, Sivapatham R, Pei Y, Gerencser AA, Momčilović O, Rao MS & Zeng X (2015) Mitochondrial Alterations by PARKIN in Dopaminergic Neurons Using PARK2 Patient-Specific and PARK2 Knockout Isogenic iPSC Lines. *Stem Cell Reports* **4:** 847–859

Shin BH, Lim Y, Oh HJ, Park SM, Lee S-K, Ahnn J, Kim DH, Song WK, Kwak TH & Park WJ (2013) Pharmacological Activation of Sirt1 Ameliorates Polyglutamine-Induced Toxicity through the Regulation of Autophagy. *PLoS ONE* **8:** e64953

Shirendeb U, Reddy AP, Manczak M, Calkins MJ, Mao P, Tagle DA & Reddy PH (2011) Abnormal mitochondrial dynamics, mitochondrial loss and mutant huntingtin oligomers in Huntington's disease: Implications for selective neuronal damage. *Human Molecular Genetics* **20:** 1438–1455

Shirendeb UP, Calkins MJ, Manczak M, Anekonda V, Dufour B, McBride JL, Mao P & Reddy PH (2012) Mutant Huntingtin's interaction with mitochondrial protein Drp1 impairs mitochondrial biogenesis and causes defective axonal transport and synaptic degeneration in Huntington's disease. *Human Molecular Genetics* **21:** 406–420

Siddiqui A, Rivera-Sánchez S, Castro M del R, Acevedo-Torres K, Rane A, Torres-Ramos CA, Nicholls DG, Andersen JK & Ayala-Torres S (2012) Mitochondrial DNA damage Is associated with reduced mitochondrial bioenergetics in Huntington's disease. *Free Radical Biology and Medicine* **53:** 1478–1488

Silva AC, Almeida S, Laço M, Duarte AI, Domingues J, Oliveira CR, Januário C & Rego a C (2013) Mitochondrial respiratory chain complex activity and bioenergetic alterations in human platelets derived from pre-symptomatic and symptomatic Huntington's disease carriers. *Mitochondrion* **13:** 801–9

Smirnova E, Griparic L, Shurland D-L & van der Bliek AM (2001) Dynamin-related Protein Drp1 Is Required for Mitochondrial Division in Mammalian Cells. *Molecular Biology of the Cell* **12:** 2245–2256

Solans A, Zambrano A, Rodríguez M & Barrientos A (2006) Cytotoxicity of a mutant huntingtin fragment in yeast involves early alterations in mitochondrial OXPHOS complexes II and III. *Human Molecular Genetics* **15:** 3063–3081

Song W, Chen J, Petrilli A, Liot G, Klinglmayr E, Zhou Y, Poquiz P, Tjong J, Pouladi MA, Hayden MR, Masliah E, Ellisman M, Rouiller I, Schwarzenbacher R, Bossy B, Perkins G & Bossy-Wetzel E (2011) Mutant huntingtin binds the mitochondrial fission GTPase dynamin-related protein-1 and increases its enzymatic activity. *Nature Medicine* **17:** 377–382

Song W, Song Y, Kincaid B, Bossy B & Bossy-Wetzel E (2013) Mutant SOD1G93A triggers mitochondrial fragmentation in spinal cord motor neurons: Neuroprotection by SIRT3 and PGC-1?? *Neurobiology of Disease* **51:** 72–81

Squitieri F, Cannella M, Sgarbi G, Maglione V, Falleni A, Lenzi P, Baracca A, Cislaghi G, Saft C, Ragona G, Russo MA, Thompson LM, Solaini G & Fornai F (2006) Severe ultrastructural mitochondrial changes in lymphoblasts homozygous for Huntington disease mutation. *Mechanisms of Ageing and Development* **127:** 217–220

Steffan JS (2004) SUMO Modification of Huntingtin and Huntington's Disease Pathology. *Science* **304:** 100–104

Steffan JS, Kazantsev a, Spasic-Boskovic O, Greenwald M, Zhu YZ, Gohler H, Wanker EE, Bates GP, Housman DE & Thompson LM (2000) The Huntington's disease protein interacts with p53 and CREB-binding protein and represses transcription. *Proceedings of the National Academy of Sciences of the United States of America* **97:** 6763–8

Strappazzon F, Nazio F, Corrado M, Cianfanelli V, Romagnoli A, Fimia GM, Campello S, Nardacci R, Piacentini M, Campanella M & Cecconi F (2015) AMBRA1 is able to induce mitophagy via LC3 binding, regardless of PARKIN and p62/SQSTM1. *Cell Death and Differentiation* **22:** 419–432

Su YC & Qi X (2013) Inhibition of excessive mitochondrial fission reduced aberrant autophagy and neuronal damage caused by LRRK2 G2019S mutation. *Human Molecular Genetics* **22:** 4545–4561

Subramaniam S, Sixt K, Barrow R & Snyder S (2009) Rhes, a striatal specific protein, mediates mutant-huntingtin cytotoxicity. *Science* **324:** 1327–1330

Tabrizi SJ, Cleeter MWJ, Xuereb J, Taanman JW, Cooper JM & Schapira AH V (1999) Biochemical abnormalities and excitotoxicity in Huntington's disease brain. *Annals of Neurology* **45:** 25–32

Tan C-C, Yu J-T, Tan M-S, Jiang T, Zhu X-C & Tan L (2014) Autophagy in aging and neurodegenerative diseases: implications for pathogenesis and therapy. *Neurobiology of Aging* **35:** 941–957

Tanner KG, Landry J, Sternglanz R & Denu JM (2000) Silent information regulator 2 family of NAD- dependent histone/protein deacetylases generates a unique product, 1-O-acetyl-ADP-ribose. *Proceedings of the National Academy of Sciences of the United States of America* **97:** 14178–14182

Thomas EA, Coppola G, Desplats PA, Tang B, Soragni E, Burnett R, Gao F, Fitzgerald KM, Borok JF, Herman D, Geschwind DH & Gottesfeld JM (2008) The HDAC inhibitor 4b ameliorates the disease phenotype and transcriptional abnormalities in Huntington's disease transgenic mice. *Proceedings of the National Academy of Sciences of the United States of America* **105:** 15564–15569

Trettel F, Rigamonti D, Hilditch-Maguire P, Wheeler VC, Sharp a H, Persichetti F, Cattaneo E & MacDonald ME (2000) Dominant phenotypes produced by the HD mutation in STHdh(Q111) striatal cells. *Human Molecular Genetics* **9:** 2799–2809

Trushina E, Dyer RB, Badger JD, Ure D, Eide L, Tran DD, Vrieze BT, Legendre-Guillemin V, McPherson PS, Mandavilli BS, Van Houten B, Zeitlin S, McNiven M, Aebersold R, Hayden M, Parisi JE, Seeberg E, Dragatsis I, Doyle K, Bender A, et al (2004) Mutant Huntingtin Impairs Axonal Trafficking in Mammalian Neurons In Vivo and In Vitro. *Molecular and Cellular Biology* **24:** 8195–8209

Tseng AHH, Shieh SS & Wang DL (2013) SIRT3 deacetylates FOXO3 to protect mitochondria against oxidative damage. *Free Radical Biology and Medicine* **63:** 222–234

Tsoi H & Chan HYE (2013) Expression of Expanded CAG Transcripts Triggers Nucleolar Stress in Huntington's Disease. *The Cerebellum* **12:** 310–312

Tsunemi T, Ashe TD, Morrison BE, Soriano KR, Au J, Roque RA V., Lazarowski ER, Damian VA, Masliah E & La Spada AR (2012) PGC-1 Rescues Huntington's Disease Proteotoxicity by Preventing Oxidative Stress and Promoting TFEB Function. *Science Translational Medicine* **4:** 142ra97–142ra97

Twig G & Shirihai OS (2011) The Interplay Between Mitochondrial Dynamics and Mitophagy. *Antioxidants & Redox Signaling* **14:** 1939–1951

Ueda M, Li S, Itoh M, Hayakawa-Yano Y, Wang M, Hayakawa M, Hasebe-Matsubara R, Ohta K, Ohta E, Mizuno A, Hida Y, Matsumoto M, Chen H & Nakagawa T (2014) Polyglutamine

expansion disturbs the endoplasmic reticulum formation, leading to caspase-7 activation through Bax. *Biochemical and Biophysical Research Communications* **443:** 1232–1238

Valenza M & Cattaneo E (2010) Neuroprotection and brain cholesterol biosynthesis in Huntington's disease. *Proceedings of the National Academy of Sciences* **107:** E143–E143

Valor LM & Guiretti D (2014) What's wrong with epigenetics in Huntington's disease? *Neuropharmacology* **80:** 103–114

Verdin E, Hirschey MD, Finley LWS & Haigis MC (2010) Sirtuin regulation of mitochondria: Energy production, apoptosis, and signaling. *Trends in Biochemical Sciences* **35:** 669–675

Walker FO (2007) Huntington's disease. *Lancet* **369:** 218–228

Waltregny D (2005) Histone deacetylase HDAC8 associates with smooth muscle -actin and is essential for smooth muscle cell contractility. *The FASEB Journal* **19:** 966–968

Wang DB, Garden G a, Kinoshita C, Wyles C, Babazadeh N, Sopher B, Kinoshita Y & Morrison RS (2013) Declines in Drp1 and Parkin Expression Underlie DNA Damage-Induced Changes in Mitochondrial Length and Neuronal Death. *Journal of Neuroscience* **33:** 1357–1365

Wang DB, Kinoshita C, Kinoshita Y & Morrison RS (2014) p53 and mitochondrial function in neurons. *Biochimica et Biophysica Acta (BBA) - Molecular Basis of Disease* **1842:** 1186–1197

Wang H, Lim PJ, Karbowski M & Monteiro MJ (2009) Effects of overexpression of Huntingtin proteins on mitochondrial integrity. *Human Molecular Genetics* **18:** 737–752

Warby SC, Doty CN, Graham RK, Shively J, Singaraja RR & Hayden MR (2009) Phosphorylation of huntingtin reduces the accumulation of its nuclear fragments. *Molecular and Cellular Neuroscience* **40:** 121–127

Wareski P, Vaarmann A, Choubey V, Safiulina D, Liiv J, Kuum M & Kaasik A (2009) PGC-1alpha and PGC-1beta Regulate Mitochondrial Density in Neurons. *Journal of Biological Chemistry* **284:** 21379–21385

Webster BR, Scott I, Han K, Li JH, Lu Z, Stevens M V, Malide D, Chen Y, Samsel L, Connelly PS, Daniels MP, McCoy JP, Combs C a, Gucek M & Sack MN (2013) Restricted mitochondrial protein acetylation initiates mitochondrial autophagy. *Journal of Cell Science* **126:** 4843–4849

Webster BR, Scott I, Traba J, Han K & Sack MN (2014) Regulation of autophagy and mitophagy by nutrient availability and acetylation. *Biochimica et Biophysica Acta - Molecular and Cell Biology of Lipids* **1841:** 525–534

Wellington CL, Leavitt BR & Hayden MR (2000) Huntington disease: new insights on the role of huntingtin cleavage. *Journal of Neural Transmission. Supplementum* **58:** 1–17

Weydt P, Pineda V V, Torrence AE, Libby RT, Satterfield TF, Lazarowski ER, Gilbert ML, Morton GJ, Bammler TK, Strand AD, Cui L, Beyer RP, Easley CN, Smith AC, Krainc D, Luquet S, Sweet IR, Schwartz MW & La Spada AR (2006) Thermoregulatory and metabolic defects in Huntington's disease transgenic mice implicate PGC-1α in Huntington's disease neurodegeneration. *Cell Metabolism* **4:** 349–362

Whitworth AJ & Pallanck LJ (2009) The PINK1/Parkin pathway: a mitochondrial quality control system? *Journal of Bioenergetics and Biomembranes* **41:** 499–503

Wickramasekera NT & Das GM (2014) Tumor suppressor p53 and estrogen receptors in nuclear–mitochondrial communication. *Mitochondrion* **16:** 26–37

Wong YC & Holzbaur ELF (2014) The Regulation of Autophagosome Dynamics by Huntingtin and HAP1 Is Disrupted by Expression of Mutant Huntingtin, Leading to Defective Cargo Degradation. *Journal of Neuroscience* **34:** 1293–1305

Xia J (2003) Huntingtin contains a highly conserved nuclear export signal. *Human Molecular Genetics* **12:** 1393–1403

Xu W, Li Y, Liu C & Zhao S (2014) Protein lysine acetylation guards metabolic homeostasis to fight against cancer. *Oncogene* **33:** 2279–85

Yanai A, Huang K, Kang R, Singaraja RR, Arstikaitis P, Gan L, Orban PC, Mullard A, Cowan CM, Raymond LA, Drisdel RC, Green WN, Ravikumar B, Rubinsztein DC, El-Husseini A & Hayden MR (2006) Palmitoylation of huntingtin by HIP14is essential for its trafficking and function. *Nature Neuroscience* **9:** 824–831

Yang H, Yang T, Baur JA, Perez E, Matsui T, Carmona JJ, Lamming DW, Souza-Pinto NC, Bohr VA, Rosenzweig A, de Cabo R, Sauve AA & Sinclair DA (2007) Nutrient-Sensitive Mitochondrial NAD+ Levels Dictate Cell Survival. *Cell* **130:** 1095–1107

Yano H, Baranov S V, Baranova O V, Kim J, Pan Y, Yablonska S, Carlisle DL, Ferrante RJ, Kim AH & Friedlander RM (2014) Inhibition of mitochondrial protein import by mutant huntingtin. *Nature Neuroscience* **17:** 822–831

Yu Z-X, Li S-H, Evans J, Pillarisetti A, Li H & Li X-J (2003) Mutant huntingtin causes context-dependent neurodegeneration in mice with Huntington's disease. *Journal of Neuroscience* **23:** 2193–2202

Yuan H, Su L & Chen W (2013) The emerging and diverse roles of sirtuins in cancer: A clinical perspective. *OncoTargets and Therapy* **6:** 1399–1416

Zhang H, Li Q, Graham RK, Slow E, Hayden MR & Bezprozvanny I (2008) Full length mutant huntingtin is required for altered Ca2+ signaling and apoptosis of striatal neurons in the YAC mouse model of Huntington's disease. *Neurobiology of Disease* **31:** 80–88

Zhang XD, Wang Y, Wang Y, Zhang X, Han R, Wu JC, Liang ZQ, Gu ZL, Han F, Fukunaga K & Qin ZH (2009) P53 mediates mitochondria dysfunction-triggered autophagy activation and cell death in rat striatum. *Autophagy* **5:** 339–350

Zheng Z, Li A, Holmes BB, Marasa JC & Diamond MI (2013) An N-terminal Nuclear Export Signal Regulates Trafficking and Aggregation of Huntingtin (Htt) Protein Exon 1. *Journal of Biological Chemistry* **288:** 6063–6071

Zhu J, Wang KZQ & Chu CT (2013) After the banquet: Mitochondrial biogenesis, mitophagy, and cell survival. *Autophagy* **9:** 1663–1676

Zhu Y, Chen G, Chen L, Zhang W, Feng D, Liu L & Chen Q (2014) Monitoring Mitophagy in Mammalian Cells. In *Methods in Enzymology* pp 39–55. Elsevier Inc.

Zinsmaier KE, Babic M & Russo GJ (2009) Mitochondrial transport dynamics in axons and dendrites. *Results and Problems in Cell Differentiation* **48:** 107–139

Zuccato C (2001) Loss of Huntingtin-Mediated BDNF Gene Transcription in Huntington's Disease. *Science* **293:** 493–498

ATTACHMENTS

1. SUPPLEMENTARY METHODS

1.1. Macro used to design ROIs

```
/*
   MitProt_AutoROIsupervised is an ImageJ macro developed to design ROIS of neurons to be used to analyze mitochondria, protein levels and colocalization with MitoProt_analyzer
   Copyright (C) 2014  Jorge Valero Gómez-Lobo.

   MitProt_AutoROIsupervised is free software: you can redistribute it and/or modify  it under the terms of the GNU General Public License as published by the Free Software Foundation, either version 3 of the License, or (at your option) any later version.

   MitProt_AutoROIsupervised is distributed in the hope that it will be useful, but WITHOUT ANY WARRANTY; without even the implied warranty of MERCHANTABILITY or FITNESS FOR A PARTICULAR PURPOSE.  See the GNU General Public License for more details.

   You should have received a copy of the GNU General Public License along with this program.  If not, see <http://www.gnu.org/licenses/>.
*/

//This macro has been developed by Dr Jorge Valero (jorge.valero@cnc.uc.pt).
//If you have any doubt about how to use it, please contact me.

//License
Dialog.create("GNU GPL License");
Dialog.addMessage(" MitProt_AutoROIsupervised  Copyright (C) 2014 Jorge Valero Gomez-Lobo.");
Dialog.setInsets(10, 20, 0);
Dialog.addMessage(" MitProt_AutoROIsupervised  comes with ABSOLUTELY NO WARRANTY; click on help button for details.");
Dialog.setInsets(0, 20, 0);
Dialog.addMessage("This is free software, and you are welcome to redistribute it under certain conditions; click on help button for details.");
Dialog.addHelp("http://www.gnu.org/licenses/gpl.html");
Dialog.show();

// This macro helps on ROI design and storage for posterior analysis

//Select initial folder

dir=getDirectory("Please, select the initial folder");
if (File.exists(dir+"ROIS/")==false) File.makeDirectory(dir+"ROIS");
        dirRois=dir+"ROIS"+File.separator;
if (File.exists(dir+"Processed/")==false) File.makeDirectory(dir+"Processed");
        dirPro=dir+"Processed"+File.separator;
if (File.exists(dir+"NONProcessed/")==false) File.makeDirectory(dir+"NONProcessed");
        dirNONPro=dir+"NONProcessed"+File.separator;

//detect Images folder
level1=getFileList(dir);
i=0;
while (i<level1.length) {
        if (level1[i]=="Images/") imagedir=dir+level1[i];
        i++;
}
```

```
52          //error message if no Images folder exists
53          if (i==level1.length+1){
54                  showMessage("NO Images folder found");
55                  beep();
56                  exit();
57          }
58
59          //detect n folder
60          level2=getFileList(imagedir);
61          for (i=0; i<level2.length; i++) {
62                  ene=File.getName(imagedir+level2[i]);
63                  enesem=substring(ene, 1);
64                  if (endsWith(level2[i], "/")){
65                          direne=imagedir+level2[i];
66
67                          //detect group folder
68                          level3=getFileList(direne);
69                          for (ii=0; ii<level3.length; ii++){
70                                  group=File.getName(direne+level3[ii]);
71                                  diris=newArray(ene, group);
72                                  if (File.exists(dirRois+ene+"/"+group+"/")==false) creardir(dirRois,
73  diris);
74                                  dirRoisgroup=dirRois+ene+"/"+group+"/";
75                                  if   (File.exists(dirPro+ene+"/"+group+"/")==false)   creardir(dirPro,
76  diris);
77                                  dirProgroup=dirPro+ene+"/"+group+"/";
78                                  if (endsWith(level3[ii], "/")){
79                                          dirgroup=direne+level3[ii];
80
81                                          //detect images
82                                          level4=getFileList(dirgroup);
83                                          for (iii=0; iii<level4.length; iii++){
84                                                  imagepath=dirgroup+level4[iii];
85                                                  work();
86                                          }
87                          }
88                  }
89          }
90  }
91
92  function work(){
93          //Open image
94          run("Bio-Formats    Importer",    "open=["+imagepath+"]    color_mode=Default    open_files
95  view=Hyperstack stack_order=XYCZT");
96          //get image name
97          imopen=getTitle();
98          imagename=File.name;
99          raiz=File.nameWithoutExtension;
100         run("Red");
101         // ROIs design
102         cont=false;
103         skip=false;
104         while (cont==false){
105
106                 autoroi();
107                 rois=roiManager("count");
108                 if (rois==0) {
109                         waitForUser("NO ROIS DETECTED");
110                         skip=getBoolean("Do you want to skip this image?");
111                         if (skip==true) cont=true;
```

```
112                             else Roidesign();
113                     }
114                     else {
115                             roiManager("Show All");
116                             cont=getBoolean("Do you want to continue with the next image?");
117                             if (cont==false) {
118                                     roiManager("Deselect");
119                                     roiManager("Delete");
120                                     Dialog.create("OPTIONS");
121                                      Dialog.addChoice("Select an option:", newArray("Separate cells
122     using a line", "Design ROIs by myself", "Try to improve the image"))
123                                      Dialog.show();
124                                     option=Dialog.getChoice();
125                                     if (option=="Separate cells using a line") Lineseparator();
126                                     if (option=="Design ROIs by myself") {
127                                             Roidesign();
128                                             cont=true;
129                                             rois=0;
130                                     }
131                                     if (option=="Try to improve the image") waitForUser("Now you
132     have time to improve the image");
133                             }
134                     }
135             }
136             if (skip==true) {
137                     if (File.exists(dirNONPro+ene+"/"+group+"/")==false) creardir(dirNONPro, diris);
138                     dirNONProgroup=dirNONPro+ene+"/"+group+"/";
139                     File.rename(imagepath, dirNONProgroup+imagename);
140                     selectWindow(imopen);
141                     close();
142             }
143             if (skip==false && rois>0){
144                     roiManager("Save", dirRoisgroup+raiz+".zip");
145                     roiManager("Deselect");
146                     roiManager("Delete");
147                     File.rename(imagepath, dirProgroup+imagename);
148                     selectWindow(imopen);
149                     close();
150             }
151
152     }
153     // this function creates folders
154     function creardir(inidir, pathes){
155             for (i=0; i<pathes.length; i++){
156                     File.makeDirectory(inidir+pathes[i]);
157                     inidir=inidir+pathes[i]+"/";
158             }
159
160     }
161     //automatic detection of cells
162     function autoroi(){
163             selectWindow(imopen);
164             run("Channels Tool...");
165             run("Make Composite", "display=Composite");
166             Stack.setDisplayMode("composite");
167             Stack.setActiveChannels("1011");
168             run("Stack to RGB");
169             run("8-bit");
170             run("Median...", "radius=5");
171             setAutoThreshold("Triangle dark");
```

```
172             run("Analyze Particles...", "size=150-Infinity add");
173             close();
174             roiManager("Select",0);
175     }
176
177     function Roidesign(){
178             cont=false;
179             skip=false;
180             while (cont==false){
181                     setTool("polygon");
182                     waitForUser("Please, draw ROIs and add to ROI Manager by pressing t");
183                     rois=roiManager("count");
184                     if (rois==0) {
185                             waitForUser("NO ROIS DESIGNED");
186                             skip=getBoolean("Do you want to skip this image?");
187                             if (skip==true) cont=true;
188                     }
189                     else {
190                             roiManager("Show All");
191                             cont=getBoolean("Do you want to continue with the next step?");
192                     }
193             }
194             if (skip==true) {
195                     if (File.exists(dirNONPro+ene+"/"+group+"/")==false) creardir(dirNONPro, diris);
196                     dirNONProgroup=dirNONPro+ene+"/"+group+"/";
197                     File.rename(imagepath, dirNONProgroup+imagename);
198             }
199             else{
200                     roiManager("Save", dirRoisgroup+raiz+".zip");
201                     roiManager("Deselect");
202                     roiManager("Delete");
203                     File.rename(imagepath, dirProgroup+imagename);
204             }
205             selectWindow(imopen);
206             close();
207     }
208
209     function Lineseparator() {
210             lines=0;
211             while(lines==0){
212                     selectWindow(imopen);
213                     setTool("line");
214                     waitForUser("Please draw lines and add to the ROi manager");
215                     lines=roiManager("count");
216                     if (lines>0){
217                             for (i=0; i<lines; i++){
218                                     roiManager("Select", i);
219                                     run("Line to Area");
220                                     run("Enlarge...", "enlarge=2 pixel");
221                                     setBackgroundColor(0, 0, 0);
222                                     run("Clear");
223                             }
224                             roiManager("Deselect");
225                             roiManager("Delete");
226                     }
227                     else{
228                             nolines=getBoolean("No lines, do you want to retry without lines?");
229                             if (nolines==true) lines=-1;
230                     }
231             }
```

```
}
```

1.2. Macro used to analyze mitochondrial morphology and protein colocalization

```
/*
   MitoProt_analyzer is an ImageJ macro developed to analyze mitochondria, protein levels and colocalization
   Copyright (C) 2014  Jorge Valero Gómez-Lobo.

   MitoProt_analyzer is free software: you can redistribute it and/or modify it under the terms of the GNU General Public License as published by the Free Software Foundation, either version 3 of the License, or (at your option) any later version.

   MitoProt_analyzer is distributed in the hope that it will be useful, but WITHOUT ANY WARRANTY; without even the implied warranty of MERCHANTABILITY or FITNESS FOR A PARTICULAR PURPOSE.  See the GNU General Public License for more details.

   You should have received a copy of the GNU General Public License along with this program.  If not, see <http://www.gnu.org/licenses/>.
*/

//This macro has been developed by Dr Jorge Valero (jorge.valero@cnc.uc.pt).
//If you have any doubt about how to use it, please contact me.

//License
Dialog.create("GNU GPL License");
Dialog.addMessage(" MitoProt_analyzer  Copyright (C) 2014 Jorge Valero Gomez-Lobo.");
Dialog.setInsets(10, 20, 0);
Dialog.addMessage(" MitoProt_analyzer  comes with ABSOLUTELY NO WARRANTY; click on help button for details.");
Dialog.setInsets(0, 20, 0);
Dialog.addMessage("This is free software, and you are welcome to redistribute it under certain conditions; click on help button for details.");
Dialog.addHelp("http://www.gnu.org/licenses/gpl.html");
Dialog.show();

//This Macro does not work adequately using Batchmode

//This is a global variable that it will be used by infoTab to substitute return;
var infovar=0;
var GFP=false;
var nonprot=0;

//Dialog of initial parameters

Dialog.create("MITOCHONDRIA PARAMETERS");

  Dialog.addNumber("Background subtraction rollingball radius:", 10)

  Dialog.addMessage("FIND FOCI parameters")
  Dialog.addNumber("Gaussian blur:", 0.5);
  Dialog.addNumber ("Absolute threshold:", 10);
  Dialog.addNumber("Peak Search parameter", 0.3);
  Dialog.addNumber("Peak fusion parameter", 0.5);
  Dialog.addNumber("Minimum size", 5);
  Dialog.show();
```

```
rolling=Dialog.getNumber();
gaussian=Dialog.getNumber();
backparam=Dialog.getNumber();
searchparam=Dialog.getNumber();
peakparam=Dialog.getNumber();
minsize=Dialog.getNumber();

Dialog.create("PROT PARAMETERS");

  Dialog.addNumber("Background subtraction rollingball radius:", 10)

  Dialog.addMessage("FIND FOCI VALUES:")
  Dialog.addNumber("Gaussian Blur:", 0.5);
  Dialog.addNumber ("Absolute threshold:", 8);
  Dialog.addNumber("Peak Search parameter", 0.3);
  Dialog.addNumber("Peak fusion parameter", 0.253);
  Dialog.addNumber("Minimum size", 2);
       Dialog.show();

rollingProt=Dialog.getNumber();
gaussianProt=Dialog.getNumber();
backparamProt=Dialog.getNumber();
searchparamProt=Dialog.getNumber();
peakparamProt=Dialog.getNumber();
minsizeProt=Dialog.getNumber();

Dialog.create("GFP PARAMETERS");

  Dialog.addNumber("Background subtraction rollingball radius:", 30)

  Dialog.addMessage("FIND FOCI VALUES:")
  Dialog.addNumber("Gaussian Blur:", 0.5);
  Dialog.addNumber ("Absolute threshold:", 8);
  Dialog.addNumber("Peak Search parameter", 0.1);
  Dialog.addNumber("Peak fusion parameter", 0.253);
  Dialog.addNumber("Minimum size", 5);
       Dialog.show();

rollingGFP=Dialog.getNumber();
gaussianGFP=Dialog.getNumber();
backparamGFP=Dialog.getNumber();
searchparamGFP=Dialog.getNumber();
peakparamGFP=Dialog.getNumber();
minsizeGFP=Dialog.getNumber();

Dialog.create("Nuclei PARAMETERS");

  Dialog.addMessage("FIND FOCI VALUES:")
  Dialog.addNumber("Gaussian Blur:", 1.0);
  Dialog.addNumber ("Absolute threshold:", 10);
  Dialog.addNumber("Peak Search parameter", 0.0);
  Dialog.addNumber("Peak fusion parameter", 1);
  Dialog.addNumber("Minimum size", 3);
       Dialog.show();

gaussianN=Dialog.getNumber();
backparamN=Dialog.getNumber();
searchparamN=Dialog.getNumber();
peakparamN=Dialog.getNumber();
minsizeN=Dialog.getNumber();
```

```
349
350 //This helps to localize the folders
351
352 dir=getDirectory("Please, select the initial folder");
353 dirRois=dir+"ROIS"+File.separator;
354 dirPro=dir+"Processed"+File.separator;
355 if (File.exists(dir+"Results/")==false) File.makeDirectory(dir+"Results");
356 dirRes=dir+"Results"+File.separator;
357
358 //detect Images folder
359 level1=getFileList(dir);
360 i=0;
361 while (i<level1.length) {
362         if (level1[i]=="Processed/") imagedir=dir+level1[i];
363         i++;
364 }
365         //error message if no Processed folder exists
366         if (i==level1.length+1){
367                 showMessage("NO Processed folder found");
368                 beep();
369                 exit();
370         }
371
372         //detect n folder
373         level2=getFileList(imagedir);
374         for (i=0; i<level2.length; i++) {
375                 ene=File.getName(imagedir+level2[i]);
376                 enesem=substring(ene, 1);
377                 summtables();
378                 if (endsWith(level2[i], "/")){
379                         direne=imagedir+level2[i];
380
381                         //detect group folder
382                         level3=getFileList(direne);
383                         for (ii=0; ii<level3.length; ii++){
384                                 group=File.getName(direne+level3[ii]);
385                                 diris=newArray(ene, group);
386                                 dirRoisgroup=dirRois+ene+"/"+group+"/";
387                                 if  (File.exists(dirRes+ene+"/"+group+"/")==false)  creardir(dirRes,
388 diris);
389                                 dirResgroup=dirRes+ene+"/"+group+"/";
390                                 if (endsWith(level3[ii], "/")){
391                                         dirgroup=direne+level3[ii];
392
393                                         //detect images
394                                         level4=getFileList(dirgroup);
395                                         sptables();
396                                         for (iii=0; iii<level4.length; iii++){
397                                                 imagepath=dirgroup+level4[iii];
398                                                 work();
399                                         }
400                         }
401                         printsumm();
402                 }
403                 savesumm();
404                 print("Number of cells with no protein levels: "+nonprot);
405                 savetab("Log", dirRes+ene+"/");
406                 selectWindow("Log");
407                 run("Close");  ;
408         }
```

```
}

function work(){
	run("Bio-Formats Importer", "open=["+imagepath+"] color_mode=Default open_files
view=Hyperstack stack_order=XYCZT");
	run("Red");
	//run("Bio-Formats Importer", "open=["+imagepath+"] color_mode=Default open_files
view=[Standard ImageJ] stack_order=Default");

	//get image name;
	imopen=getTitle();
	imagename=File.name;
	raiz=File.nameWithoutExtension;
	getPixelSize(unit, pixelWidth, pixelHeight);

	//open rois
	roiManager("Open", dirRoisgroup+raiz+".zip");
	rois=roiManager("count");
	//analyze each roi
	for (iroi=0; iroi<rois; iroi++){
		selectWindow(imopen);
		roiManager("Select", 0);
		roiManager("Measure");
		Roiarea=getResult("Area", iroi);
		hayprot=protpresence();
		selectWindow("prot");
		close();
		if (hayprot!=-1){
			mitos();
			prot();
			if (GFP==true) GFPdata();
			closing();
		}
		else {
			closingnonprot();
			nonprot++;
		}
	}
	selectWindow(imopen);
	close();
}

function protpresence(){
	run("Duplicate...", "title=Duplicate duplicate channels=1-4");
	roiManager("Add");
	roiManager("Deselect");
	run("Duplicate...", "title=prot duplicate channels=4");
	run("Subtract Background...", "rolling="+rollingProt);
	run("FindFoci", "mask=[None] background_method=Absolute
background_parameter="+backparamProt+" auto_threshold=Otsu statistics_mode=Both
search_method=[Fraction of peak - background] search_parameter="+searchparamProt+"
minimum_size="+minsizeProt+" minimum_above_saddle minimum_peak_height=[Relative above
background] peak_parameter="+peakparamProt+" sort_method=[Total intensity]
maximum_peaks=1000000000 show_mask=Threshold fraction_parameter=1.0
gaussian_blur="+gaussianProt+" centre_method=[Max value (search image)] centre_parameter=2.0");
	run("Set Scale...", "distance=1 known="+pixelWidth+" pixel=1 unit="+unit);
	setThreshold(3, 10000000000000000000);
	run("Create Selection");
	return(selectionType());
}
```

```
469
470 function mitos(){
471         run("Set Measurements...", "area perimeter shape feret's area_fraction redirect=None
472 decimal=3");
473         selectWindow("Duplicate");
474         run("Duplicate...", "title=Mitos duplicate channels=1");
475         run("Grays");
476         run("Subtract Background...", "rolling="+rolling);
477         run("FindFoci", "mask=[None] background_method=Absolute
478 background_parameter="+backparam+" auto_threshold=Otsu statistics_mode=Both
479 search_method=[Fraction of peak - background] search_parameter="+searchparam+"
480 minimum_size="+minsize+" minimum_above_saddle minimum_peak_height=[Relative above
481 background] peak_parameter="+peakparam+" sort_method=[Total intensity]
482 maximum_peaks=1000000000 show_mask=Threshold fraction_parameter=1.0
483 gaussian_blur="+gaussian+" centre_method=[Max value (search image)] centre_parameter=2.0");
484         run("Set Scale...", "distance=1 known="+pixelWidth+" pixel=1 unit="+unit);
485         setAutoThreshold("Default dark");
486         setOption("BlackBackground", false);
487
488         run("Duplicate...", "title=MaskMit");
489         setThreshold(2, 255);
490         run("Convert to Mask");
491
492         selectWindow("Mitos FindFoci");
493         close();
494         selectWindow("MaskMit");
495         rename("Mitos FindFoci");
496         roiManager("Select", 0);
497         roiManager("Delete");
498         TOTROIS=roiManager("count");
499         inirois=rois-iroi;
500         ROIS=TOTROIS-inirois;
501         mitoarr=newArray(ROIS);
502         for (i=0; i<ROIS; i++) mitoarr[i]=i+inirois;
503         roiManager("Select", mitoarr);
504         roiManager("Combine");
505         roiManager("Add");
506         roiManager("Select", mitoarr);
507         roiManager("Delete");
508         roiManager("Select", inirois);
509         setBackgroundColor(0, 0, 0);
510         run("Clear");
511         selectWindow("Mitos");
512         close();
513
514         //To know whether the cell is GFP positive
515         selectWindow("Duplicate");
516         roiManager("Deselect");
517         run("Duplicate...", "title=GFP duplicate channels=2");
518         run("Subtract Background...", "rolling="+rollingGFP);
519         run("FindFoci", "mask=[None] background_method=Absolute
520 background_parameter="+(backparamGFP+12)+" auto_threshold=Otsu statistics_mode=Both
521 search_method=[Fraction of peak - background] search_parameter="+searchparamGFP+"
522 minimum_size="+minsizeGFP+" minimum_above_saddle minimum_peak_height=[Relative above
523 background] peak_parameter="+peakparamGFP+" sort_method=[Total intensity]
524 maximum_peaks=1000000000 show_mask=Threshold fraction_parameter=1.0
525 gaussian_blur="+gaussianGFP+" centre_method=[Max value (search image)] centre_parameter=2.0");
526         run("Set Scale...", "distance=1 known="+pixelWidth+" pixel=1 unit="+unit);
527         setThreshold(1, 10000000000000000000);
528         run("Create Selection");
```

```
529		select=selectionType();
530		if (select!=-1){
531			GFP=true;
532			run ("Select None");
533		}
534		else GFP=false;
535
536
537		//take values
538		infoTab("Summary", 1, 3);
539		area=infovar;
540		infoTab("Summary", 1, 5);
541		perim=infovar;
542		Round=0;
543		AR=0;
544		perim=0;
545		areabis=0;
546		selectWindow("Results");
547		ress=getInfo();
548		row=split(ress, "\n");
549		limit=row.length-1;
550		for(irow=0; irow<limit; irow++){
551			Round=Round+getResult("Round", irow);
552			AR=AR+getResult("AR", irow);
553			perim=perim+getResult("Perim.",irow);
554			areabis=areabis+getResult("Area",irow);
555		}
556		Round=Round/limit;
557		AR=AR/limit;
558		selectWindow("Mitos FindFoci");
559		roiManager("Select", inirois-1);
560		run("Measure");
561		perArea=getResult("%Area", limit);
562
563		//populate tables
564		tablearray=newArray(ene, group, imagename, iroi, Roiarea, area, perim, Round, AR,
565	perArea);
566		if (GFP==true) tableprinter(ene+ group+ " Mit parameters GFP", tablearray);
567		else {
568			tableprinter(ene+ group+ " Mit parameters NONGFP", tablearray);
569			selectWindow("GFP FindFoci");
570			close();
571			selectWindow("GFP");
572			close();
573		}
574
575		//IJ.renameResults(name);
576		//savetab(tablename, dirdest);
577		selectWindow("Results");
578		run("Close");
579		selectWindow("Summary");
580		run("Close");
581	}
582
583		//Prot measurements
584	function prot(){
585		selectWindow("Duplicate");
586		roiManager("Deselect");
587		run("Duplicate...", "title=prot duplicate channels=4");
588		selectWindow("prot FindFoci");
```

```
589             run("Set Scale...", "distance=1 known="+pixelWidth+" pixel=1 unit="+unit);
590             setThreshold(3, 10000000000000000000);
591             run("Create Selection");
592             select=selectionType();
593             if (select!=-1){
594                     roiManager("Add");
595                     selectWindow("prot FindFoci");
596                     close();
597                     selectWindow("Mitos FindFoci");
598                     ROIS=roiManager("count");
599                     roiManager("Select", ROIS-1);
600                     run("Set Measurements...", "area mean integrated area_fraction redirect=None
601     decimal=3");
602                     run("Measure");
603                     selectWindow("prot");
604                     roiManager("Select", ROIS-1);
605                     run("Measure");
606
607             }
608
609             //get results
610             area=getResult("Area", 1);
611             IntDen=getResult("IntDen", 1);
612             meanint=getResult("Mean", 1);
613             perArea=getResult("%Area", 0);
614
615             //obtain data about prot into the mitochondria
616             rois=roiManager("count");
617             jeje=newArray(2);
618             jeje[0]=rois-2;
619             jeje[1]=rois-1;
620             selectWindow("prot");
621             roiManager("Select", jeje);
622             roiManager("AND");
623             run("Measure");
624             if (getResult("IntDen",0)!=0){
625                     protquantmit=getResult("IntDen", 2);
626                     perprotmit=(100/IntDen)*protquantmit;
627                     IDRoi=(IntDen/Roiarea);
628             }
629             else{
630                     protquantmit=0;
631                     perprotmit=0;
632             }
633
634             //populate tables
635                     tablearray=newArray(ene, group, imagename, iroi, Roiarea, area, IntDen, IDRoi,
636     meanint, perprotmit , protquantmit);
637                     if (GFP==true) tableprinter(ene+group+" Prot analysis GFP", tablearray);
638                     else tableprinter(ene+group+" Prot analysis NONGFP", tablearray);
639
640             //eliminating prot images and rois
641                     selectWindow("prot");
642                     close();
643                     selectWindow("Results");
644                     run("Close");
645                     roiManager("Deselect");
646                     roiManager("Select", rois-1);
647                     roiManager("Delete");
648     }
```

```
649
650             //GFP analysis
651     function GFPdata(){
652
653             selectWindow("GFP FindFoci");
654             setThreshold(1, 10000000000000000000);
655             run("Create Selection");
656                     roiManager("Add");
657                     selectWindow("GFP FindFoci");
658                     close();
659
660                     //data about GFP in GFP
661                     selectWindow("GFP");
662                     ROIS=roiManager("count");
663                     roiManager("Select", ROIS-1);
664                     run("Set Measurements...", "area mean integrated area_fraction redirect=None
665     decimal=3");
666                     run("Measure");
667
668                     //data about GFP in mitochondria
669                     selectWindow("Mitos FindFoci");
670                     roiManager("Select", ROIS-1);
671                     run("Measure");
672                     a=ROIS-2;
673                     b=ROIS-1;
674                     mitGFP=newArray(a,b);
675                     selectWindow("GFP");
676                     roiManager("Select", mitGFP);
677                     roiManager("AND");
678                     run("Measure");
679                     roiManager("Deselect");
680
681                     //data about GFP in nuclei
682                     selectWindow("Duplicate");
683                     run("Select None");
684                     run("Duplicate...", "title=Nucl duplicate channels=3");
685                     run("FindFoci", "mask=[None] background_method=Absolute
686     background_parameter="+backparamN+" auto_threshold=Otsu statistics_mode=Both
687     search_method=[Above background] search_parameter="+searchparamN+"
688     minimum_size="+minsizeN+" minimum_above_saddle minimum_peak_height=[Relative above
689     background] peak_parameter="+peakparamN+" sort_method=[Total intensity] maximum_peaks=1
690     show_mask=Threshold fraction_parameter=1.0 gaussian_blur="+gaussianN+" centre_method=[Max
691     value (search image)] centre_parameter=2.0");
692                     run("Set Scale...", "distance=1 known="+pixelWidth+" pixel=1 unit="+unit);
693                     setThreshold(1, 10000000000000000000);
694                     run("Convert to Mask");
695                     roiManager("Select", ROIS-2);
696                     setBackgroundColor(255, 255, 255);
697                     run("Clear");
698                     run("Create Selection");
699                     roiManager("Add");
700                     roiManager("Select", ROIS-1);
701                     run("Measure");
702                     a=ROIS-1;
703                     nucleiGFP=newArray(a, ROIS);
704                     selectWindow("GFP");
705                     roiManager("Select", nucleiGFP);
706                     roiManager("AND");
707                     run("Measure");
708
```

```
709                     //get data
710                     area=getResult("Area", 0);
711                     IntDen=getResult("IntDen",0);
712                     meanint=getResult("Mean", 0);
713                     if (getResult("IntDen", 1)!=0) perGFPmit=(100/IntDen)*getResult("IntDen",2);
714                     else perGFPmit=0;
715                     if (getResult("IntDen", 3)!=0) perGFPNucl=(100/IntDen)*getResult("IntDen",4);
716                     else perGFPNucl=0;
717
718                     //populate table
719                     tablearray=newArray(ene, group, imagename, iroi, Roiarea, area, IntDen, meanint,
720     perGFPmit, perGFPNucl);
721                     tableprinter (ene+group+" GFP localization", tablearray);
722
723                     //clear GFP things
724                     selectWindow("GFP");
725                     close();
726                     selectWindow("Nucl FindFoci");
727                     close();
728                     selectWindow("Nucl");
729                     close();
730                     roiManager("Deselect");
731                     rois=roiManager("count");
732                     for (i=1; i<3; i++){
733                             roiManager("Select", rois-i);
734                             roiManager ("Delete");
735                     }
736                     selectWindow("Results");
737                     run("Close");
738             }
739
740     function creardir(inidir, pathes){
741             for (i=0; i<pathes.length; i++){
742                     File.makeDirectory(inidir+pathes[i]);
743                     inidir=inidir+pathes[i]+"/";
744             }
745     }
746
747     function tablecreator(tabname, tablearray){
748             run("New... ", "name=["+tabname+"] type=Table");
749             headings=tablearray[0];
750             for (i=1; i<tablearray.length; i++)headings=headings+"\t"+tablearray[i];
751             print ("["+tabname+"]", "\\Headings:"+ headings);
752     }
753
754     function tableprinter(tabname, tablearray){
755             line=tablearray[0];
756             for (i=1; i<tablearray.length; i++) line=line+"\t"+tablearray[i];
757             print ("["+tabname+"]", line);
758     }
759
760
761     //This function obtains info from Threshold table channel "chann" and column "column", values should
762     be numeric
763
764     function infoTab(tablename, line, column){
765             selectWindow(tablename);
766             tableinfo=getInfo();
767             Ltab=split(tableinfo, "\n");
768             Ctab=split(Ltab[line], "\t");
```

```
769             infovar=Ctab[column];
770     }
771
772     function copytable(oldname, newname){
773             first=0;
774             if (isOpen(newname)==false) {
775                     run("New... ", "name=["+newname+"] type=Table");
776                     first=1;
777             }
778             selectWindow(oldname);
779             tableinfo=getInfo();
780             linetable=split(tableinfo, "\n");
781             for (t=0; t<linetable.length; t++){
782             if (t==0 && first==1) print("["+newname+"]","\\Headings:"+linetable[t]);
783             else if (t!=0) print("["+newname+"]",""+linetable[t]);
784             }
785     }
786
787     function mean(oldname, newname){
788             first=0;
789             if (isOpen(newname)==false) {
790                     run("New... ", "name=["+newname+"] type=Table");
791                     first=1;
792             }
793             selectWindow(oldname);
794             tableinfo=getInfo();
795             linetable=split(tableinfo, "\n");
796             for (t=0; t<linetable.length; t++){
797             if (t==0 && first==1) print("["+newname+"]","\\Headings:"+linetable[t]);
798             else if (t!=0) print("["+newname+"]",""+linetable[t]);
799             }
800     }
801
802     function  savetab(tablename, dirdest){
803             //tablename=getList("window.titles");
804                     selectWindow(tablename);
805                      saveAs("Text", dirdest+tablename+".xls");
806             }
807
808     function closing(){
809             selectWindow("Mitos FindFoci");
810             close();
811             selectWindow("Duplicate");
812             close();
813             rois=roiManager("Count");
814             for (i=1; i<3; i++){
815                     roiManager("Select", rois-i);
816                     roiManager("Delete");
817             }
818     }
819
820     function closingnonprot(){
821             selectWindow("prot FindFoci");
822             close();
823             selectWindow("Duplicate");
824             close();
825             rois=roiManager("Count");
826             for (i=1; i<3; i++){
827                     roiManager("Select", rois-i);
828                     roiManager("Delete");
```

```
829             }
830     }
831
832     function sptables(){
833             //creating tables
834                             tablearray=newArray("Exp group", "Genotype", "Image", "ROI",
835     "ROIArea", "Area", "Perimeter", "Round", "AR", "Roundness", "Connectivity", "% Area Mit into
836     cells");
837                             tablecreator (ene+ group+ " Mit parameters NONGFP", tablearray);
838                             tablecreator (ene+group+" Mit parameters GFP", tablearray);
839
840                             tablearray=newArray("Exp group", "Genotype", "Image", "ROI",
841     "ROIArea", "Area", "Int Den.", "ID/ROI area", "Mean", "%Prot in Mit", "Quantity of prot in Mit");
842                             tablecreator (ene+group+" Prot analysis NONGFP", tablearray);
843                             tablecreator (ene+group+" Prot analysis GFP", tablearray);
844
845                             tablearray=newArray("Exp group", "Genotype", "Image", "ROI",
846     "ROIArea", "Area", "Int Den.", "Mean", "%GFP in Mit", "%GFP Nucl");
847                             tablecreator (ene+group+" GFP localization", tablearray);
848     }
849
850     function summtables(){
851             //creating tables
852                             tablearray=newArray("Exp group", "Genotype", "Area", "Perimeter",
853     "Round", "AR", "Roundness", "Connectivity", "% Area Mit into cells");
854                             tablecreator (ene+" Summary Mit parameters", tablearray);
855
856                             tablearray=newArray("Exp group", "Genotype", "Area", "Int Den.", "ID/ROI
857     area", "Mean", "%Prot in Mit", "Quantity of prot in Mit");
858                             tablecreator (ene+" Summary Prot analysis", tablearray);
859
860                             tablearray=newArray("Exp group", "Genotype", "Area", "Int Den.", "Mean",
861     "%GFP in Mit", "%GFP Nucl");
862                             tablecreator (ene+" Summary GFP localization", tablearray);
863     }
864
865     function printsumm(){
866
867             meandata(ene+ group+ " Mit parameters NONGFP", ene+" Summary Mit parameters", "");
868             savetab(ene+ group+ " Mit parameters NONGFP", dirResgroup);
869             selectWindow(ene+ group+ " Mit parameters NONGFP");
870             run("Close");
871
872             meandata(ene+group+" Mit parameters GFP", ene+" Summary Mit parameters", "GFP");
873             savetab(ene+ group+ " Mit parameters GFP", dirResgroup);
874             selectWindow(ene+ group+ " Mit parameters GFP");
875             run("Close");
876
877             meandata(ene+group+" Prot analysis NONGFP", ene+" Summary Prot analysis", "");
878             savetab(ene+ group+ " Prot analysis NONGFP", dirResgroup);
879             selectWindow(ene+ group+ " Prot analysis NONGFP");
880             run("Close");
881
882             meandata(ene+group+" Prot analysis GFP", ene+" Summary Prot analysis", "GFP");
883             savetab(ene+ group+ " Prot analysis GFP", dirResgroup);
884             selectWindow(ene+ group+ " Prot analysis GFP");
885             run("Close");
886
887             meandata(ene+group+" GFP localization", ene+" Summary GFP localization", "");
888             savetab(ene+ group+ " GFP localization", dirResgroup);
```

```
889             selectWindow(ene+ group+ " GFP localization");
890             run("Close");
891     }
892
893     //print mean tables
894     function meandata(datatab, destinytab, extra){
895             selectWindow(datatab);
896             tableinfo=getInfo();
897             linetable=split(tableinfo, "\n");
898             if (linetable.length>1){
899             coltable=split(linetable[1], "\t");
900             means=newArray(coltable.length-2);
901             infoTab(datatab, 1, 0);
902             means[0]=infovar;
903             infoTab(datatab, 1, 1);
904             means[1]=infovar+" "+extra;
905             for(c=4; c<coltable.length; c++){
906                     n=0;
907                     for (t=1; t<linetable.length; t++){
908                             infoTab(datatab, t, c);
909                             infovar=parseFloat(infovar);
910                             means[c-2]=means[c-2]+infovar;
911                             n++;
912                     }
913                     means[c-2]=means[c-2]/n;
914             }
915             tableprinter(destinytab, means);
916             }
917     }
918
919     function savesumm(){
920             savetab(ene+" Summary Mit parameters", dirRes+ene+"/");
921             selectWindow(ene+" Summary Mit parameters");
922             run("Close");
923
924             savetab(ene+" Summary Prot analysis", dirRes+ene+"/");
925             selectWindow(ene+" Summary Prot analysis");
926             run("Close");
927
928             savetab(ene+" Summary GFP localization", dirRes+ene+"/");
929             selectWindow(ene+" Summary GFP localization");
930             run("Close");
931     }
932
```

2. SUPPLEMENTARY DATA

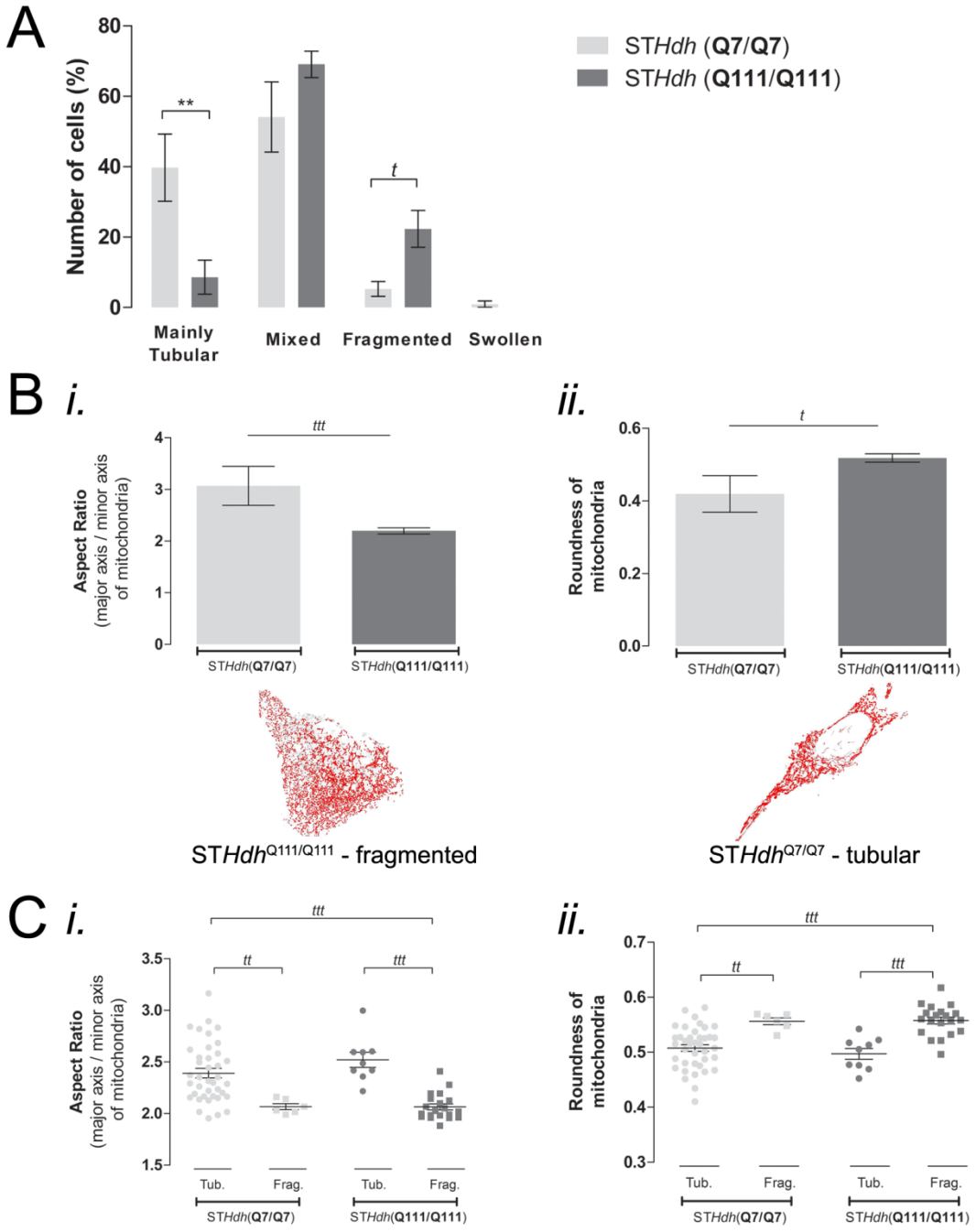

Fig. S 1 | Study of the variables Aspect Ratio and Roundness and their adequacy towards the categorization of mitochondrial morphology.

Aspect Ratio and Roundness were quantified using Image J and only untransfected cells were considered. **A)** Cells were placed in different categories according to their mitochondrial morphology, visually assessed by a not blinded observer. Data is presented as the mean ± SEM of 4 experiments. **B)** A cell with an obviously fragmented mitochondrial network and one with tubular mitochondria were considered for the analysis. Each value derived represents a single mitochondrion. **C)** Values from cells considered to have a fragmented or tubular mitochondrial morphology in (**A**) were considered separately. Data is presented as the mean ± SEM of 4 experiments. Statistical significance: $^{t}P<0.05$, $^{tt}P<0.01$, $^{ttt}P<0.001$ (two-tailed Student's *t*-test) and $^{**}P<0.01$ (two-way ANOVA, followed by Bonferroni *post-hoc* test).